POLITECNICO
MILANO 1863

SCUOLA DI INGEGNERIA INDUSTRIALE
E DELL'INFORMAZIONE

Executive Summary of the Thesis

Counter rotating electric fan, mission analysis and preliminary sizing

Laurea Magistrale in Aeronautical Engineering - Ingegneria Aeronautica

Author: Matteo Baldassarri

Advisor: Prof. Paolo Gaetani

Co-advisor: Prof. Fabrizio Fontaneto, Dr. Manas Madasseri Payyappalli

Academic year: 2021-2022

1. Introduction

To satisfy the increasingly limitations in terms of emitted pollutants and noise, in the last years also the aeronautical field started to consider the electric propulsion. The main problem is that an aircraft requires propulsion systems that have to be light and powerful, therefore it is important to consider new engine designs and components, like counter-rotating (CR) machines. These machines present some benefits, for example some studies demonstrated that ducted or unducted CR fans can save fuel up to 35 %. Unfortunately, there are very few example of these machines in the past due to their complexity from a mechanical point of view. However, the technological level reached in these last years have resulted in a revival of the CR machines. In Figure 1 is represented an example of an unducted CR fan.

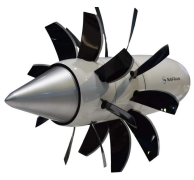

Figure 1: Safran open rotor model, 2017.

This thesis fits exactly in this context, in fact the main focus will be on electric CR fan engines. At first the CR fan component will be modeled in an existing commercial modelling tool called EcosimPro. From that component different models of the electric CR fan engine will be proposed, which will be then analyzed from a design and off-design point of view. In the last part of this thesis, their performances will be tested in different flight missions. Each flight mission considered is the result of different combinations of range (short / medium / long), hybrid system used (CASE 1 / 1bis / 2 / 2bis) and electric CR fan engine used. The hybrid systems will be presented in Section 4. The electric CR fan engines were modeled depending in which flight mission they will perform, in which configuration they will be mounted (classic or distributed) and for which speed ratio they will work.

2. EcosimPro

EcosimPro is a simulation tool used for modelling physical processes. It has an important role in this thesis, in fact it was used to create the CR fan component. Moreover, it was used also to model and test the off-design conditions of all the engines presented in this manuscript. One of the main references used in this work is the user manual of EcosimPro [1], from which it was possible to learn how to use this software and how

to program in EL (EcosimPro language).

2.1. CR fan component

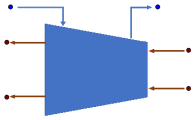

Figure 2: EcosimPro component: CR fan.

The first result obtained in this thesis was the creation of the CR fan component in EcosimPro (Figure 2). The work of Alexiou et al. [2] was used as reference. It was coded in EL and it was modeled in order to be compatible with the other components in the aeroengine dedicated library called turbojet. The CR fan component presents two gas ports (blue) and four mechanical ports (brown). From the formers are exachanged thermodynamic quantities, like the total quantities and the mass flow. Instead, from the latters are exchanged the mechanical power and rotational speed for each shaft.

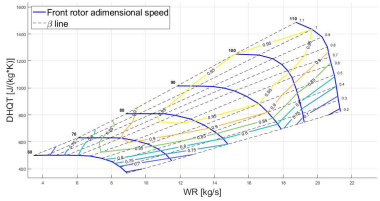

(a) Performance map.

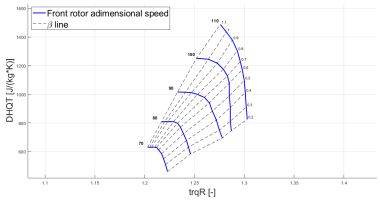

(b) Torque ratio map.

Figure 3: CR fan non-scaled maps for $N_{ratio} = 1$. Inside the component are embedded also the maps for $N_{ratio} = 0.9$ and $N_{ratio} = 1.1$.

In the CR fan code are implemented several equations, like for example the conservation of mass and power, but none of them is associated to the component geometry. In fact, the CR fan component was modeled in 0D. In the code, all the component characteristics are embedded in its performance and torque ratio maps, which are depicted in Figure 3. The three main parameters of the CR fan are the speed, power and torque ratio, defined as:

$$N_{ratio} = \frac{N_{FR}}{N_{RR}};\ P_{ratio} = \frac{P_{FR}}{P_{RR}};\ T_{r_{ratio}} = \frac{T_{r,FR}}{T_{r,RR}}.$$

2.2. Engines modelling

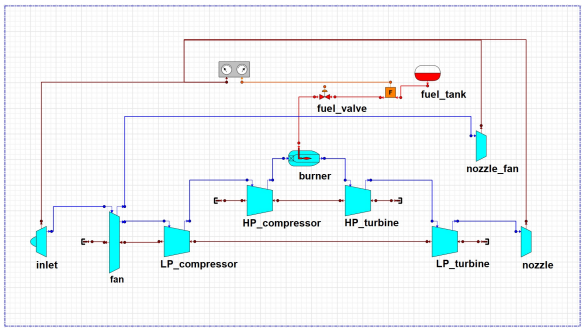

Figure 4: Turbofan schematic.

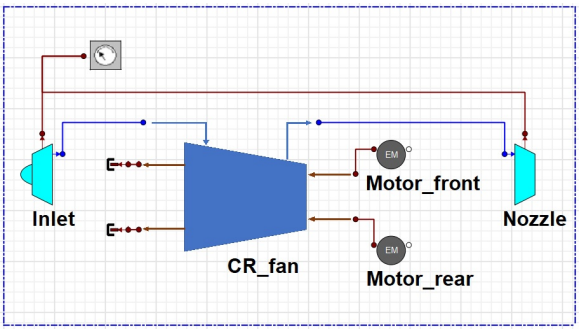

Figure 5: Electric CR fan schematic.

Once the CR fan modelling was completed, the second part of this thesis is dedicated to the design and off-design analysis of all the engines. At first, two turbofans were analyzed: CFM56-7B24 and GEnx-1B64. These are very common turbofans in civil aviation and they were used as references. Note that the CFM56-7B24 will be used as reference for short and medium range missions, instead the GEnx-1B64 for the long ones. In order to design an engine in EcosimPro, at first its engine schematic has to be created. The engine schematic used for the two turbofans is depicted in Figure 4, instead the one used for the electric CR fans is the one in Figure 5. After that, throught the imposition of specific boundary conditions, it is possible to obtain the engine models. As said before, the turbofans designed are 2. Instead the electric CR fans designed are 12 and are reported in Figure 6. This figure should be read in this

way. The acronym HYB-CF1 indicates that the electric CR fan is designed for short or medium range missions. The acronyms 2eng or 10 eng indicate if the engine was designed to be mounted in a configuration with 2 or 10 engines. The acronyms DPref, DP1 and DP2 indicate respectively if the engine was designed at $N_{ratio} = 1$, $N_{ratio} = 0.9$ or $N_{ratio} = 1.1$. Therefore, the electric CR fan engines in the group HYB-CF1-2eng will be named HYB-CF1-2eng-DPref, HYB-CF1-2eng-DP1 and HYB-CF1-2eng-DP2. The same nomenclature is applied for HYB-CF2.

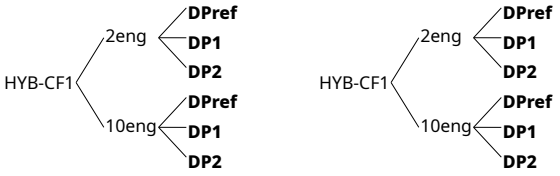

(a) Engines for short and medium range missions.

(b) Engines for long range missions.

Figure 6: All electric CR fan engines modeled.

From the off-design analysis it is possible to obtain the so called "engine maps". Each engine has its own engine map and its meaning is simple. In Figure 7 and 8 are reported two examples of engine maps. These are basically a cloud of points, in which each of them defines a particular engine off-design condition at a certain z, M and $\dot{m}_f$ (or electric power P for electric CR fan engines). In each point are saved all the engine performances, like the thrust, in that off-design condition. The main scope of the engine map is to transfer the engine model from EcosimPro to Matlab, but also some considerations can be done. For example it can be highlighted that the electric CR fans have an higher rangeability.
All the boundary conditions used come from both real data [3] and realistic assumptions. The engine models were validated comparing the outputs of the off-design simulation with both real values and values obtained through simple isentropic relations.
The contributions of this section are three. The first one is the creation of a new component. The second one is the design of different engine models. The last one is the creation in EL of the code that generates the engine map.

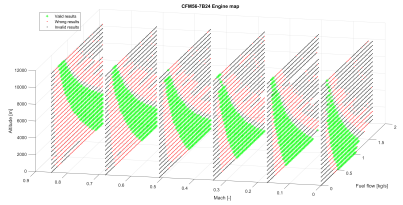

Figure 7: CFM56-7B24: Engine map.

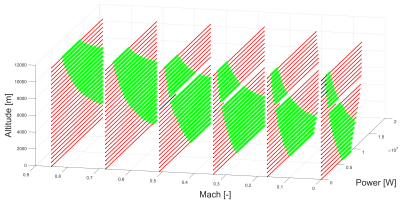

Figure 8: HYB-CF1-2eng-DPref: Engine map.

3. Implementation of the flight missions

The flight mission analysis was implemented in Matlab, because it was more easy to create a code flexible enough to be used to analyze different flight missions.

3.1. Models used

This code receives in input several models, that are:

- the atmosphere model;
- the engine model;
- the aircraft model.

The atmosphere model used is the simple International Atmosphere Model(ISA).
The engine models are added converting their engine maps in tables. In this way Matlab can read them and obtain the value of thrust when the engine is at a certain z, M and $\dot{m}_f$ (or P). The aircraft was considered as a point mass.

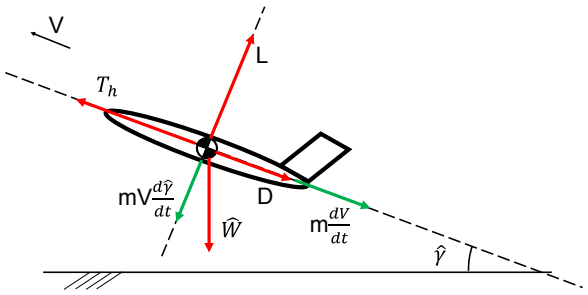

Figure 9: Aircraft model.

The equations of motion come from the equilib-

rium of forces and are here reported:

$$\begin{cases} T_h - D - \hat{W}\sin(\hat{\gamma}) = m\dfrac{\mathrm{d}V}{\mathrm{d}t}, \\ L - \hat{W}\cos(\hat{\gamma}) = mV\dfrac{\mathrm{d}\hat{\gamma}}{\mathrm{d}t}. \end{cases} \quad (1)$$

Equations (1) are referred to Figure 9.
Note that the atmosphere and aircraft model are the same for all the missions, instead the engine model changes dependig on the engine used.

3.2. Input data

The flight mission code in Matlab receives in input also several data, which are:

- the aircraft data;
- the flight mission data;
- the engine data (only for the electric CR fan engines).

The aircraft data are referred to Boieng 737-800 and Boeing 787-800. The former was used in the short and medium range missions, instead the latter in the long ones. These data are the wing surface, the payload weight, the weight of the empty aircraft, the max take-off weight and the values of CD_0 for different flight phases. Note that, for the reference cases, on Boeing 737-800 can be mounted only the CFM56-7B24, instead on Boeing 787-800 can be mounted only the GEnx-1B64. In both cases these engines are mounted in two engines configuration.
The flight mission data come from Eurocontrol [4] and they define the flight path of the three flight missions: short, medium and long range. All these flight missions were divided in three main phases: climb, cruise and descent.

Component	Var.	Value	Unit
Battery	η	0.99	-
Battery	SP	1000	$\frac{W}{kg}$
Battery	SE	720000	$\frac{J}{kg}$
Electric gen.	η	0.95	-
Electric gen.	SP	9500	$\frac{W}{kg}$
Electric motor	η	0.95	-
Electric motor	SP	9500	$\frac{W}{kg}$
Power electronics	η	0.98	-
Power electronics	SP	62000	$\frac{W}{kg}$

Table 1: Electric components data.

The engines data are needed only for the hybrid system. In particular, these are the intial values of the specific fuel consumption (SFC_{init}) for the turbogas generator (GT) and the values of efficiency (η), specific power (SP) and specific energy (SE) for the electric components. These data are reported in Table 1.
A further explanation about the hybrid systems used will be provided in Sub-section 3.3.

3.3. Hybrid systems

The electric CR fan engines need a source of electric power. For this thesis two different hybrid systems were considered:

- hybrid-electric serial (hy-el se), which uses energy from both the GT and the battery. This layout comprises an electric generator and electric motors that work in AC. Since the battery works only in DC, the presence of the power electronics is necessary;
- turbo-electric power controlled (tu-el pc), which uses energy only form the GT. Between the generator and the electric motors there is the power electronics, which adjust the current to the value needed by the electric motors.

In Figures 10 these two systems are reported.

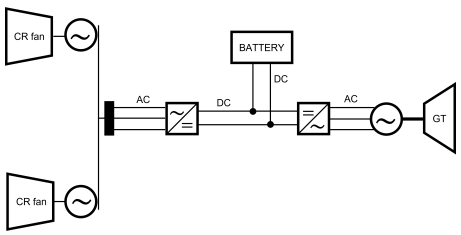

(a) Hy-el se with 2 electric CR fan engines.

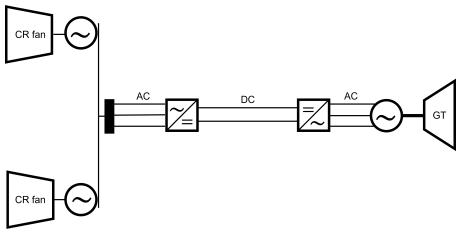

(b) Tu-el pc with 2 electric CR fan engines.

Figure 10: These are the two hybrid layout used in this thesis. The former is used in CASE 1 and CASE 1bis, instead the latter is used in CASE 2 and CASE 2bis. The cases with 10 electric CR fan engines are analogous.

In the last chapter will be analzyed the flight mission analysis. The flight missions will be perfomed considering four different "CASEs", which are reported in Table 2. CASE 1 and 1bis are perfomed with the layout hy-el se. The difference from the two is in the different use of the battery. CASE 2 and 2bis are perfomed with the layout tu-el pc. Here the difference is in the aircraft weight considered. In the sense that in CASE 2bis the aircraft weight is imposed equal to the reference case. CASE 2bis will be used to compare directly the electric CR fan engines with the reference turbofans.
The main reference used for the implementation of the flight mission analysis was the work of Hendrik et al. [5].

	1	1bis	2	2bis
Take-off	GT	GT	GT	GT
Init. climb	GT	GT	GT	GT
Climb 1	GT	GT	GT	GT
Climb 2	GT	GT	GT	GT
Const. M climb	GT	GT	GT	GT
Cruise	GT	GT	GT	GT
Init. descent	B	B	GT	GT
Descent	B	B	GT	GT
Approach	B	GT	GT	GT

Table 2: Different use of the hybrid system during a certain flight mission. The four columns are the different CASEs. In this table B is the battery.

4. Flight mission analysis

The last part of this thesis is dedicated to the flight mission analysis. Several flight missions were analyzed and each flight mission is the result of different combinations between:

- range, the three ranges considered are short (500 [km]), medium (2000 [km]) and long (6500 [km]);
- engine, the two turbofans and the twelve electric CR fans;
- hybrid system, hence CASE 1, 1bis, 2 and 2bis.

The notation used to identify the single flight mission will be "range / engine / CASE". Hence, for example, a flight mission could be "short / HYB-CF1-2eng-DP1 / CASE 1bis".

The results of each flight mission will be presented mainly in terms of fuel saved and reduction in payload mass (m_{PAY}) with respect the reference case. Morevoer, it will be provided also the SFC target value (SFC_{target}) for the GT. Before explaining its meaning, let's introduce how works the Matlab code in the case of the hybrid aircraft. The flight mission code computes the fuel and the electric component masses through successive iterations. The code has to satisfy two conditions: the first one is mandatory and is $m_{TOT} < m_{MTOW}$, the second one is that the hybrid aircraft has to consume less fuel with respect the reference case, hence $m_{FUEL_{hyb}} < m_{FUEL_{ref}}$. In order to satisfy these two conditions, the code (if necessary) at first will start to reduce the GT SFC, hence $m_{FUEL_{hyb}}$. If it is not enough, the code will start to reduce m_{PAY}. The SFC at maximum can be reduced by 38 %, instead the m_{PAY} by 90 %. The obtained value of SFC is the SFC_{target}, which is the SFC value that the GT should have in order to make the flight with the hybrid configuration possible (i.e. $m_{TOT} < m_{MTOW}$) and more sustainable (i.e. $m_{FUEL_{hyb}} < m_{FUEL_{ref}}$).

4.1. Short range mission

The fuel consumed in the reference case is $m_{FUEL} = 2133$ [kg]. In Table 3 are reported the key results for the different cases. The units are [kg] for m_{FUEL} and [%] for SFC and m_{PAY} reduction. Note that to have m_{FUEL} saved >0 is a positive result, instead to have m_{PAY} and SFC reduction <0 is a negative result. The latter tells that the hybrid aircraft can't bring the same payload of the reference case and that an improvement on the GT SFC is needed.

CASE	m_{FUEL} **saved**	m_{PAY} **reduc.**	SFC **reduc.**
1	+1002	-43.2	-38
1bis	+826	-27	-38
2	+1	0	-9
2bis	+20	0	-5

Table 3: Results reported for HYB-CF1-2eng-DP1 which is the engine that showed the best performances.

4.2. Medium range mission

The fuel consumed in the reference case is $m_{FUEL} = 6223$ [kg].

CASE	m_{FUEL} saved	m_{PAY} reduc.	SFC reduc.
1	+1641	-78.1	-38
1bis	+1462	-48.2	-38
2	+5	0	-18
2bis	+15	0	-13

Table 4: Results reported for HYB-CF1-2eng-DP1 which is the engine that showed the best performances.

4.3. Long range mission

The fuel consumed in the reference case is $m_{FUEL} = 46082$ [kg].
Note that CASE 1 and 1bis were not performed because with the battery the condition $m_{TOT} < m_{MTOW}$ can't be satisfied.

CASE	m_{FUEL} saved	m_{PAY} reduc.	SFC reduc.
2	+5730	0	-36
2bis	+516	0	-23

Table 5: Results reported for HYB-CF2-10eng-DP1 which is the engine that showed the best performances.

5. Conclusions

The main scope of this thesis was to assess the feasibility of the CR fan engines, providing models and guidelines for future researches. In particular, the CR fan component can be re-used to built new schematics or its code can be used as a basis for more detailed modelling. A suggestion is to continue the analysis of these propulsion systems in PROOSIS, which is a software compatible with EcosimPro, but designed for aero-engines.
From the off-design analysis it was possible to highlight the higher rangeability of the electric CR fan engines compared to the one of the turbofans. From the flight mission analysis emerged that the hybrid system hy-el se can make sense only for short range missions, in which the power and energy required is relatively low. In fact, the main problem of the hybrid system is the battery weight. The hybrid layout tu-el pc could be a possible solution for both the short and medium range missions, instead for the long ones there are some problems. In fact, to provide the power to an intercontinental aircraft the electric components should be very powerful, hence heavy. Among all the possible electric CR fan models the best results are obtained for $N_{ratio} = 0.9$. Note that this result is very sensitive to the non-scaled performance maps used. Changing these maps, the results could be different. A more detailed analysis about that aspect is required.
The distributed propulsion has a certain potential because it permits to increase the propulsive efficiency throught the reduction of the compression ratio. The drawback is that having more engines the losses are higher.
In all the hybrid cases the SFC_{target} value is lower with respect the initial one. Further studies should be performed about the GT in order to achieve the required SFC_{target}, for example considering also a small amount of thrust generated by the GT itself (in analogy of a turbofan core).

References

[1] *EcosimPro 5.2 modelling and simulation software - User Manual.*

[2] A. Alexiou, I. Roumeliotis, N. Aretakis, A. Tsalavoutas, and K. Mathioudakis. Modeling Contra-Rotating Turbomachinery Components for Engine Performance Simulations: The Geared Turbofan With Contra-Rotating Core Case. *Journal of Engineering for Gas Turbines and Power*, 134(11), 09 2012. 111701.

[3] Mark Daly. *Jane's Aero-Engines: 2019-2020.* Jane's by IHS Markit, 2019.

[4] Eurocontrol. Aircraft performance database. [12/03/2022].

[5] Hendrik Gesell, Florian Wolters, and Martin Plohr. System analysis of turbo-electric and hybrid-electric propulsion systems on a regional aircraft. *The Aeronautical Journal*, 123(1268):1602–1617, 2019.

POLITECNICO
MILANO 1863

SCUOLA DI INGEGNERIA INDUSTRIALE
E DELL'INFORMAZIONE

Counter rotating electric fan, mission analysis and preliminary sizing

Tesi di Laurea Magistrale in
Aeronautical Engineering - Ingegneria Aeronautica

Author: **Matteo Baldassarri**

Student ID: 944649
Advisor: Prof. Paolo Gaetani
Co-advisors: Prof. Fabrizio Fontaneto, Dr. Manas Madasseri Payyappalli
Academic Year: 2021-2022

Abstract

The effects of climate change are visible all around the world and their impact on our society is increasing year after year. This is why the European Union is encouraging a lot of research to make our economy more sustainable and resource-efficient. This thesis fits perfectly in this context, in fact it will be used by the von Karman Institute (VKI) as a starting point of a new research area dedicated to novel aircraft engine concepts. The engine that will be analyzed is the electric counter-rotating (CR) fan. The main scope of this thesis, therefore, will be to assessing the feasibility of this particular new engine and providing guidelines for future researches.
The modelling and analysis of all the engines were performed in EcosimPro, which is a commercial modelling tool. In particular, the turbojet library was used as a reference. At first, using this software, the CR fan component was created. It was coded in order to be compatible with the other components in the turbojet library, therefore it will be more easy to re-use it for future studies. Then, starting from that component, several electric CR fan engine models were generated. Each engine was designed using different boundary conditions, with a particular regard to the speed ratio, which is a key parameter of the CR fan. Moreover, a comparison of the performance of the CR fan engines in a classic 2 engines configuration and in a distributed 10 engines configuration was carried out. As next step, two turbofans were modeled in order to be used as reference cases: the CFM56-7B24 and GEnx-1B64.
The last part of this thesis is dedicated to the flight mission analysis, which was performed in Matlab. Each flight mission considered is the result of different combinations of mission range, engines mounted on the aircraft and hybrid system layout considered. These results will be useful to define for which configurations and missions the electric CR fans are more suited for.

Keywords: EcosimPro, turbofan, electric counter-rotating fan, hybrid propulsion, flight mission analysis.

Abstract in lingua italiana

Gli effetti dei cambiamenti climatici sono ormai visibili in tutto il mondo e le ripercussioni che hanno sulla nostra società sono sempre più evidenti. Proprio per questo motivo l'Unione Europea sta investendo molte risorse per rendere la nostra economia più sostenibile ed efficiente. Questa tesi si inserisce proprio in questo contesto, infatti è uno dei primi lavori svolti al von Karman Institute (VKI) all'interno della nuova area di ricerca dedicata a sistemi di propulsione innovativi, come per esempio il fan elettrico contro-rotante. Quest'ultimo, sarà il propulsore trattato in questo manoscritto. Il principale scopo di questa tesi sarà quello di valutarne la fattibilità di utilizzo, fornendo anche linee guida per ricerche future.
Per modellare i vari propulsori è stato usato EcosimPro (software commerciale specifico per le modellizzazioni) ed in particolare la libreria turbojet. Come primo step, è stata creata la componente fan contro-rotante. Il suo codice è stato scritto in modo tale da risultare compatibile con le altre componenti presenti nella libreria turbojet, così facendo sarà più facile riutilizzarlo in studi futuri. Come step successivo, a partire da questa componente, differenti fan elettrici contro-rotanti sono stati generati. Ognuno di questi propulsori è stato definito imponendo differenti condizioni al contorno ed in particolare un parametro chiave utilizzato è stato il rapporto delle velocità del fan contro-rotante. Inoltre, verrà svolta una breve comparazione tra le performance di questi motori installati in una configurazione a 2 o 10 motori . Conclusa questa parte, lo step seguente è stato quello di modellare due propulsori di riferimento e per questa tesi sono stati scelti i turbofan CFM56-7B24 e GEnx-1B64.
Questo lavoro si conclude con l'analisi di varie missioni di volo, le quali sono state effettuate con Matlab. Ogni missione analizzata è il risultato di diverse combinazioni di range, propulsori montati sul velivolo e sistema ibrido utilizzato. Tutti questi risultati saranno utili in futuro per definire per quali missioni e con quali configurazioni i motori elettrici contro-rotanti sono più adatti.

Parole chiave: EcosimPro, turbofan, fan elettrici contro-rotanti, propulsione ibrida, analisi di missione di volo.

Contents

1 | Introduction

The aeronautical industry is continuously increasing the gas turbine efficiency [5]. The results are less fuel burned, reduced operating costs and a less evironmental impact both in terms of emitted pollutants and noise. In order to achieve these results, it is essential to consider new engine designs and some of them contain CR turbomachinery components (fans, propellers, compressors, and turbines). These components have certain advantages compared to the corresponding conventional ones. For example, the use of CR shafts reduce the engine gyroscopic moment and since the CR components can achieve high pressure ratios with less stages, the size and weight of the engine (in theory) can be reduced. At the same time, a CR stage can achieve the same pressure ratio of a classic one with decreased rotational speed and this aspect is very important in noise reduction. However, the CR concept found limited applications in the past due to its considerable mechanical complexity. Instead, nowadays the technological improvements achieved with respect the design and hardware implementation have resulted in a revival of the CR machines.

For this reason, VKI dedicated a new research area to them. In this thesis the CR fans will be at first designed and analyzed in design and off-design and then implemented in an hybrid system in order to perform a flight mission analysis. The hybrid systems considered are two: turbo-electric and hybrid-electric. Instead, the flight mission ranges considered are three: short range, medium range and long range. In EcosimPro the CR fan component was created and used to built the electric CR fan engine schematic. From that schematic different electric CR fan engine models were generated, each one of them modeled considering a different design point condition. The engine schematic is simply the generic representation of the engine. Then, imposing different boundary conditions, it is possible to generate different electric CR fan engines. Some of the data used for the boundary conditions are real, instead others come from reasonable assumptions. The validation of these models was made through the comparison of real data and data obtained through basic relations. Finally, the flight missions can be defined considering the all possible combinations between: flight mission range, hybrid system and electric CR fan engine. These missions can be simulated through Matlab and the results obtained com-

pared to the two reference cases, which were performed using the turbofans CFM56-7B24 and GEnx-1B64.

1.1. Thesis contribution

This thesis will be used as a reference for future researches about electric CR machines at the VKI, therefore its contributions are different and they can be summarized in the following points:

- provide guidelines on how perform engine designs and off-design simulations in EcosimPro;
- provide the models in EcosimPro of two of the most common turbofans in civil aviation: the CFM56-7B24 and the GEnx-1B64. The former used for short and medium range missions and the latter used for long range missions. These models can be used as references also for other researches;
- provide the CR fan component and the electric CR fan engine schematic in EcosimPro. In this way, simply by modifying the schematic boundary conditions, it will be possible to obtain and test different engine models;
- provide different electric CR fan engine models. The values obtained will be used as initial guesses for more complete designs;
- the final contribution comes from the flight mission analysis. The results obtained will give some indications about which hybrid propulsive system use depending on the flight mission.

Since this thesis is the starting point of a more complex research about CR fans, all the results obtained are preliminary results. These results are intended to be used as baselines for future studies.

1.2. Thesis structure

The thesis is organized as follows. In Chapter 2 the theoretical background needed to go through this thesis will be presented. This is a review about CR machines, turbofan engines and hybrid systems. In this chapter will be also presented the models used for the atmosphere and the aircraft. In Chapter 3, EcosimPro and the turbojet library will be explained. Moreover, the compressor, fan and turbine components will be described in order to understand better how the CR fan component was coded. In Chapter 4 the

design and off-design analysis of the two reference turbofans will be presented. Chapter 5 is analogous to Chapter 4, but in this case the engines analyzed are the electric CR fans. Note that these engines will be subdivided at first depending on the mission range. The engines designed for short and medium range missions will be identified by the initials "HYB-CF1", instead the ones designed for long range missions will be identified by the initials "HYB-CF2". Then, they will be subdivided depending if they will be mounted in a classic configuration (2 engines) or in a distributed configuration (10 engines). The formers will be identified by the initials "2eng", instead the latters by the initials "10eng". The last subdivision depends for which values of speed ratio and power ratio the electric CR fan engines will be designed. Depending on the values of these two parameters, the engines will be identified by the initials "DPref" or "DP1" or "DP2" or "DP3" or "DP4". In Chapter 6 all the data used in the flight mission analysis will be presented. Finally, in Chapter 7 the flight mission analysis results will be showed.

2 | Theoretical Background

2.1. Turbomachinery overview

The economy around the gas turbines is in the order of magnitude of billions of dollars each year and this business is expected to continuosly grow in the next future [7]. The gas turbine industry is characterized by internationality, competitivity and high tecnhology. These three aspects are strictly connected each other in fact, even if the working principle of a turbomachine is simple, these are machines very complex from both an aerodynamic and a mechanical point of view. Therefore, it means that for the design and production of a single gas turbine a lot of different competences are required. In general these machines produce power in the order of MW, hence a small increase in the machine efficiency means a significant increase in power. Unfortunately, not always a tecnhological improvement is positive, because the life cycle cost can't increase too much.
The gas turbines have the great advantage to be light and small in size with respect the power that they can produce, this is why these machines are widely used in air, sea and land applications.

The schematic of a gas turbine engine is extremely simple [6], in fact it is composed by:

- compressor, in which the air is compressed. Its role is to create the necessary condition for the fuel combustion in the combustion chamber;
- combustion chamber, in which the fuel is trasformed in heat;
- turbine, in which the gas coming from the combustion chamber is expanded. Its role is to extract power form the gas flow and so transfer mechanical power to the compressor.

From a theoretical thermodynamic point of view, the gas turbines can be considered continuous and internal combustion engines based on the open Joule-Brayton cycle (Figure 2.1). The ideal cycle is characterized by four different thermodynamic processes:

1. isentropic compression;

2. isobar combustion;
3. isentropic expansion;
4. heat rejection.

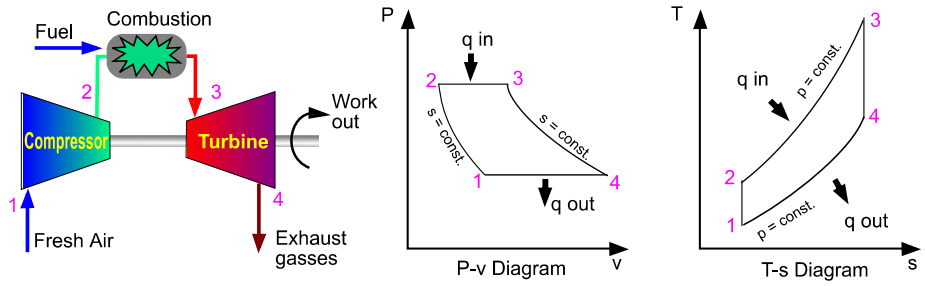

Figure 2.1: Ideal cycle Joule-Brayton [37].

The two main components of a gas turbine engine are the compressor and the turbine, which are turbomachines. By definition [32], a turbomachine is a machine that exchanges mechanical work with continuous working fluid and they can be subdivided in two main categories:

- work-absorbing turbomachines, that absorb mechanical power from the shaft and they transfer it to the working fluid. Some examples of that kind of turbomachines are compressors and pumps;
- work-producing turbomachines, that extract work from the working fluid and they transform it in mechanical power. The typical example are the turbines.

Moreover, the turbomachines can be classified depending also on the meridional flow path. In fact, it is possible to define:

- axial turbomachines, in which the meridional flow path is parallel with respect the axis of rotation;
- radial turbomachines, in which the meridional flow path is perpendicular with respect the axis of rotation.

Both compressors and turbines can be axial or radial.
The last major classification regards the working fluid, which can be compressible or incompressible:

- compressible turbomachines, in which the fluid changes the density during the path;

- incompressible turbomachines, in which the fluid density is considered constant. Usually this approximation is valid for fluid or when the gas velocity is $M \leq 0.3$.

This thesis deals with axial turbomachines, in particular compressors, ducted fans, ducted CR fans and turbines. All the computations at engine level were done using EcosimPro and in this case the working fluid is the air, which was considered compressible and subsonic.

2.1.1. Axial compressor

Considering the propulsion systems for civil aviation, one of most used work-absorbing turbomachine is the axial compressor (Figure 2.2). During the years, this solution was preferred instead of the radial compressor, because has several advantages [12]. First of all, an axial machine is able to process an higher volumetric flow rate or, in other words, considering the same volumetric flow rate, the frontal area is less. Hence, the engine drag is reduced. Another advantage is that, thanks to the technological improvements in the last decades, an axial compressor is more efficient with respect a radial one. Of course axial compressors have also drawbacks, like a lower increment of pressure for single stage and a poor rangeability.

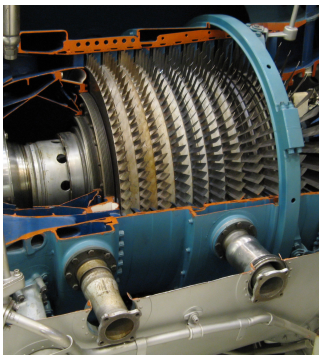

Figure 2.2: View of an axial HP compressor in a Pratt & Whitney TF30 turbofan engine.

A typical axial compressor performance map is the one reported in Figure 2.3. In this case the map is dimensional, because in the x-axis there is the mass flow rate and the iso-speed lines are defined as % of the nominal rotational speed.

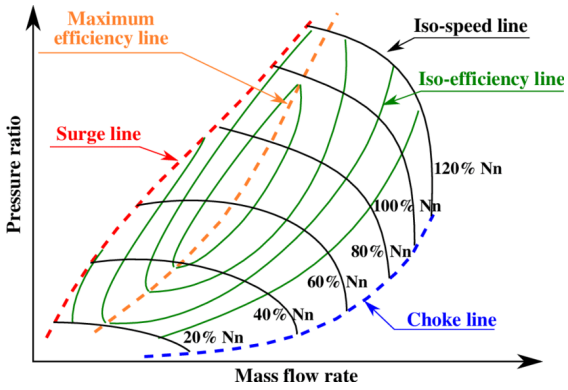

Figure 2.3: Typical operating curve for an axial compressor [40].

The variables are:

- pressure ratio $\rightarrow \beta_c = \frac{p_{T_{out}}}{p_{T_{in}}}$;
- mass flow rate $\rightarrow \dot{m} = \rho A V$.

It is important to note that usually the operating curves are given in terms of dimensionless or reduced quantities. These quantities are very useful, because they allow to use the concept of similariry and so the same performance map can be used for describing the performance of compressors that are similar each other. A better description of a compressor performance map, in terms of reduced quantities, will be done in the next chapters. The two most important lines are the surge line and the chocke line. The former is a limit at low flow rate due to operating instability, instead the latter is a limit at high flow rate due to supersonic mach number.

A conventional axial compressor stage is composed of two blade rows [32]: a rotating part called rotor and a fixed part called stator. The rotor provides energy to the fluid increasing its total pressure. The stator does not provide energy to the fluid. Its role is to convert kinetic energy into static pressure. In order to understand the energy conversion process, the Euler work equation and the rotor-stator velocity triangle will be described.

Euler work

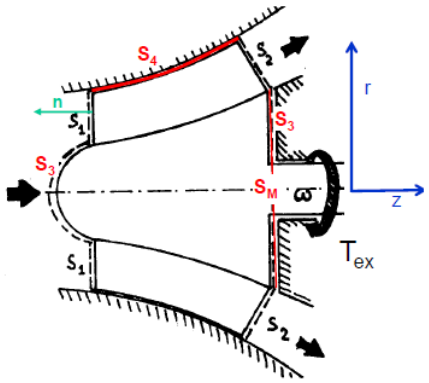

Figure 2.4: Control volume used to demostrate the Euler work [12].

To demostrate the Euler work [12] is possible to start from the momentum definition, that is:

$$\vec{q} = m \cdot \vec{V}. \tag{2.1}$$

Then, $\vec{r}$ can be defined as the distance between the axis z and the point of the momentum application (Figure 2.4). The vector product between $\vec{q}$ and $\vec{r}$ is defined as angular momentum:

$$\vec{M} = \vec{r} \times \vec{q}. \tag{2.2}$$

Substituting Equation (2.1) into Equation (2.2) and then computing the total derivative of $\vec{M}$ projected in direction z, that is called M_z, it is possible to define the torque (T) applied to the system "turbomachine". The resulting expression is:

$$T = \frac{DM_z}{Dt} = \frac{\partial M_z}{\partial t} + \int_S \vec{r} \times \rho \vec{V}(\vec{V} \cdot \vec{n}) \, \mathrm{d}S = \int_S \vec{r} \times \vec{\sigma}_n \, \mathrm{d}S + \int_\Omega \vec{r} \times \vec{f} \, \mathrm{d}\Omega + T_{ex}, \tag{2.3}$$

with S that is the control volume (c.v.) surface, Ω the c.v. volume and T_{ex} the external torque applied to the shaft. Referring to Figure 2.4, the following hypothesis can be made:

- $S = S_1 + S_2 + S_3 + S_4 + S_n$;
- $\frac{\partial}{\partial t} = 0$, steady state;
- S_3 and S_4, no flow rate.

Then, it is possible to rewrite the terms in Equation (2.3) as following:

- $\begin{cases} \vec{r} \times \rho \vec{V} = r \rho V_t \\ \vec{V} \cdot \vec{n} = V_n \end{cases} \longrightarrow \int_S \vec{r} \times \rho \vec{V}(\vec{V} \cdot \vec{n}) \, \mathrm{d}S = \int_S r \rho V_t V_n \, \mathrm{d}S.$

Moreover, this last expression can be rewritten as a term average in time plus a term due to turbulence. The latter can be neglected. Therefore, the resulting expression is:

$$\int_S r\rho V_t V_n \, \mathrm{d}S = \int_S r \, \overline{\rho V_t V_n} \, \mathrm{d}S + \cancel{T_{turb}} = \int_{S_2} r \, \overline{V_t \, \mathrm{d}\dot{m}} - \int_{S_1} r \, \overline{V_t \, \mathrm{d}\dot{m}};$$

- $\frac{\partial M_z}{\partial t} = 0$;
- $\int_\Omega \vec{r} \times \vec{f} \, \mathrm{d}\Omega = 0$, because there is no weight contribution in the torque;
- $\int_S \vec{r} \times \vec{\sigma}_n \, \mathrm{d}S = T_\tau$, that is a torque that acts always against the rotational speed. It is due to friction.

Substituting them into Equation (2.3) the result is:

$$\int_{S_2} r \, \overline{V_t \, \mathrm{d}\dot{m}} - \int_{S_1} r \, \overline{V_t \, \mathrm{d}\dot{m}} - T_\tau = T_{ex}. \tag{2.4}$$

Finally, considering mean values over the c.v. surface, from Equation (2.4) is possible to obtain the power balance:

$$\omega \, \overline{\overline{r_2 V_{2t}} \, \dot{m}} - \omega \, \overline{\overline{r_1 V_{1t}} \, \dot{m}} - \overline{P_\tau} = \overline{P_{ex}}, \tag{2.5}$$

And dividing for $\dot{m}$, the work balance can be obtained:

$$\omega \, \overline{\overline{r_2 V_{2t}}} - \omega \, \overline{\overline{r_1 V_{1t}}} - \overline{L_\tau} = \overline{L_{ex}}. \tag{2.6}$$

Considering an ideal case, and so $\overline{L_\tau} = 0$, remembering that the rotor peripheal speed U is defined as $U = \omega \, r$ and simplifying the notation, the Euler work equation can be written as:

$$L_{Eul} = U_2 V_{2t} - U_1 V_{1t}. \tag{2.7}$$

This equation describes the work exchanged between blades and fluid and in this case is defined as $[\frac{\mathrm{J}}{\mathrm{kg}}]$. It is important to note that $L_{Eul} > 0$ means that the fluid energy is increasing, therefore this is the case of a compressor. The opposite is for turbines. Equation (2.7) confirms also what was written before about rotor and stator. In a stator $U_2 = U_1 = 0$ and so it can't exchange energy with the fluid.

Velocity triangle

In a stream that is adiabatic, through the energy conservation the total entalphy (h_t) can be defined as [12]:

$$h_t = h + \frac{V^2}{2}. \tag{2.8}$$

In this expression h is the static enthaply and V is the absolute velocity. V is composed of three terms: axial (V_z), tangential (V_t) and radial (V_r). These are defined according to the cylindrical system of coordinates in Figure 2.5.

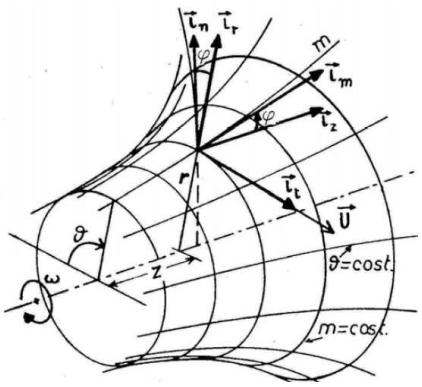

Figure 2.5: Axial turbomachine: cylindrical coordinate [12]. The velocity vector is defined as $\vec{V} = V_r\ \vec{i_r} + V_t\ \vec{i_t} + V_z\ \vec{i_z}$.

It is immediate to note that:

- V_z is associated to the mass flow, so for continuity $V_z = cost.$;
- V_n is associated to the radial equilibrium, hence it will be not considered;
- V_t is associated to the Euler work, so in a compressor rotor stage this velocity increases because the fluid energy is increasing.

Using the enthalpy definition $h = C_p\ T$ and after some passages, the Equation (2.8) can be rewritten in terms of total temperature:

$$T_t = T + \frac{V^2}{2C_p}. \tag{2.9}$$

If the process is also isoentropic, starting from Equation (2.9) it is possible to define also the total pressure:

$$P_t = P\left(\frac{T_t}{T}\right)^{\frac{\gamma}{\gamma-1}}. \tag{2.10}$$

These passages show that the total quantities are composed by a static and a dynamic

contribution and, in an ideal case, only rotor components can change these quantities because they can vary the fluid energy. Stator components can only increase pressure while reducing velocity or viceversa, they can't change the energy system.

The detailed velocity triangles in an axial compressor stage are illustrated in Figure 2.6.

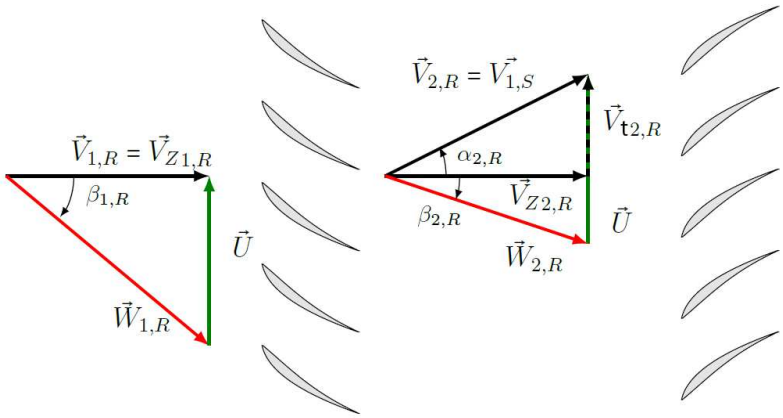

Figure 2.6: Axial compressor: Rotor-Stator stage [32].

In Figure 2.6 the subscript R is for the rotor and S for the stator, meanwhile the subscript 1 is for the component inlet and 2 for the component outlet [32]. For simplicity, the fluid enters the rotor axially with an absolute inlet velocity $\vec{V}_{1,R}$. Subtracting vectorially the blade speed $\vec{U}$ gives the inlet relative velocity $\vec{W}_{1,R}$ at angle $\beta_{1,R}$. Note that $\vec{W}_{1,R}$ is almost parallel to the rotor blade angle at their leading edge at design condition. While passing through the rotor, the flow is turned to the direction $\beta_{2,R}$ at outlet with a relative velocity $\vec{W}_{2,R}$. This turning $\Delta\beta$ can be reflected by the increase of the tangential velocity of the fluid ΔV_t and so to energy transfer from the rotor to the fluid. On the other hand, the fluid approaches the stator with an absolute velocity $\vec{V}_{1,S} = \vec{V}_{2,R}$, by adding vectorially the blade speed $\vec{U}$ to $\vec{W}_{2,R}$ at outlet of the rotor. When passing through the stator, the flow is diffused and deflected towards the axis and gets an outlet velocity $\vec{V}_{2,S}$. The work is 0 and static pressure is recovered.

2.1.2. Counter-rotating fan

A CR fan consists of two counter-rotating rotors [32], called respectively front rotor (FR) and rear rotor (RR). Each of them is located on its shaft and there is no stator in between. An example is reported in Figure 2.7.

Figure 2.7: Safran open rotor model, 2017

From Figure 2.8, it can be seen that the relative velocity at the inlet of the RR ($\vec{W}_{1,RR}$) is bigger then the previous case of a classic stage. This is due to the counter rotation and so to the vectorial sum $\vec{U}_{FR} + \vec{U}_{RR}$. Then, the air enters in the RR that not only recovers the static pressure, but also supplies energy to the working fluid. From a first comparison between the classic axial compressor stage and a CR fan emerges that CR fans can be very useful. In fact, both in the FR and RR the gas energy is increased. These machines have the potential to be better with respect the classic ones, but unfortunately present also some problems. A literature review about this topic will be made in the following lines.

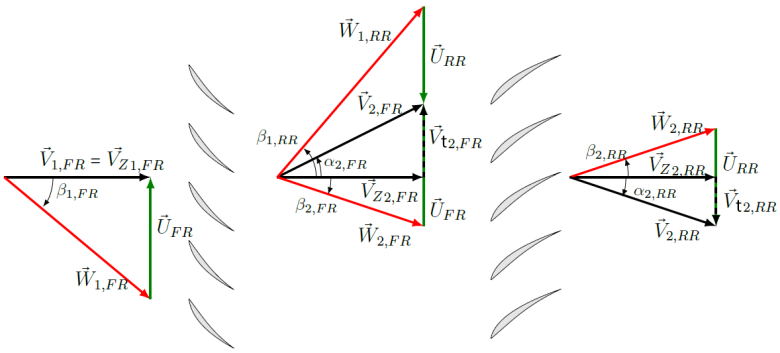

Figure 2.8: Counter-rotating fan: counter Rotor-Rotor stage [32]

A brief literature review

One of the first researches about the counter-rotating machines was done by Leslec [18], that tried to find out the condition of max thrust in the case of two CR propellers. He tested also tandem air propellers [19] and he demostrated that, at the same rotational speed, with a smaller diameter, lower tip speed and greater efficiency, a noise reduction is possible. Two years later, Lesley tested the tandem configuration with three blades per propeller [20]. He pointed out that the tandem propellers had 2 to 15 % greater maximum

efficiency than the single six blade propeller. After that, several reasearches were done about CR machines. Some of them estimated that with the use of ducted or unducted CR fans is possible to save fuel up to 35%. Schimming [26] conducted several experiments on the CR shrouded fan, demonstrating that these propulsors are a valid alternative for high bypass engines. In fact, because of the swirl-free exit flow, they have an higher efficiency compared to the classic propulsors. The problem, in particular for open rotor CR fans, is the high level of noise produced by this configuration. Others relevant reasearches are the ones done by Young [39] and Wilcox [38], that in the 1950s proposed a CR configuration for compression in order to achieve an higher pressure rise. Then, Sharma et al. [29] [28] and Roy et al. [24] explored through experimental works the benefits of a CR fan concept for low pressure configuration. Also Newton [22], Saunder and Glassman [25] studied this concept and they recognized its potential to significantly reduce fuel consumption in high-bypass engines. In general, a lot of researches are about parameter influence in CR machines. For example, in 1996 Sharma et al. [3] presented a review of the aerodynamic and aeroacustic aspect of performance of a ducted single stage CR axial flow compressor. In that paper were also discussed the effects of some parameters:

- speed ratio, defined as front rotor velocity over rear rotor velocity;
- hun-tip ratio;
- inlet flow distorsion;
- casing treatment.

What was demonstrated is that an increase in the speed ratio provides an improvement in aerodynamic performance, but the aeroacoustic performance is deteriorated. Fortunally, a trade-off between aerodynamic and aeroacoustic performance can be made by selecting a suitable axial gap. Moreover, an increase in the hub-tip ratio is also found to improve the aerodynamic performance of a CR stage and the stall flow margin shows a considerable improvement. Sharma et al. found difficulties in defining the Reynolds number, as the relative flow velocities for the rotors are significantly different. Another important research was done by Shigemitsu et al. [30] that, by both experiments and numerical simulations, investigated the influence of blade row distance on the static pressure and velocity field of small-size CR axial fans. From static pressure rise curves, they noticed that the static pressure was almost constant as the axial spacing was < 30 [mm], but decreased for higher values of axial spacing. It could be concluded that there is a limit axial distance, beyond which the performance deteriorates. The last presented result is the one of Minstry et Pradeep [21], who found that a higher rotational speed in the rear rotor could improve the overall machine operating range and efficiency.

2.2. Low specific fuel consumption aircraft engine: Turbofan

In aviation a key design driver is the fuel economy, both for an economic and environmental point of view [7]. In fact, the fuel weight at take-off can reach up to 40% of the total aircraft weight. In order to reduce the engine fuel consumption, it is important that the engine has a very low SFC. Engines with very low SFC are: turbofans, turboprops and unducted fans. These machines are designed with high turbine entry temperature (TET) and β_c to achieve high thermal efficiency and with high bypass ratio (BPR) to achieve high propulsive efficiency. The main engine thermodynamic parmaters are:

- TET;
- β_c;
- BPR;
- $\dot{m}$.

Each one of these cycle parameters brings benefits and design challenges (often conflicting) requiring compromises. Their selection depends on the mission requirements, the technology maturity and the technology strenghts of the manufacturer/s. In the following lines will be presented an explanation of why turbofans are so used in civil aviation [11].

Two important requirements of an aeroengine are: small weight/size and low fuel consumption. Unfortunately, these two requirements are in conflict. For example a military engine is light and small in size, but will be costly in terms of fuel consumption. The opposite applies for civil engines. In a thermodynamic sense the parameter that is associated to the fuel economy is the specific fuel consumption (SFC):

$$SFC = \frac{\dot{m}_f}{T_h}.$$

Instead, the one associated to the size of the engine is the specific thrust (I_a):

$$I_a = \frac{T_h}{\dot{m}}.$$

The meaning of the SFC is straightforward: at fixed T_h a low value of SFC means a low value of $\dot{m}_f$. The I_a is the value of T_h per unit of $\dot{m}$, so an higher value of I_a means a low value of $\dot{m}$. Usually a low $\dot{m}$ is associated to small engines. Other key engine parameters are the thermal efficiency (η_{th}), β_c and the turbomachine component isentropic efficiency

(η_{is}). The two parameters that describe the aeroengine heat conversion, from fuel to useful work, are I_a and η_{th}. The latter is defined as the amount of useful work delivered per unit of heat input supplied and its definition is:

$$\eta_{th} = \frac{P_u}{\dot{m}_f \cdot LHV}.$$

The max value of TET sets the amount of energy that can be added in compression and heating. This value is determined by the max temperature that the turbine blades can substain. Typically, high compression with modest heat addition will yield a high efficiency gas turbine of a larger size, while modest compression with a large amount of heat addition will deliver a smaller but less efficient engine (Figure 2.9). The losses are quantified by the η_{is}.

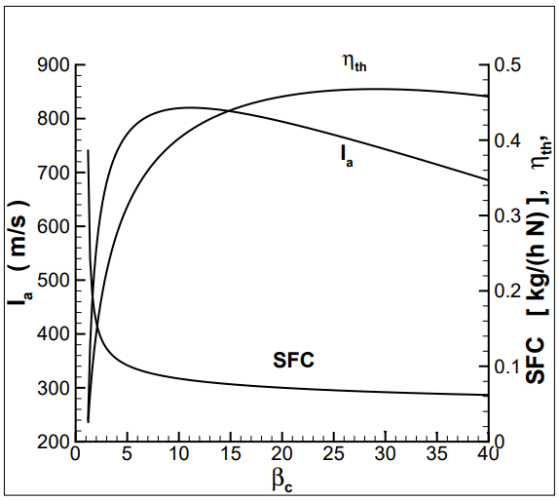

Figure 2.9: Effect of β_c on SFC, η_{th} and I_a. It is possible to observe that SFC and η_{th} are linked each other, instead I_a has a different trend [11].

The useful work of a jet engine is delivered through thrust, that in the case of a single exhaust can be written as:

$$T_h = \dot{m}(V_{exit} - V_0) + A_{exit}(P_{exit} - P_{atm}),$$

With V_{exit} that is the nozzle exit velocity, V_0 the flight velocity, A_{exit} the nozzle exit area, P_{exit} the static pressure at nozzle exit and P_{atm} the ambient pressure. When producing thrust, not all the kinetic energy available in the high pressure gas is transformed in thrust, some of it is lost. The fraction of kinetic energy converted into thrust is called

propulsive efficiency (η_{prop}). The overall engine efficiency for a jet engine is simple:

$$\eta_{tot} = \eta_{th} \cdot \eta_{prop}.$$

After some passages, the following result can be obtained:

$$SFC \propto \frac{1}{\eta_{tot}} = \frac{1}{\eta_{th} \cdot \eta_{prop}}.$$

The easy conclusion is that in order to increase SFC is possible to increase both η_{th} and η_{prop}. To increase η_{prop} an aircreaft engine can be designed with a second stream that enables jet engines designs with lower exhaust jet velocities. This second stream is called: bypass stream. The ratio between the bypass stream ($\dot{m}_2$) and the core stream ($\dot{m}_1$) is the BPR:

$$BPR = \frac{\dot{m}_2}{\dot{m}_1}.$$

The classic bypass engine is the turbofan.

Now should be more clear why in civil aviation the turbofan is a very common engine. In this thesis the reference engines will be the CFM56-7B24 and the GEnx-1B64, that are two of the most used turbofans.

2.3. Hybrid aircraft propulsive systems

The increasing environmental regulations in terms of pollutant emissions in the air transport, moved the elctric propulsion systems into the focus of aviation research [15]. Some small aircrafts are already equipped with electric power systems, but there is still a lot of work to do for higher power class aircrafts.

2.3.1. Hybrid configurations

This manuscript is about electric CR fans. In order to test their performances during a flight mission, different hybrid propulsion systems can be considered [15]: the turbo-electric power controlled (tu-el pc), the turbo-electric direct (tu-el dir), the hybrid-electric serial (hy-el se) and the pure electric (p-e). These configurations are represented in Figure 2.10.

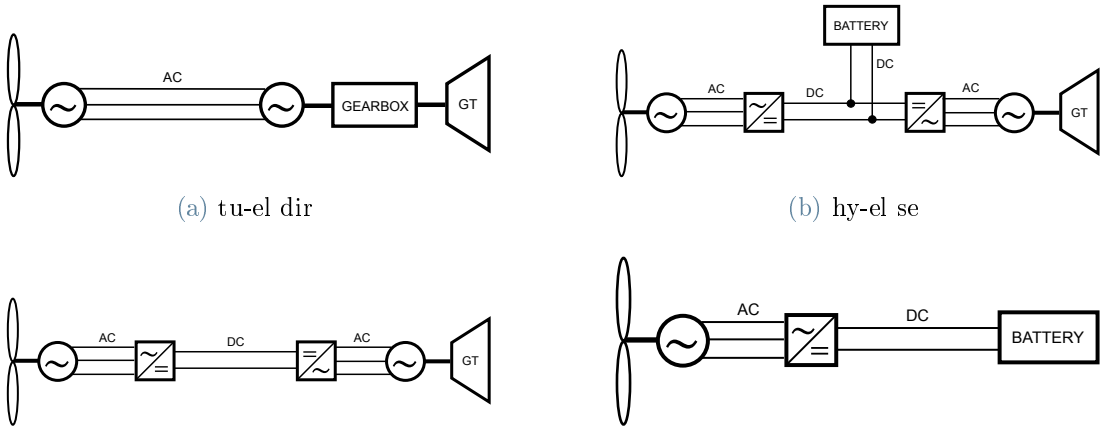

(a) tu-el dir

(b) hy-el se

(c) tu-el pc

(d) p-e

Figure 2.10: Hybrid propulsion systems.

In the turbo-electric concept, only the turbogas generator (GT) provides energy to the system. In this concept only a large GT is present, because generally a larger GT is more efficient with respect a smaller one. The main disadvantage with this configuration, is the loss of redundancy. It is possible to think to two variations of turbo-electric propulsion system:

- tu-el pc (Figure 2.10c). In this case, between the GT and the electric motor, a DC/AC and a AC/DC converter are present. For simplicity, from now on in this thesis the DC/AC and the AC/DC will be considered generically power electronics. In fact, in this work there isn't a detailed model of the electric system and so these two devices are considered just devices that controls the electric power. The role of the power electronics is to first convert the current from AC, the one that comes from the GT, in high voltage DC in order to reduce the losses. Then, to convert it back to the right value of voltage and frequency to drive the electric motor, which usually is in AC. In this way the gearbox is not necessary;
- tu-el dir (Figure 2.10a). In this case there isn't the power electronics, in fact the generated electricity is conducted without any conversion to the motor. That causes a direct link between the rotational speed of the power turbine and the propulsion system. In order to match the different requests of rotational speed, a gearbox between the GT and the electric generator is necessary.

The hybrid-electric concept instead, uses energy from both the GT and the battery. The main advantage is that during the different flight phases, the total power can be balanced between these two sources in order to optimize the global energy consumption. The major

limitation is the battery specific energy (SE $[\frac{J}{kg}]$) and power (SP $[\frac{W}{kg}]$), hence the battery weight. In the case of the hy-el se propulsion system (Figure 2.10b), the GT and the electric propulsion are decoupled. This layout comprises an electric generator and an electric motor that works in AC. Since the batteries work only in DC, the presence of the power electronics is necessary. The decoupling between the two power sources permits to have a large flexibility in the power management. In fact, during the different phases of a flight mission, the power can come only from the battery or only from the GT or could be a trade-off between the two.
The last possible concept is the p-e. This is the simplest layout, in fact there is a battery that supplies electric power to the electric motor. In between there is the power electronics. The global efficiency of this system is very high, but unfortunately the battery technology is not mature enough. As reported in [14], for an use in civil aviation the battery specific energy should be greater than 800 $[\frac{Wh}{kg}]$, which is about four times the actual value.

The main focus of this manuscript is on electric CR fans, which will be considered also in a distributed configuration. The layout considered will be:

- tu-el pc, because the main idea is to have a GT well designed around a specific design point. Then, the power electronics adapt the voltage and frequency values in order to match with the ones required by the CR fans. In particular, in the distributed propulsion case, the power electronics is necessary to adapt the right power parameters for each engine;
- hy-el se, which is similar to tu-el pc, but in this case there is another degree of freedom due to the battery presence.

Tu-el dir and p-e concept will be not considered, because the former has too less flexibility and the latter has a not ready techological level.

2.3.2. Electric components

As suggested by Trainelli et al. [31], from a system analysis point of view the electric components can be considered as a "black box" defined by an efficiency and a specific power (or energy). This is a strong semplification, but the main advantage is that the all computation is simple. Even if the results are not extremely precise, they are good enough for a preliminary design.

The electric motors, the electric generator and the power electronics are defined by their efficiency and SP, from which it is possible to compute the component weight. Only the battery has an additional parameter, which is the SE. The battery weight is obtained as

the larger between the one obtained by the SP and the one obtained by the SE.

2.4. Flight mission analysis

One of the main focus of this thesis will be the comparison between a reference flight mission, performed by a standard civil aircraft propelled by a turbofan, and the same flight mission with the same aircraft, but with a different propulsive system. In order to do that, it is essential to have a mathematical model for the engines, for the atmosphere and for the aircraft. The engine models will be discussed later, now the atmosphere and the aircraft model are presented.

2.4.1. Atmosphere model

The atmosphere is the medium in which the aircraft moves, this is why it is important to choose the correct model [1]. The atmosphere is a not homogeneous mixture of different gasses and small particles, that are present in different level of concentration. This concentration vary with location, altitude, season and also from day to night. The interaction between the aircraft and all these variables generates different forces, but it is impossible to take in account everything. Therefore, in the past, the scientists defined the International Atmosphere Model (ISA), that is a static atmospheric model in which pressure, temperature, density and viscosity change over the altitude. The variations of these variables are computed starting from their values in standard condition, that are: $P_0 = 101325$ [Pa], $\rho_0 = 1.225$ $[\frac{\text{kg}}{\text{m}^3}]$ and $T_0 = 288$ [K]. The air is considered a perfect gas under the effect of the gravitaitonal force. The main atmosphere regions defined in this model are:

- troposphere, is the region between 0 to 11 [km] of altitude;
- stratosphere; is the region above 11 [km] of altitude;
- high atmosphere, is the region between 50 to 100 [km] of altitude.

In this thesis all the flight missions are performed below 12 [km], so the models of troposphere and stratosphere were used.

The perfect gas equation is a relation that links the pressure (P), the temperature (T) and the density (ρ) through the universal gas constant for the air (R). Its expression is:

$$P = \rho R T. \tag{2.11}$$

The pressure varies with the altitude and its variation is described by the following relation:

$$\mathrm{d}P = -\rho g \ \mathrm{d}\hat{z}, \tag{2.12}$$

instead, the temperature variation with the altitude is described by a linear relation:

$$T(z) = T_0 + T_z \ z = 288 - 0.0065 \ z. \tag{2.13}$$

Then, combining Equations (2.11), (2.12) and (2.13), it is possible to obtain:

$$\frac{\mathrm{d}P}{P} = -\frac{g \ \mathrm{d}\hat{z}}{R \ T(z)}, \tag{2.14}$$

and integrating Equation (2.14) between the generic altitude z and 0 the result is:

$$ln\frac{P}{P_0} = -\frac{g}{R}\int_0^z \frac{\mathrm{d}\hat{z}}{T(z)} = \frac{g}{R \ T_z} \ln\left(1 + \frac{T_z}{T_0} z\right), \tag{2.15}$$

from which the relation of the pressure variation with altitude can be written:

$$P = P_0\left(1 + \frac{T_z}{T_0} z\right)^{-\frac{g}{R \ T_z}}. \tag{2.16}$$

Finally, ρ can be computed from Equation (2.11).

In the stratosphere the relations are simpler, because the T is constant with the altitude:

$$T(z) = T = cost. \tag{2.17}$$

The pressure at the generic altitude $z > 11000$ [m] can be computed combining Equations (2.17) and (2.12) and integrating from 11000 [m] and z:

$$\ln \frac{P}{P_{11000}} = -\frac{g}{R \ T}(z - 11000) \tag{2.18}$$

and so

$$P = P_{11000} \ e^{-\frac{g}{R \ T}(z - 11000)}. \tag{2.19}$$

As before, ρ can be computed through Equation (2.11).

2.4.2. Aircraft model: Point mass approach

In order to perform the flight mission analysis, an aircraft model has to be defined. The scope of this thesis is to obtain some initial results that can be used as initial guesses for future and more detailed researches. Therefore, in this case is better to use a simple model.

The model used for the aircraft is the point mass [1]. All the aircraft mass is concentrated in the centre of gravity and the only forces considered are: thrust (T_h), drag (D), lift (L), weight ($\hat{W}$) and inertial forces. The considered frame of reference is the body frame of reference. The origin is the centre of gravitiy and the axis are: roll axis ($\vec{b_1}$), pitch axis ($\vec{b_2}$) and the yaw axis ($\vec{b_3}$). The frame of reference scheme and the forces scheme are reported respectively in Figures 2.11a and 2.11b.

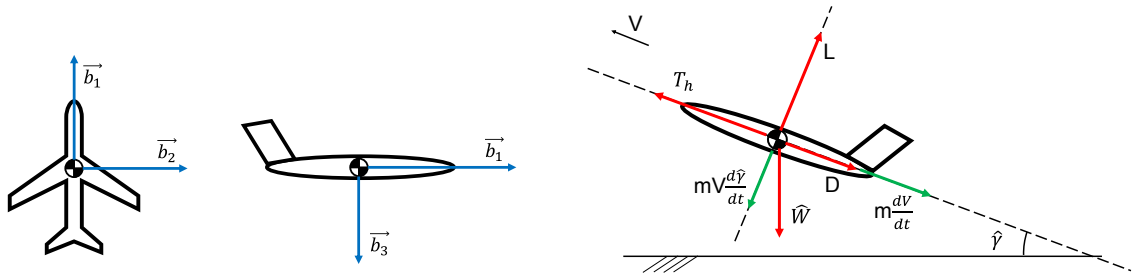

(a) Body frame of reference (b) Scheme of forces

Figure 2.11: Aircraft model.

The general equation of motions can be written from the force equilibrium:

$$\begin{cases} T_h - D - \hat{W}\sin(\hat{\gamma}) = m\dfrac{\mathrm{d}V}{\mathrm{d}t}, \\ L - \hat{W}\cos(\hat{\gamma}) = mV\dfrac{\mathrm{d}\hat{\gamma}}{\mathrm{d}t}. \end{cases} \tag{2.20}$$

In Equations (2.20) the value of T_h is computed using EcosimPro, while the values of L and D are computed using the linear aerodynamic model, so respectively:

$$L = \frac{1}{2}\rho V^2 S C_L, \tag{2.21}$$

$$D = \frac{1}{2}\rho V^2 S C_D. \tag{2.22}$$

It is important to note that the angle of attack was considered negligible.
Moreover, in order to simplify the matlab code, the rate of climb (RC) was considered

constant:

$$RC = V \sin(\hat{\gamma}) = cost. \tag{2.23}$$

3 | EcosimPro

In this chapter will be presented at first a description about EcosimPro, then a description about the turbomachine components that are inside the turbojet library and in the end a presentation about the new component CR fan. EcosimPro has an important role in this work, since all the engines analyzed were modeled using it. This software is used by industries and also by ESA, which developed their own library called ESPSS that is very useful for modelling rocket and satellite propulsion systems. EcosimPro is used for system analysis and this is the reason why it was chosen for this thesis.

3.1. Software introduction

EcosimPro is an object-oriented multidisciplinary simulation platform [2] [16]. In EcosimPro user manual, a more precise definition is given:

> "EcosimPro is a simulation tool with a user-friendly environment (...) for modelling simple and complex physical processes that can be expressed in terms of differential-algebraic equations or ordinary-differential equations and discrete events".

The physical components are modeled using the EcosimPro language (EL), which is similar to a standard modelling language, but flexible enough to model continuos and discrete processes. Inside the software are already present different libraries (hydraulic, turbojet, etc...) which contain different components. These components can be used to model new systems, to model new components or they can be modified in order to obtain more realistic components. Two or more components can be connected via ports, from which set of variables can be exchanged. A brief description of the principal aspects of EcosimPro will be done in the following paragraphs. In Figure 3.1 are indicated the main EcosimPro interface areas.

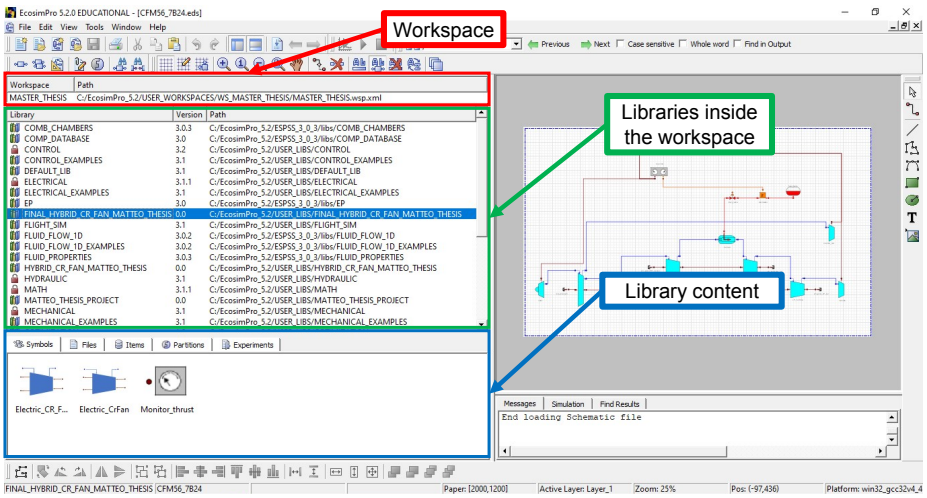

Figure 3.1: EcosimPro interface.

Workspaces and libraries

The workspace contains a set of libraries related to the specific simulation environment that the user is working with [2]. It is possible to create a personal simulation environment, hence a personal workspace. The workspace created for this thesis is called "*MASTER_THESIS*" and it is visible in the red box of Figure 3.1. Inside the green box of Figure 3.1 are present all the libraries contained in the selected workspace. A library can be defined as a collection of components related to a specific simulation environment (example: thermal, turbojet, etc...). The library created for this thesis is called "FINAL_HYBRID_CR_FAN_MATTEO_THESIS". Also ports and partitions are included inside the library. The library content is represented by the blue box in Figure 3.1.

Textual and graphical modelling

There are two methods to model a new component:

- the first method consists in code a new component using the EL. The code can be done from scratch or starting from the code of an existing component. One of the powerful thing of this method is the possibility to re-use the code. In fact a new component can inherit the codes of other components. Thanks to this characteristic, it is very useful to define the so called "abstract components" when a new family of components has to be designed. A better explanation of this concept, will be given in the Sub-section 3.2.1;
- the second method consists in built a new graphical model called schematics. When

two or more components are connected each other through their ports they form a schematic, which can be identified by a new symbol. At this point, this new schematic is a new component. A simple example could be the connection between a compressor, a burner and a turbine. The resulting schematic can be called turbojet and it can be represented by a new symbol. It is important to note that once a schematic is created, it is not mandatory to define a new symbol. The schematic can be left as a connection of components. This is useful when the user wants to show the layout of a particular system. In this thesis the schematics builted are the ones of the two turbofan reference engines, the CFM56-7B24 (Figure 4.2) and the GEnx-1B64 (Figure 4.15), and the ones of the electric CR fans (Figure 5.2 and 5.11). These schematics will be described respectively in Sections 4.1 , 4.2 , 5.1 and 5.2 .

The component created in this work is the CR fan, that will be well described in Section 3.3.

Create a partition

The mathematical representation of a physical model, under a given set of conditions, is called partition. A single component can have more than one associated partition [2]. A component represents a physical system which is defined by its system of equations [16]. This system, in general, is not mathematically closed and it can include implicit equations and non-linear equation systems. When a partition is created, all the mathematical formulations and functions of each component are embedded inside. A set of differential-algebraic equations is created and a state vector $x(t)$ is obtained from this set. In order to obtain the solution, boundary and initial conditions $x(t_0)$ have to be provided. The set of equations can be written in the form:

$$F(\dot{x}, x, t, u(t)) = 0.$$

Where t is the time and $u(t)$ the control law (if present). In EcosimPro there are two main ways to generate a partition:

- the default partition, which is the one automatically generated by the software. EcosimPro selects the most suitable boundary conditions, the variables that should be used as algebraic in the non-linear system of equations and, only if necessary, the derivative values that should be excluded. This way to generate partitions was never used in this manuscript;

- the custom partion, which does the same thing of the default one, but it has two main advantages. The first one is that the user can choose which variables use as algebraic, which boundary conditions use and which derivatives exclude. Therefore, it is more flexible. The second one is that is possible to create the so called design model. This is a special partition case designed to carry out design calculations. In this case, a specific amount of data is released so it can ben calculated on the basis of additional boundary conditions. If for example is required to compute the exit area of a turbojet nozzle in a certain condition, thanks to this design partition is possible to transform the nozzle area from data to variable and then compute its value.

The custom partition was largely used in this thesis, both for the design of all the engines considered and also to perform the off-design analysis. These partitions are represented in Figure 3.2.

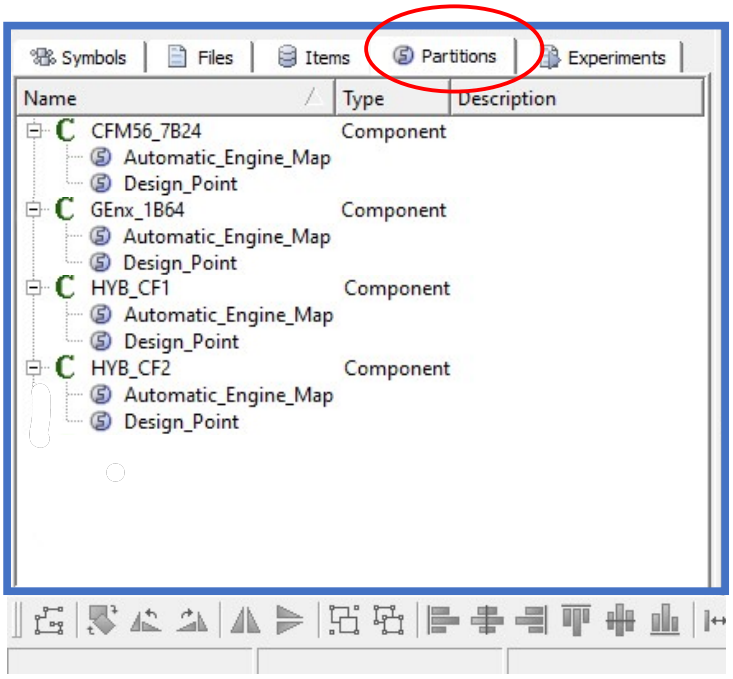

Figure 3.2: For each schematic builted (CFM56-7B24, GEnx-1B64, HYB-CF1 and HYB-CF2), two partitions has been generated: "Automatic_Engine_Map" and "Design_Point". The first one is refererred to the off-design analysis, the second one is referred to the design analysis (i.e. design model partition).

Create an experiment

Once the partition is created, the final step is to configure the simulation and then simulate the model [2]. In EcosimPro the simulation can be generated through the EL or through the experiment wizard, which is a graphical assistant that makes the experiment set up easier. The three major types of calculations are the steady, transient and parametric. The parametric calculation could be both steady and transient. In this thesis the experiments were first set up using the wizard, then transformed in EL and in the end modified with direct coding. The cases considered were steady and steady parametric, in fact the steady case was considered sufficient for this preliminary study.
The all experiments performed for this theisis are reported in Figure 3.3. Note that the experiments performed for each schematic follow the same scheme. As reported in Figure 3.2, for each schematic are present two partitions: design and off-design. For each design model partition is present a single steady experiment (created through wizard) called "Design_Point". For each off-design partition are present two steady parametric experiments: "Engine_Data_Flight_Mission" and "Engine_Data_Flight_Mission_CODE". The first one was created using the wizard command and it was used to generate a baseline EL code. This code was then modified in order to make all the simulation more robust (for more details see Section 4.1). The result is the experiment called "Engine_Data_Flight_Mission_CODE". Hence, the off-design analysis was performed only by using the latter. In the two elctric CR fan schematics (HYB-CF1 and HYB-CF2) the scheme is the same, but two different engines were analyzed: a big electric CR fan engine used in 2 engines configuration and a smaller one used in 10 engines configuration. All these experiments will be discussed in more detail in Chapters 4 and 5.

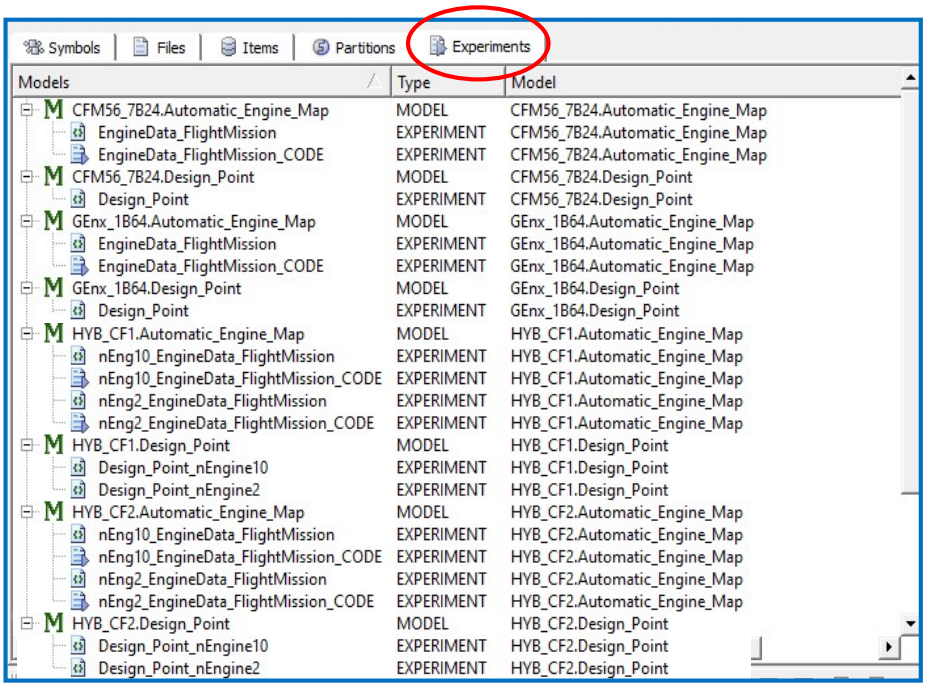

Figure 3.3: Experiments created.

3.2. Turbojet library: Turbomachine components

The most used library in this work is the turbojet library. This library is included in EcosimPro and it contains the most common elements of a turboengine. Moreover, also some examples about turbofans, turbojets with and without afterburner, etc... are present. Here are reported the description of all turbomachine components used and also the explanation of how the new CR fan component was coded.

3.2.1. Compressor

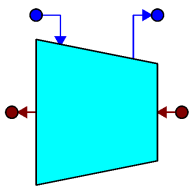

Figure 3.4: EcosimPro component: Compressor

The all compressor characteristics in terms of data, variables and the mathematical model, can be found in the component code and in the component documentation. As written before, each component can inherit the mathematical model (variables, data, equations,

etc...) of other components and/or abstract components. Now, some definitions will be given [2]:

- ports, which are connection points between two or more component. The connection ports are part of the component interface. Each port must have a direction mode, either IN or OUT and different port types should be defined for different kind of connections. Ports are essential for modelling a system in a modular way;
- abstract components, which are coded in the same way of a component, but do not represent any phisical components. It can only be used as a base component for other components. An abstract component can contain only connection ports or it can contain also equations. In the first case any child component will inherit the same ports. In the second case the component will inherit also the equations;
- data, which are simply the component data;
- decls, which are variables that have no connection outside the component and they are normally used only inside the component.

The compressor is a concrete component, in the sense that it represents a physical component. It inherits data and equations from an abstract component called GasTurbo, which inherits data and equations from an abstract component called GasChannel, which inherits data and equations from an abstract component called GasInGasOut. Hence, the compressor inheritance tree is:

$$\text{GasInGasOut} \rightarrow \text{GasChannel} \rightarrow \text{GasTurbo} \rightarrow \text{Compressor}$$

These abstract components are now presentend in detail:

- GasInGasOut, which is the basis of most of the components in the turbojet library. It is an abstract component that contains an inlet gas port and an outlet gas port, therefore it can be used to define all the components that has a gas flow that pass through them. The variables exchanged through the gas port are presented in Table 3.1. The GasInGasOut ports are the ones highlighted in green in Table 3.3;

EcosimPro Name	Thesis Name	Initial value	Description	Unit
FAR	FAR	-	Fuel air ratio	-
H	h_T	700000	Total enthalpy	$\frac{J}{kg}$
P	p_T	-	Total pressure	Pa
T	T_T	500	Total temperature	K
W	$\dot{m}$	-	Mass flow	$\frac{kg}{s}$
WF	$\dot{m}_f$	-	Fuel flow	$\frac{kg}{s}$
WH	WH	-	Energy flow	W

Table 3.1: Variables exchanged through the components connected with a gas port.

- GasChannel, which is an abstract component and it is the child of GasInGasOut. The GasChannel ports are the ones highlighted in green in Table3.3, in fact GasChannel inherited them from GasInGasOut. In this abstract component are defined three decls, that are the ones in the red cells in Table 3.5. One of them is β_c, instead the other two are θ and δ:

$$\theta = \frac{T_{T_{in}}}{T_0}, \tag{3.1}$$

$$\delta = \frac{p_{T_{in}}}{p_0}; \tag{3.2}$$

- GasTurbo, which is an abstract component and it is used to define all turbomachine components. It is the child of GasChannel, so it means that GasTurbo ports are the ones highlighted in green in Table3.3 and the decls are the ones highlighted in red in Table 3.5. In addition, other data, decls and ports are defined and are the ones highlighted in yellow in Table 3.3, 3.4 and 3.5. In Table 3.2 all the variables exchanged through the shaft port are reported.

EcosimPro Name	Thesis Name	Initial value	Description	Unit
N	N	-	Rotational speed	rpm
P	P_{shaft}	-	Shaft mechanical power	W

Table 3.2: Variables exchanged through the components connected with a shaft port.

In the GasTurbo code are embedded Equations (3.2) and (3.1), plus other equations

that are the definition of the corrected mass flow

$$\dot{m}_{corr} = \frac{\dot{m}_{in} \cdot \sqrt{\theta}}{\delta}, \tag{3.3}$$

the definition of power for a generic turbomachine

$$P = \dot{m}_{in} \cdot (h_{T_{in}} - h_{T_{out}}), \tag{3.4}$$

and the shaft power balance

$$P + P_{shaft_{in}} - P_{shaft_{out}} = I \cdot \left(\frac{\pi}{30}\right)^2 \cdot N \cdot \dot{N}. \tag{3.5}$$

PORTS

EcosimPro Name	Direction	Description
g_in	IN	Inlet gas port
g_out	OUT	Outlet gas port
sh_in	IN	Input mechanical port
sh_out	OUT	Output mechanical port

Table 3.3: Compressor connection ports. The ports highlighted in green are defined in GasInGasOut, instead the ones highlighted in yellow are defined in GasTurbo.

DATA

EcosimPro Name	Thesis Name	Type	Default	Description	Unit
$CG1$	$CG1$	REAL	1	Correction coefficient for corrected mass flow	-
$CG2$	$CG2$	REAL	1	Correction coefficient for efficiency	-
$CG4$	$CG4$	REAL	1	Correction coefficient for compression work	-
$F1$	$F1$	TABLE_2D	-	Compression work vs adimensional speed and beta parameter	$\frac{\mathrm{J}}{\mathrm{kg \cdot K}}$
$F2$	$F2$	TABLE_2D	-	Efficiency vs adimensional speed and beta parameter	-
$F3$	$F3$	TABLE_2D	-	Corrected mass flow vs adimensional speed and beta parameter	$\frac{\mathrm{kg}}{\mathrm{s}}$
I	I	REAL	10	Inertial moment	$\mathrm{kg \cdot m^2}$
ND	N_D	REAL	10000	Design rotational speed	rpm

Table 3.4: Compressor data. The data highlighted in yellow is defined in *GasTurbo*.

DECLS

EcosimPro Name	Thesis Name	Type	Default	Description	Unit
$DHQT$	L_c	REAL	-	Compression work	$\frac{J}{kg \cdot K}$
$DHQTJ$	L_c^{NS}	REAL	-	Non scaled compression work	$\frac{J}{kg \cdot K}$
DN	$\dot{N}$	REAL	-	Derivative of rotational speed	$\frac{rpm}{s}$
EPD	η_{is}	REAL	-	Efficiency	-
$EDPJ$	η_{is}^{NS}	REAL	-	Non-scaled efficiency	-
N	N	REAL	-	Rotational speed	rpm
$PCNR$	N_{ad}	REAL	-	Adimensional rotational speed	%
PQ	β_c	REAL	-	Pressure quotient	-
$Power$	P	REAL	-	Mechanical power	W
WR	$\dot{m}_{corr}$	REAL	-	Corrected flow rate	$\frac{kg}{s}$
WRJ	$\dot{m}_{corr}^{NS}$	REAL	-	Non-scaled corrected mass flow	$\frac{kg}{s}$
$beta$	$beta$	REAL	0.7	Beta parameter	-
$delta$	δ	REAL	-	Adimensionalised inlet total pressure	-
$theta$	θ	REAL	-	Adimensionalised inlet total temperature	-

Table 3.5: Compressor decls. The decls highlighted in yellow are defined in *GasTurbo*, instead the ones highlighted in red are defined in *GasChannel*.

The compressor component ports, data and decls are reported respectively in Tables 3.3, 3.5 and 3.4 and they are the result of the ones inherited from GasTurbo plus the ones defined in the compressor code. The four ports are clearly visible in Figure 3.4, with the blue ones that are the gas ports and the brown ones that are the mechanical ports. The compressor equations are the ones inherited from GasTurbo (i.e. Equations (3.1), (3.2), (3.3), (3.4) and (3.5)), plus the ones defined in the component itself. The equations added

in the compressor code are the conservation of air mass

$$\dot{m}_{in} = \dot{m}_{out}, \tag{3.6}$$

the conservation of fuel mass

$$FAR_{in} = FAR_{out}, \tag{3.7}$$

the adimensional rotational speed

$$N_{ad} = \frac{100 \cdot \frac{N}{N_D}}{\sqrt{\theta}}, \tag{3.8}$$

the non-scaled quantities extraction through a spline interpolation from the compressor tables

$$\begin{cases} L_c^{NS} = splineInterp2D(F1, beta, N_{ad}), & \text{(3.9a)} \\ \eta_{is}^{NS} = splineInterp2D(F2, beta, N_{ad}), & \text{(3.9b)} \\ \dot{m}_{corr}^{NS} = splineInterp2D(F3, beta, N_{ad}), & \text{(3.9c)} \end{cases}$$

the correction coefficients computation

$$\begin{cases} CG1 = \dfrac{\dot{m}_{corr}}{\dot{m}_{corr}^{NS}}, & \text{(3.10a)} \\ CG2 = \dfrac{\eta_{is}}{\eta_{is}^{NS}}, & \text{(3.10b)} \\ CG4 = \dfrac{L_c}{L_c^{NS}}, & \text{(3.10c)} \end{cases}$$

the definition of the compression work

$$L_c = \frac{h_{T_{out}} - h_{T_{in}}}{T_{T_{in}}}, \tag{3.11}$$

and the definition of the compressor efficiency

$$\eta_{is} \cdot (\Phi_{out} - \Phi_{in}) = R \cdot \ln(\beta_c). \tag{3.12}$$

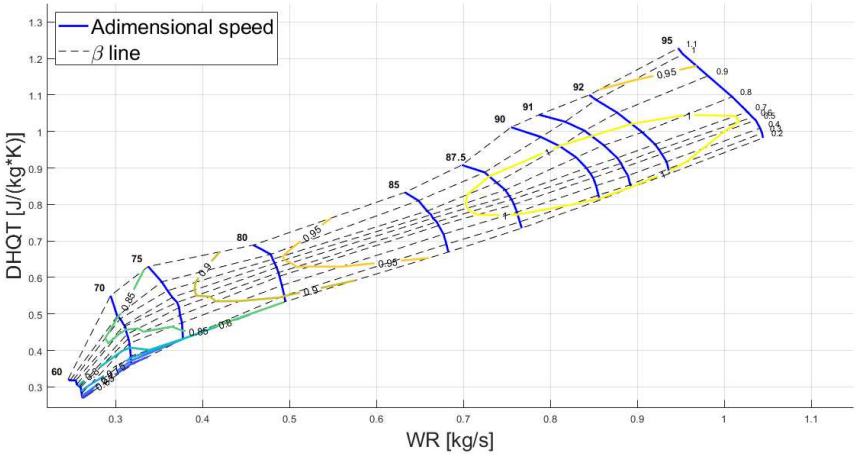

Figure 3.5: Non-scaled fan and compressor performance map.

It is important to know that in EcosimPro the turbomachine components are defined by their generic (i.e. non-dimensional) non-scaled performance map (or maps). The non-scaled performance map used for the compressor is the one depicted in Figure 3.5. This map describes the performance of a conventional 0D compressor component [17] and it is added in EcosimPro through three 2D tables called $F1$, $F2$ and $F3$. This map receives in input *beta* and N_{ad} and provides in output the values of L_c^{NS}, η_{is}^{NS} and $\dot{m}_{corr}^{NS}$, as reported respectively in Equations (3.9a), (3.9b) and (3.9c). Then, these quantities are computed also through the thermodynamic quantities, hence the correction coefficients can be computed using Equations (3.10a), (3.10b) and (3.10c). During the design phase these correction coefficients are computed in order to obtain the scaled performance map. Once the latter is obtained, the off-design analysis can be performed. Note that the parameter *beta* is simply a parameter needed by the solver. As reported in [27]: "*beta* serves simply as an array address and avoids the problem of horizontal and vertical portions constant N_{ad} lines".
This generic non-scaled performance map does not contain the surge line and the chocke line, this is why also points outside the map can be considered. In order to add the surge and the chocke line a more complex compressor model is needed, but this will not be the scope of this thesis.

All these equations introduced should be clear to the reader. The only equation that needs a better explanation is Equation (3.12), in particual the meaning of Φ. Φ can be explained starting from the enthalpy definition:

$$h = u + pv, \tag{3.13}$$

with u that is the internal energy and v the specific volume. Then, differentiating Equation (3.13) it is possible to obtain:

$$\mathrm{d}h = \mathrm{d}u + \mathrm{d}(pv). \tag{3.14}$$

The definition of $\mathrm{d}u$ is:

$$\mathrm{d}u = T\mathrm{d}s - p\mathrm{d}v. \tag{3.15}$$

Substituting Equation (3.15) into Equation (3.14) and making some passages:

$$\mathrm{d}h = T\mathrm{d}s - p\mathrm{d}v + p\mathrm{d}v + v\mathrm{d}p = T\mathrm{d}s + v\mathrm{d}p = T\mathrm{d}s + \frac{\mathrm{d}p}{\rho},$$

and remembering also the equation of perfect gases, Equation (3.14) can be rewritten as:

$$\mathrm{d}h = T\Big(\mathrm{d}s + R\frac{\mathrm{d}p}{p}\Big). \tag{3.16}$$

The definition of the entropy differentiation is:

$$\mathrm{d}s = \frac{\mathrm{d}h}{T} - R\frac{\mathrm{d}p}{p}. \tag{3.17}$$

The enthalpy can be defined also as:

$$\mathrm{d}h = C_p\mathrm{d}T \tag{3.18}$$

hence, Equation (3.17) can be rewritten as:

$$\mathrm{d}s = C_p\frac{\mathrm{d}T}{T} - R\frac{\mathrm{d}p}{p}. \tag{3.19}$$

In EcosimPro the component efficiency is defined as the isentropic efficiency and so, referring to Figure 3.6, it is defined as:

$$\eta_{is} = \frac{L_{c_{is}}}{L_c} = \frac{h_{2i} - h_1}{h_2 - h_1} = \frac{\int_1^{2i}\mathrm{d}h}{\int_1^2\mathrm{d}h}. \tag{3.20}$$

Then, substituting into Equation (3.20) the Equation (3.16) and considering for the nu-

merator that $\mathrm{d}s = 0$, the following steps can be done:

$$\eta_{is} = \frac{\int_1^{2i} RT\frac{\mathrm{d}p}{p}}{\int_1^2 T\left(\mathrm{d}s + R\frac{\mathrm{d}p}{p}\right)}. \tag{3.21}$$

Knowing that $p_{2i} = p_2$ and subsituting in Equation (3.21) the Equation (3.18) and the definition of β_c, it can be written that:

$$\eta_{is} \cdot \int_1^2 \left(C_p \frac{\mathrm{d}T}{T}\right) = R\ln(\beta_c). \tag{3.22}$$

At this point the Nasa polynomials are introduced in order to rewrite the term $C_p\frac{\mathrm{d}T}{T}$ as:

$$\left(C_p \frac{\mathrm{d}T}{T}\right) = \sum_{i=1}^{N}(a_i \cdot T^{i-1}\mathrm{d}T). \tag{3.23}$$

The coefficients a_i are called thermodynamic coefficients. Finally, adding this expression in Equation (3.22) results:

$$\eta_{is} \cdot \int_1^2 \sum_{i=1}^{N}(a_i \cdot T^{i-1}\mathrm{d}T) = R\ln(\beta_c) \tag{3.24}$$

and re-naming $\int_1^2 \sum_{i=1}^{N}(a_i \cdot T^{i-1}\mathrm{d}T)$ as $\int_1^2 \sum_{i=1}^{N}(a_i \cdot T^{i-1}\mathrm{d}T) = (\Phi_2 - \Phi_1)$, it is possible to obtain:

$$\eta_{is} \cdot (\Phi_2 - \Phi_1) = R \cdot \ln(\beta_c). \tag{3.25}$$

Equation (3.25) is exactly Equation (3.12).

Hence, in EcosimPro η_{is} is obtained through the NASA polynomials. Note that in EcosimPro the expression of $C_p\frac{\mathrm{d}T}{T}$ is more complex, because it is function both of the gas temperature and the chemical gas composition.

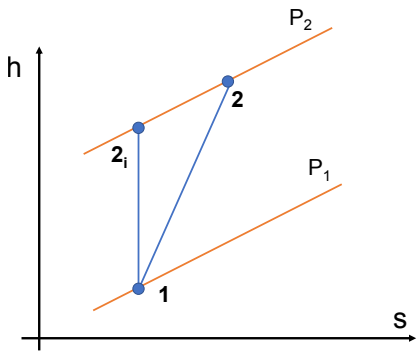

Figure 3.6: T-s diagram: Compressor isentropic efficiency.

3.2.2. Fan

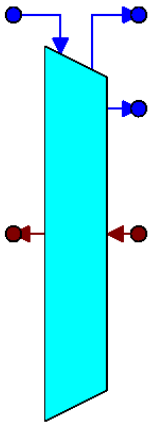

Figure 3.7: EcosimPro component: Fan.

The EcosimPro fan component is depicted in Figure 3.7. This component inherits all ports, data, decls and equations from the compressor, in fact a fan is substantially a compressor. The fan inheritance tree is:

$$\text{GasInGasOut} \rightarrow \text{GasChannel} \rightarrow \text{GasTurbo} \rightarrow \text{Compressor} \rightarrow \text{Fan}$$

The main difference from the compressor is the fact that the total mass flow is divided in:

- primary flow, that pass inside the engine core;
- secondary flow, that pass outside the engine core.

Hence, the fan component has two outlet gas ports. For the same reason also two more data are defined. The ports, data and decls added in the fan code are reported respectively in Tables 3.6, 3.7 and 3.8.

PORTS

EcosimPro Name	Direction	Description
g_pr	OUT	Outlet primary gas port

Table 3.6: New connection port defined in the fan code.

DATA

EcosimPro Name	Thesis Name	Type	Default	Description	Unit
DH_ratio	DH_{ratio}	REAL	0.9	Scalar for primary flow compression work	-
EPD_ratio	EPD_{ratio}	REAL	0.9	Scalar for primary flow efficiency	-

Table 3.7: New data defined in the fan code.

DECLS

EcosimPro Name	Thesis Name	Type	Default	Description	Unit
BPR	BPR	REAL	-	Bypass ratio	-

Table 3.8: New decls defined in the fan code.

The total fan equations are the sum of the ones inherited from the compressor plus the ones defined in the fan code. Here is present the definition of BPR plus other equations that are identical to the compressor ones (Equations (3.6), (3.7), (3.11) and (3.12)), but referred to the primary flow. The equations inherited from the compressor are used for the secondary flow. In EcosimPro the performance map used is the same as for the compressor (Figure 3.5).

3.2.3. Turbine

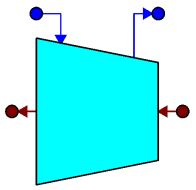

Figure 3.8: EcosimPro component: Turbine.

The turbine component code is very similar to the one of the compressor, but the turbine does not inherit the compressor mathematical model. A turbine is a turbomachine, hence the turbine inheritance tree is:

$$\text{GasInGasOut} \rightarrow \text{GasChannel} \rightarrow \text{GasTurbo} \rightarrow \text{Turbine}$$

In the turbine code are defined new data and decls, which can be found in Tables 3.9 and 3.10. Note that all the variables that are in this sub-paragraph are referred to the turbine component.

DATA

EcosimPro Name	Thesis Name	Type	Default	Description	Unit
$CG1$	$CG1$	REAL	1	Correction coefficient for corrected mass flow	-
$CG2$	$CG2$	REAL	1	Correction coefficient for efficiency	-
$CG3$	$CG3$	REAL	1	Correction coefficient for rotational speed	-
$CG4$	$CG4$	REAL	1	Correction coefficient for expansion work	-
$G1$	$G1$	TABLE_2D	-	Corrected mass flow vs power and corrected rotational speed	$\frac{kg}{s}$
$G2$	$G2$	TABLE_2D	-	Efficiency vs power and corrected rotational speed	-

Table 3.9: New data defined in the turbine code.

DECLS

EcosimPro Name	Thesis Name	Type	Default	Description	Unit
$DHQT$	L_e	REAL	-	Expansion work	$\frac{\text{J}}{\text{kg·K}}$
$DHQTJ$	L_e^{NS}	REAL	-	Non scaled expansion work	$\frac{\text{J}}{\text{kg·K}}$
EPD	η_{is}	REAL	-	Efficiency	-
$EDPJ$	η_{is}^{NS}	REAL	-	Non-scaled efficiency	-
WRJ	$\dot{m}_{corr}^{NS}$	REAL	-	Non-scaled corrected mass flow	$\frac{\text{kg}}{\text{s}}$
NR	N_{corr}	REAL	-	Corrected rotational speed	rpm
NRJ	N_{corr}^{NS}	REAL	-	Non-scaled corrected rotational speed	rpm

Table 3.10: New decls defined in the turbine code.

The equations in the turbine component are the conservation of mass and fuel that correspond to Equations (3.6) and (3.7), the definition of corrected rotational speed

$$N_{corr} = \frac{N}{\sqrt{\theta}},$$

the expansion work definition

$$L_e = \frac{h_{T_{in}} - h_{T_{out}}}{T_{T_{in}}},$$

the non-scaled quantities extraction from the turbine map

$$\begin{cases} \dot{m}_{corr}^{NS} = splineInterp2D(G1, L_e^{NS}, N_{corr}^{NS}), \\ \eta_{is}^{NS} = splineInterp2D(G2, L_e^{NS}, N_{corr}^{NS}), \end{cases}$$

the correction coefficients

$$\begin{cases} CG1 = \dfrac{\dot{m}_{corr}}{\dot{m}_{corr_{(TURB)}}^{NS}}, \\ CG2 = \dfrac{\eta_{is}}{\eta_{is}^{NS}}, \\ CG3 = \dfrac{N_{corr}}{N_{corr}^{NS}}, \\ CG4 = \dfrac{L_e}{L_e^{NS}}, \end{cases}$$

and the turbine isentropic efficiency

$$\frac{\eta_{is}}{\Phi_{out} - \Phi_{in}} = R \cdot \ln(\beta_c).$$

As for the compressor, the turbine performances are described by its generic non-scaled performance map. This map has a lot of similarities with the compressor one, but there are also some differences. The main differences are two: the first one is that this map is added in EcosimPro through two 2D tables ($G1$ and $G2$) and the second one is that this map receives in input L_e^{NS} and N_{corr}^{NS} and provides in output $\dot{m}_{corr}^{NS}$ and η_{is}^{NS}. In Figure 3.9 is represented the turbine performance map.

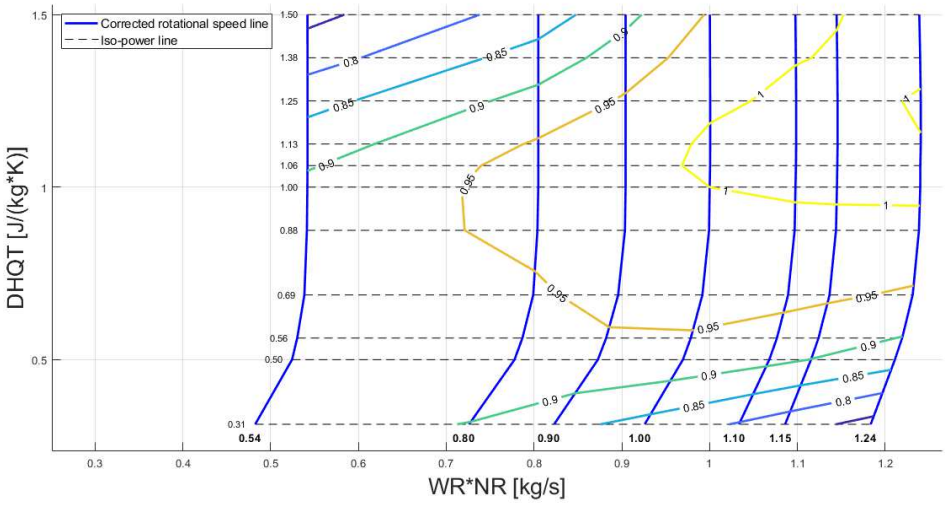

Figure 3.9: Non-scaled turbine performance map.

3.3. New component: Counter-rotating fan

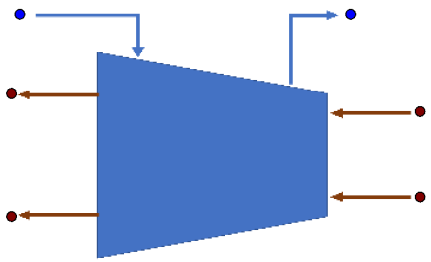

Figure 3.10: EcosimPro component: CR fan.

This thesis is about electric CR fans, but in the turbojet library there aren't CR components. This is why it was necessary to code the CR fan component, which in EcosimPro it was called "Electric_CrFan". This new component was coded with the same philosophy of the other turbomachine components, because first of all it is a turbomachine and also because it is not so different from a compressor. In order to code the CR fan, the compressor code and the work of Alexiou et al. [5] were used as references. Remember also that all the variables defined in this sub-section are referred to the CR fan component.

The first step is to choose the CR fan inheritance tree. The CR fan componet can't inherit the mathematical model from GasTurbo, because the CR fan has two shafts and so four mechanical ports. This is clearly visible in Figure 3.10. Instead, the CR fan can be the child of GasChannel, so the chosen inheritance tree is:

$$\text{GasInGasOut} \rightarrow \text{GasChannel} \rightarrow \text{Electric\_CrFan}$$

PORTS

EcosimPro Name	Direction	Description
$sh1\_in$	IN	Front rotor input mechanical port
$sh1\_out$	OUT	Front rotor output mechanical port
$sh2\_in$	IN	Rear rotor input mechanical port
$sh2\_out$	OUT	Rear rotor output mechanical port

Table 3.11: New ports defined in the CR fan code.

DATA

EcosimPro Name	Thesis Name	Type	Default	Description	Unit
$CG1$	$CG1$	REAL	1	Correction coefficient for corrected mass flow	-
$CG2$	$CG2$	REAL	1	Correction coefficient for efficiency	-
$CG4$	$CG4$	REAL	1	Correction coefficient for compression work	-
$CG5$	$CG5$	REAL	1	Correction coefficient for torque ratio	-
NR	N_{ratio}	REAL	1	Speed ratio	-
$ND1$	$N_{D,FR}$	REAL	10000	Front rotor design rotational speed	rpm
$F1$	$F1$	-	TABLE_3D	Compression work vs Front rotor adimensional speed and beta parameter and speed ratio	$\frac{J}{kg \cdot K}$
$F2$	$F2$	-	TABLE_3D	Efficiency vs Front rotor adimensional speed and beta parameter and speed ratio	-
$F3$	$F3$	-	TABLE_3D	Corrected mass flow vs Front rotor adimensional speed and beta parameter and speed ratio	$\frac{kg}{s}$
$F4$	$F4$	-	TABLE_3D	trqR vs Front rotor adimensional speed and beta parameter and speed ratio	-

Table 3.12: New data defined in the CR fan code.

DECLS

EcosimPro Name	Thesis Name	Type	Default	Description	Unit
WR	$\dot{m}_{corr}$	REAL	-	Corrected Flow Rate	$\frac{\text{kg}}{\text{s}}$
$PowerR$	P_{ratio}	REAL	-	Power ratio	-
$Power$	P	REAL	-	Total CR fan power	W
$Power1$	P_{FR}	REAL	-	Front rotor power	W
$Power2$	P_{RR}	REAL	-	Rear rotor power	W
$trq1$	$T_{r,FR}$	REAL	-	Front rotor torque	$\text{N} \cdot \text{m}$
$trq2$	$T_{r,RR}$	REAL	-	Rear rotor torque	$\text{N} \cdot \text{m}$
$N1$	N_{FR}	REAL	-	Front rotor rotational speed	rpm
$N2$	N_{RR}	REAL	-	Rear rotor rotational speed	rpm
$beta$	$beta$	REAL	0.7	Beta parameter	-
$PCNR1$	$N_{ad,FR}$	REAL	-	Front rotor adimensional speed	%
$DHQTJ$	L_c^{NS}	REAL	-	Non-scaled compression work	$\frac{\text{J}}{\text{kg}\cdot\text{K}}$
$EPDJ$	η_{is}^{NS}	REAL	-	Non-scaled efficiency	-
WRJ	$\dot{m}_{corr}^{NS}$	REAL	-	Non-scaled corrected mass flow	$\frac{\text{kg}}{\text{s}}$
$trqRJ$	$T_{r_{ratio}}^{NS}$	REAL	-	Non-scaled torque ratio	$\frac{\text{kg}}{\text{s}}$
$DHQT$	L_c	REAL	-	Compression work	$\frac{\text{J}}{\text{kg}\cdot\text{K}}$
EPD	η_{is}	REAL	-	Efficiency	-
$trqR$	$T_{r_{ratio}}$	REAL	-	Torque ratio	-

Table 3.13: New decls defined in the CR fan code.

At this point, new ports, data and decls have to be defined in order to implement the mathematical model. All these new variables, with their description, are reported in Tables 3.11, 3.12 and 3.13. Since the CR fan can be seen as a compressor, it is possible to note that the CR fan variables are similar to the compressor ones, even if there are some differences. The main difference is that, since the CR fan has two rotors, it needs a one more degree of freedom: N_{ratio}. This fact implies that now there is a different performance map for each speed ratio (Figures 3.12). Moreover, in order to compute the power split between the two shafts, also the torque ratio maps are added (Figures 3.13). As for the

performance maps, also in this case there is a different torque ratio map for each speed ratio considered. To extract the values from the performance and torque ratio maps the first parameter needed is N_{ratio}, in fact this parameter select the right performance and torque ratio map. After that, both these maps receive in input *beta* and $N_{ad,FR}$ and then the performance map provides in output L_c^{NS}, η_{is}^{NS} and $\dot{m}_{corr}^{NS}$. Instead, the torque ratio map provides $T_{r_{ratio}}^{NS}$. Note that both the performance maps and the torque ratio maps are added in EcosimPro as 3D tables, that are $F1$, $F2$, $F3$ and $F4$. A brief descprition of these 3D table is done in Figure 3.11.

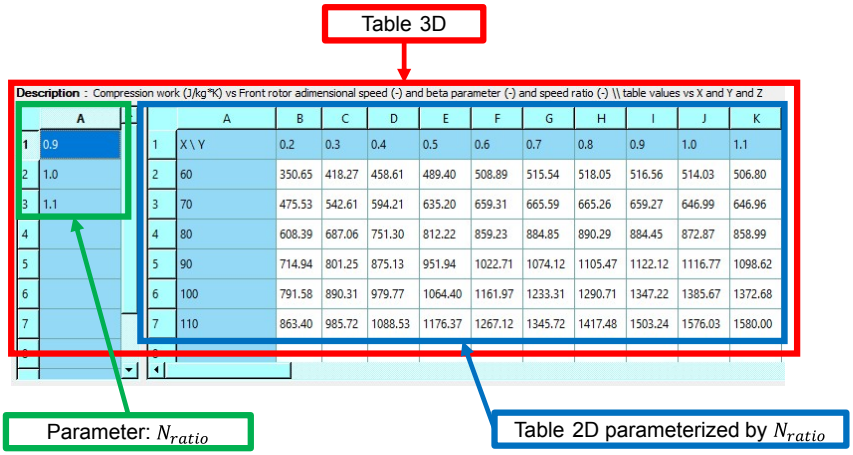

	A	B	C	D	E	F	G	H	I	J	K
1	X \ Y	0.2	0.3	0.4	0.5	0.6	0.7	0.8	0.9	1.0	1.1
2	60	350.65	418.27	458.61	489.40	508.89	515.54	518.05	516.56	514.03	506.80
3	70	475.53	542.61	594.21	635.20	659.31	665.59	665.26	659.27	646.99	646.96
4	80	608.39	687.06	751.30	812.22	859.23	884.85	890.29	884.45	872.87	858.99
5	90	714.94	801.25	875.13	951.94	1022.71	1074.12	1105.47	1122.12	1116.77	1098.62
6	100	791.58	890.31	979.77	1064.40	1161.97	1233.31	1290.71	1347.22	1385.67	1372.68
7	110	863.40	985.72	1088.53	1176.37	1267.12	1345.72	1417.48	1503.24	1576.03	1580.00

	A
1	0.9
2	1.0
3	1.1

Figure 3.11: Example of the 3D table $F1$. A 3D table is substantially a 2D table parameterized by a parameter that in this case is N_{ratio}. The N_{ratio} values are 0.9, 1 and 1.1, therefore the 3D table is the composition of three 2D tables.

The maps used are the ones of the work of Alexiou et al. [5], which were used for a CR compressor. Instead, in this work these maps were used for a CR fan. This choice was made due to three main reasons:

- the maps are non-dimensional and non-scaled, so the similarity concept can be used;
- in EcosimPro the map for the compressor and for the fan is the same;
- specific CR fan maps were not available.

The equations defined in the CR fan component are similar to the compressor ones, but adapted to the fact that now there are two shafts. Moreover, the hypothesis of steady condition was made. The equations of air and fuel conservation are identical to the compressor ones, so respectively Equations (3.6) and (3.7). $N_{ad,FR}$ is defined in the same way as N_{ad} (Equation (3.8)), but with the front rotor as subject. Other equations are the

non-scaled quantities extraction from the 3D tables through 3D linear interpolation

$$\begin{cases} T^{NS}_{r_{ratio}} = linearInterp3D(F4, N_{ad,FR}, beta, N_{ratio}), \\ \eta^{NS}_{is} = linearInterp3D(F2, N_{ad,FR}, beta, N_{ratio}), \\ \dot{m}^{NS}_{corr} = linearInterp3D(F3, N_{ad,FR}, beta, N_{ratio}), \\ L^{NS}_{c} = linearInterp3D(F1, N_{ad,FR}, beta, N_{ratio}), \end{cases}$$

the correction coefficients computation

$$\begin{cases} CG1 = \dfrac{\dot{m}_{corr}}{\dot{m}^{NS}_{corr}}, \\ CG2 = \dfrac{\eta_{is}}{\eta^{NS}_{is}}, \\ CG4 = \dfrac{L_c}{L^{NS}_c}, \\ CG5 = \dfrac{T_{r_{ratio}}}{T^{NS}_{r_{ratio}}}. \end{cases}$$

The definition of L_c is the same of Equation (3.11) and the definition of η_{is} is the same of Equation (3.12). Moreover, $\dot{m}_{corr}$ and P are defined respectively in Equations (3.3) and (3.4). Then, for the computation of power, torque and rotational speed in the two shafts, other equations are added. These equations are the definition of power ratio

$$P_{ratio} = \frac{P_{FR}}{P_{RR}},$$

the speed ratio definition

$$N_{ratio} = \frac{N_{FR}}{N_{RR}},$$

the torque ratio definiton

$$T_{r_{ratio}} = \frac{T_{r,FR}}{T_{r,RR}},$$

and the front and rear rotor power definitions

$$P_{FR} = \frac{T_{r,FR} \cdot N_{FR} \cdot \pi}{30},$$
$$P_{RR} = \frac{T_{r,RR} \cdot N_{RR} \cdot \pi}{30}.$$

The last equations refer to the power balance and are

$$
\begin{aligned}
0 &= P_{FR} + P_{shaft,FR_{in}} - P_{shaft,FR_{out}}, \\
0 &= P_{RR} + P_{shaft,RR_{in}} - P_{shaft,RR_{out}}, \\
T_{r,FR} &= \frac{30 \cdot T_{r_{ratio}} \cdot N_{ratio}}{\pi \cdot N_{FR} \cdot (1 + T_{r_{ratio}} \cdot N_{ratio})}.
\end{aligned}
$$

Now that the CR fan component is correctly coded, it can be used in EcosimPro. For completeness the its code in EL is reported in Appendix B.

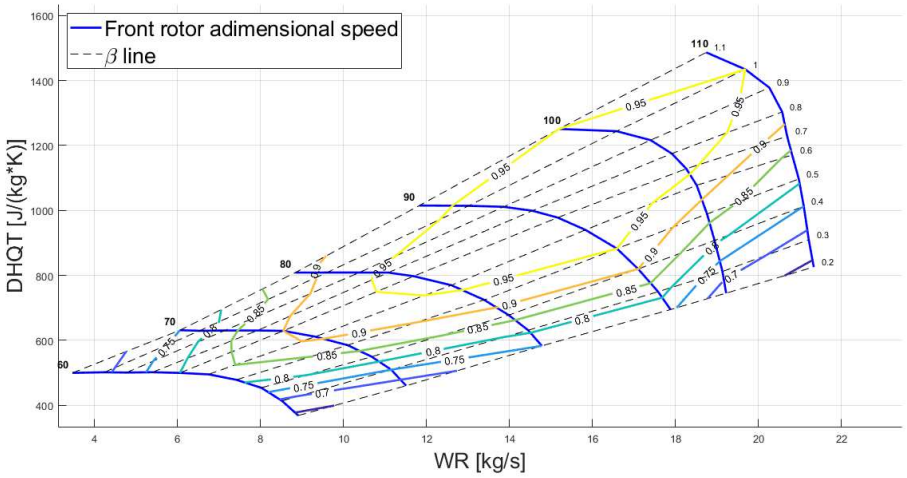

(a) $N_{ratio} = 1$

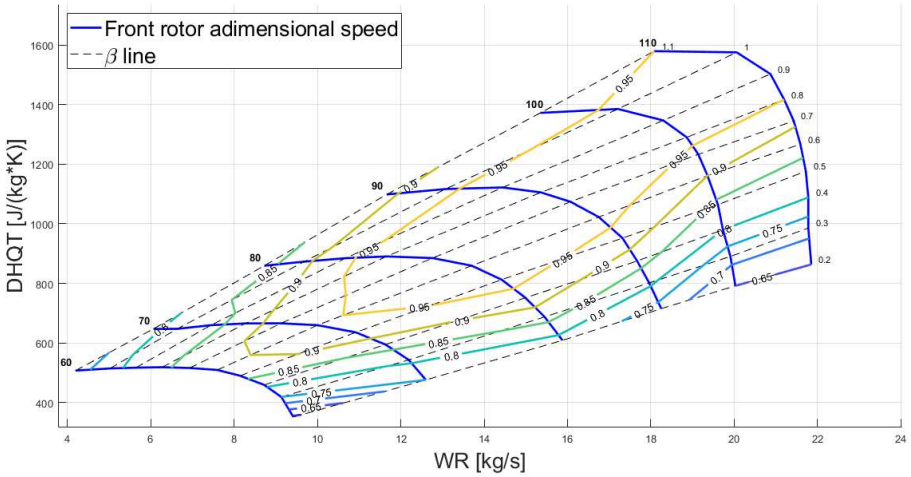

(b) $N_{ratio} = 0.9$

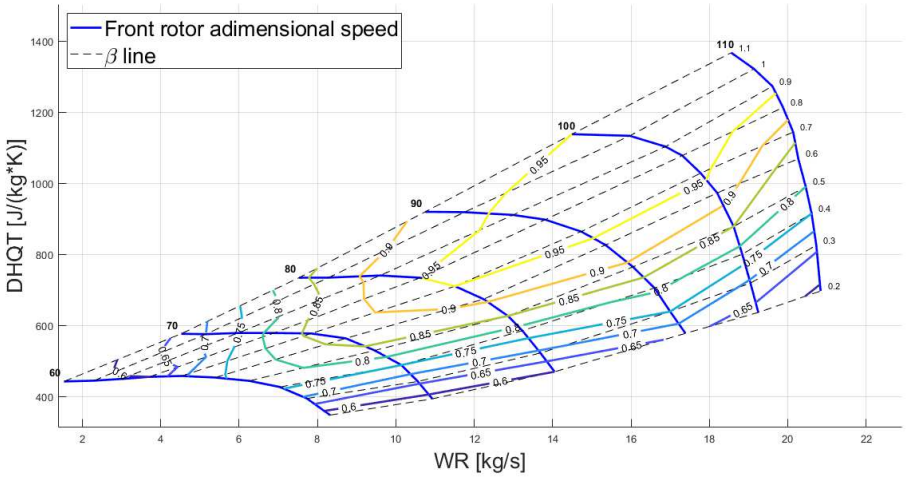

(c) $N_{ratio} = 1.1$

Figure 3.12: Non-scaled counter-rotating fan performance maps.

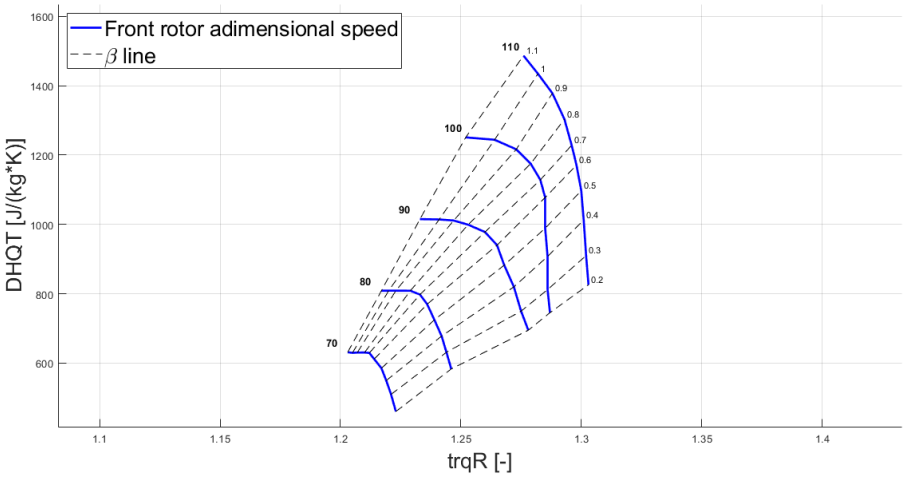

(a) $N_{ratio} = 1$

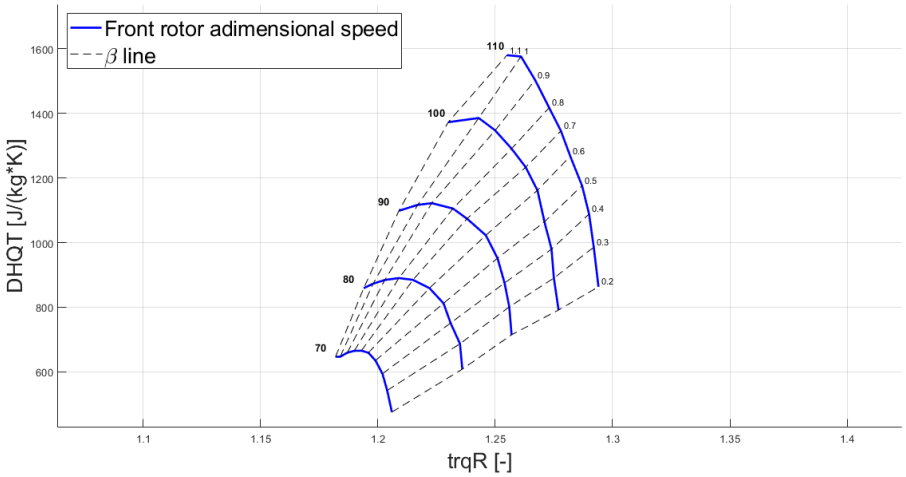

(b) $N_{ratio} = 0.9$

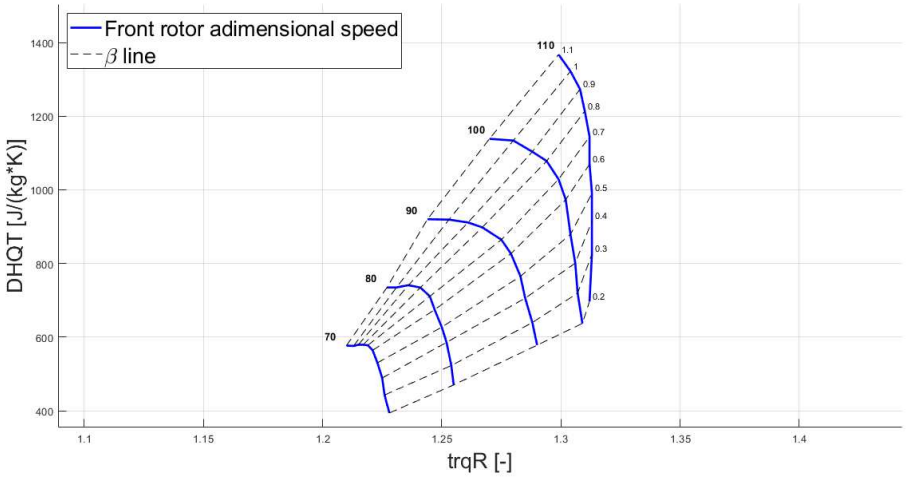

(c) $N_{ratio} = 1.1$

Figure 3.13: Non-scaled counter-rotating fan performance maps - Torque ratio.

4 | Reference turbofans modelling on EcosimPro

This chapter aims at describing all the procedures in order to define all the engine characteristics in Ecosimpro. These characteristics will be computed starting from the engine schematic and using real available data. It is important to note that not all the data are available and so, when needed, meaningful assumptions will be done. The engines analyzed in this chapter are the CFM56-7B24 and the GEnx-1B64, which will be used as references respectively for the short/medium range missions and for the long range missions. The choice of these two engines was done depending on both the modernity of the engines and the availability of data.

4.1. CFM56-7B24

Figure 4.1: CFM56-7B24.

CFM56 is a turbofan engine developed and produced by the CFM international, that is a join venture formed in 1974 between Snecma Moteurs of France and General Electric of the US. The CFM56 is one of the most popular turbofan in civil aviation and one of the latest version is the CFM56-7B24. It was chosen as a reference for the short and medium range flight missions, because it is used on the Boieng 737 next generation and

on the Airbus A318/A319/A320/A321 which are very common aircrafts for regional and continental transport [7].

CFM56-7B24 is a two-shaft turbofan without reduction gear and with no internal mixing of the primary and secodary flow exhaust. The fundamental components of that engine are: inlet, fan, low pressure (LP) compressor, high pressure (HP) compressor, HP turbine, LP turbine that provides power to the fan and the LP compressor, primary nozzle (for the core) and secondary nozzle (for the fan). The EcosimPro engine schematic is rapresented in Figure 4.2. Since during preliminary analysis generally the dynamic of the components is not considered, both the design and off-design computations will be done in steady condition.

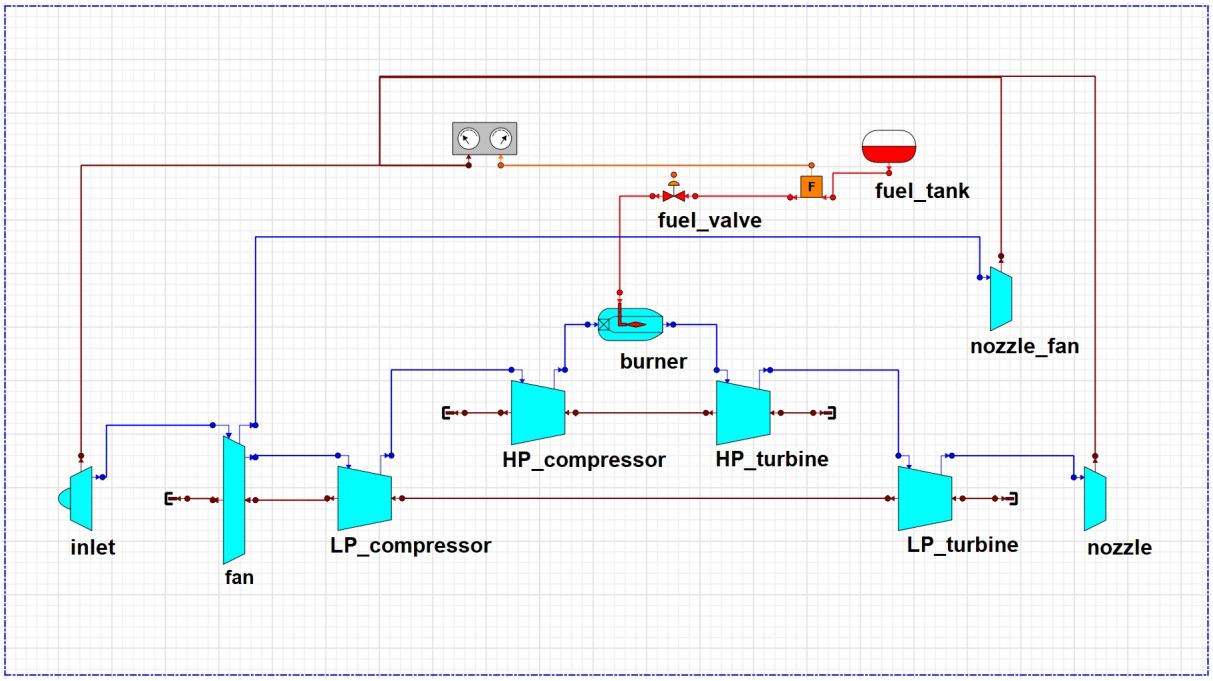

Figure 4.2: CFM56-7B24 schematic.

4.1.1. Engine design

As well described in Chapter 3, once the engine schematic is ready, the next step is to create the design partition. During this phase the engine data reported in Table 4.1 are transformed in unknows, therefore they can be computed during the schematic simulation that is called "design experiment". The data transformed in unknowns are the correction coefficients for the performance map components, the two nozzle areas, the burner volume and the burner loss coefficient.

Component	Value	Unit
Fan	$CG1$	-
	$CG2$	-
	$CG4$	-
	N_D	-
	DH_{ratio}	-
	EPD_{ratio}	-
LP compressor	$CG1$	-
	$CG2$	-
	$CG4$	-
	N_D	-
HP compressor	$CG1$	-
	$CG2$	$\frac{\text{rpm}}{\text{s}}$
	$CG4$	-
	N_D	-
Burner	ϵ	$\frac{\text{s}}{\text{kg}}$
	Vol	m^3
HP turbine	$CG1$	-
	$CG2$	-
	$CG3$	-
	$CG4$	-
LP turbine	$CG1$	-
	$CG2$	-
	$CG3$	-
	$CG4$	-
Primary nozzle	$A_{PN_{out}}$	m^2
Secondary nozzle	$A_{SN_{out}}$	m^2

Table 4.1: CFM56-7B24 and GEnx-1B64 data transformed in unknowns.

During the creation of the design partition, also the schematic boundary conditions have to be selected. Depending on the number of unknowns, EcosimPro tells to the user how many boundary conditions needs in order to solve the mathematical model. By default, EcosimPro suggests which boundary conditions use and the user can use or modify them. In this case, except for z and M, it was chosen to modify all the boundary conditions. These were selected depending on which data are easy to find in literature or at least

easy to be estimated starting from general knowledge in the aeroengine field. Note that not all the possible combinations of boundary conditions are allowed, in fact they have to be indipendent and not already present in the mathematical model. With indipendent it means that it is not possible to select both the temperature at the burner outlet and at the turbine inlet, because they are the same value. The boundary conditions chosen are reported in Table 4.2.

Once the design partition has been generated, hence the schematic mathematical model created, it is possible to associate to it the design experiment. In this case, to generate the experiment, the wizard command was sufficient. As reported in Figures 3.2 and 3.3, the CFM56-7B24 design partition is called "Design_Point" and the associated design experiment is called "Design_Point". After that, the boundary conditions and the dynamic variables can be added. The latter are needed since the simulation is steady and so now these variables are constant that the solver needs. The boundary conditions and dynamic variables are reported respectively in Table 4.2 and 4.3 and they refer to a cruise condition. This condition was chosen as design point for several reasons:

- in literature, for preliminary computations, the cruise usually is chosen as design point because it is an easy point to consider, also when regional aircrafts are analyzed;
- define a proper design point is not straightforward and not necessary in preliminary analysis;
- the CFM56-7B24 is used also for medium range missions, so it is realistic that the real design point is not too far from the cruise condition;
- in literature most of the engine data are referred to the cruise condition and in general the real design point is not reported.

Component	Variable	Value	Unit
Aircraft	z	10668	m
	M	0.8	-
Fan	BPR	5.3	-
	$\dot{N}$	0	$\frac{\text{rpm}}{\text{s}}$
	η_{is}	0.89	-
	N_{ad}	94	%
	β_c	1.6	-
	$beta$	1	-
LP compressor	η_{is}	0.9	-
	N_{ad}	92	%
	β_c	2.5	-
	$beta$	0.4	-
HP compressor	$\dot{m}_{in}$	21.6	$\frac{\text{kg}}{\text{s}}$
	$\dot{N}$	0	$\frac{\text{rpm}}{\text{s}}$
	η_{is}	0.91	-
	N_{ad}	92	%
	β_c	10	-
	$beta$	0.7	-
Burner	AL	2	$\frac{\text{kg}}{\text{s}\cdot\text{m}^3}$
	β_c	0.96	-
	$p_{T_{in}}$	1440000	Pa
	$T_{T_{in}}$	780	K
HP turbine	L_e^{NS}	1	$\frac{\text{J}}{\text{kg}\cdot\text{K}}$
	η_{is}	0.91	-
	N_{corr}^{NS}	1	$\frac{\text{r}}{\text{s}}$
	$T_{T_{in}}$	1440	K
LP turbine	L_e^{NS}	1	$\frac{\text{J}}{\text{kg}\cdot\text{K}}$
	η_{is}	0.91	-
	N_{corr}^{NS}	1	$\frac{r}{s}$

Table 4.2: CFM56-7B24 design: Boundary conditions. The blue values are known from literature [7] [35], instead the green ones are due to the fact that the simulation is steady.

Component	Variable	Value	Unit
LP compressor	N	5380	$\frac{\text{r}}{\text{min}}$
HP compressor	N	15183	$\frac{\text{r}}{\text{min}}$

Table 4.3: CFM56-7B24 design: Dynamic variables. The blue values are known from literature [35].

Since not all the input variables are known, some of them are chosen between a reasonable range of realistic values. The final choice of these values was done in order to obtain a final schematic that gives in output performances in terms of thrust and specific fuel consumption, similar to the real engine. This step is also useful to validate the engine model obtained. The results are shown in Table 4.4.

Variable	EcosimPro Value	Real engine Value	Error [%]
T_h	24.83 [kN]	24.38 [kN]	+1.8
SFC	$1.703e^{-05}$ $[\frac{\text{kg}}{\text{N}\cdot\text{s}}]$	$1.706e^{-05}$ $[\frac{\text{kg}}{\text{N}\cdot\text{s}}]$	−0.2

Table 4.4: CFM56-7B24 global performances comparison between the model and the real engine [7] in cruise condition.

The boundary conditions used and the component data obtained are realistic, moreover the values of SFC and T_h match perfectly with the ones of the real engine. However, to make a more robust validation, other checks are needed. In order to do that, the work of Stefano [23] was used. For his thesis he coded a simple thermodynamic cycle for a turbofan engine in Matlab. This code contains the basic isentropic relations corrected by the component efficiencies. Hence, adding the component data obtained in EcosimPro, it was possible to compute the thermodynamic cycle and so compare the results with the ones obtained in EcosimPro. The thermodynamic cycle obtained is represented in Figure 4.3 and the results are reported in Table 4.5.

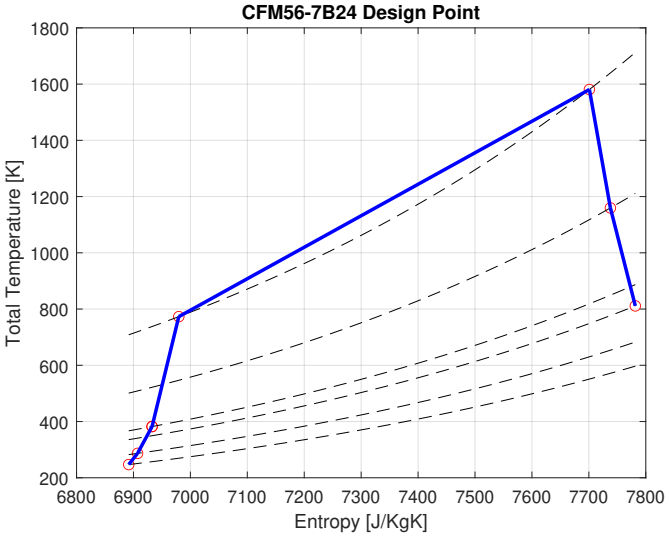

Figure 4.3: CFM56-7B24 thermodynamic cycle in design point (i.e. cruise) condition.

Component	EcosimPro Value	Matlab Value	Error [%]
Fan	5.58 [MW]	5.47 [MW]	+2
LP compressor	2.13 [MW]	2.08 [MW]	+2.6
HP compressor	8.86 [MW]	8.51 [MW]	+3.9
HP turbine	8.86 [MW]	9.35 [MW]	−5.6
LP turbine	7.71 [MW]	7.74 [MW]	−0.3

Table 4.5: CFM56-7B24 comparison between the power components computed with EcosimPro and the ones computed with Matlab in design (i.e. cruise) condition.

The results obtained are good, since the max absolute error is less than 6 %. Now that the CFM56-7B24 engine model is validated, it can be safely used for the following analysis.

4.1.2. Off-design analysis

To perform the flight mission analysis it was implemented in Matlab a code that needs the athmosphere, the aircraft and the engine mathematical models. The problem is that the engine model is in EcosimPro, so it has to be transferred in Matlab. One simple way

to do that, is to first create the so called "engine map" in EcosimPro and then upload it in the form of a table in Matlab.

To generate this map, an engine off-design analysis has to be done. Now that the CFM56-7B24 schematic is designed, it can be used to analyze the engine behaviour in conditions different from cruise. In order to do that, a new partition called "Automatic_Engine_Map" was generated (Figure 3.2). In fact the partition used for the engine design can't be used, because now the engine data are known and fixed. In this new partition, called also off-design partition, the only boundary conditions requested are z, M and $\dot{m}_f$, that are the only variables that can modify the engine performances.

The next step is to generate the experiment associated to that partition. The idea is to create a steady parametric experiment in which z, M and $\dot{m}_f$ are the parameters. In this way the engine behaviour can be obtained for different working conditions and this is the exact meaning of engine map. The output of this experiment is a table in which are saved all the engine quantities like T_h, SFC, HP compressor L_c, LP compressor L_c, etc... for different values of z, M and $\dot{m}_f$. Unfortunately, the creation of that experiment is not so easy. First of all note that the sum of the all steady calculations, each one for a certain value of z, M and $\dot{m}_f$, generates the parametric simulation. During a parametric simulation the variables obtained in a certain calculation are used to initialize the next one. If the previous calculation did not converge, the next one receives input values that does not make sense. Hence, like in a chain reaction, all the following calculations defined in the parametric simulation fail. To overcome this problem two simulations, which can be seen under the CFM56 off-design partition in Figure 3.3, were created:

- the first one is called "EngineData_FlightMission". It was generated using the wizard command and it is represented in Figure 4.4. From this figure it can be seen that this simulation is subdivided in blocks. The first block is called "Initialization", in which the design engine data are added to the model and the take-off simulation is performed. The real parametric simulation starts in the following blocks, which are subdivided for altitude ranges. This subdivision was done at the beginning of the thesis work for other reasons, but it is not mandatory. All these blocks can be seen as an unique parametric steady experiment. At first, the engine model is tested at $z = 0$ [m], $M = 0$ [$-$] and $\dot{m}_f = 0$ [$\frac{\text{kg}}{\text{s}}$], then the engine model is tested for increasing values of $\dot{m}_f$ until a certain $\dot{m}_{f_{MAX}}$ is reached. After that, the simulation re-starts from $z = 0$ [m] and $\dot{m}_f = 0$ [$\frac{\text{kg}}{\text{s}}$], but with a different value of Mach, for example $M = 0.1$ [$-$]. Again, the model is tested for increasing values of $\dot{m}_f$ and this cycle continue until the simulation at $z = 0$ [m], $M = M_{MAX}$ [$-$] and $\dot{m}_f = \dot{m}_{f_{MAX}}$ [$\frac{\text{kg}}{\text{s}}$] is reached. At this point the simulation changes the z value, so for

example $z = 1500$ [m], and M and $\dot{m}_f$ re-start from 0. The parametric simulation stops when the paramters reach $z = z_{MAX}$, $M = M_{MAX}$ and $\dot{m}_f = \dot{m}_{f_{MAX}}$. All these passages are represented in Table 4.6.

- the second simulation is called "EngineData_FlightMission_CODE" and it was builted in EL. Due to the problems explained before, "EngineData_FlightMission" can't be used to simulate different off-design conditions and so to built the engine map. The scope of "EngineData_FlightMission" is to generate a baseline EL code for the "EngineData_FlightMission_CODE", in which some modifications were added in order to solve the problems cited before. First of all, the EL code was modified in order to avoid the situation in which a new calculation is initialized by values that come from a calculation that did not converge. Then, to help the convergence of the calculations, the EL code was modified in such a way a new calculation in a certain flight condition is initialized from a previous calculation that is in the nearest flight condition. For example the off-design calculation at $z = 1500$ [m], $M = 0.5$ [$-$] and $\dot{m}_f = 0$ [$\frac{\text{kg}}{\text{s}}$] is not initialized by the previous one which is $z = 1500$ [m], $M = 0.4$ (Max) [$-$] and $\dot{m}_f = 1.4$ (Max) [$\frac{\text{kg}}{\text{s}}$], but it is initialized by the nearest flight condition valid calculation, that maybe could be $z = 1500$ [m], $M = 0.4$ (Max) [$-$] and $\dot{m}_f = 0.3$ [$\frac{\text{kg}}{\text{s}}$].

Now it should be clear why only the simulation called "EngineData_FlightMission_CODE" was used to perform the off-design calculations, hence to built the engine map.

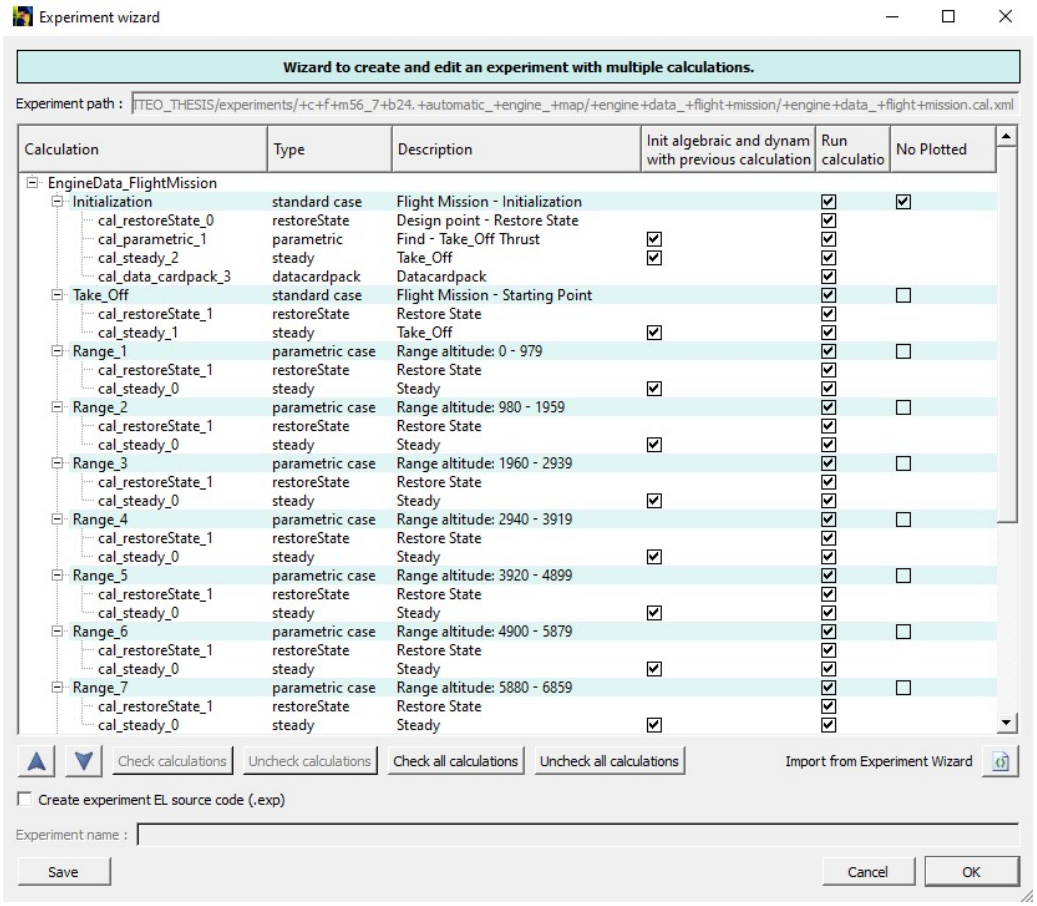

Figure 4.4: Scheme of the "*EngineData_FlightMission*" simulation.

Calculation N°	z [m]	M [−]	$\dot{m}_f$ [$\frac{kg}{s}$]
1	0	0	0
2	0	0	0.2
...	...	...	...
7	0	0	1.2
8	0	0	1.4 (Max)
9	0	0.1	0
10	0	0.1	0.2
...	...	...	...
16	0	0.1	1.4 (Max)
17	0	0.2	0
...	...	...	...
64	0	0.7 (Max)	1.4 (Max)
65	1500	0	0
66	1500	0	0.2
...	...	...	...
576	12000 (Max)	0.7 (Max)	1.4 (Max)

Table 4.6: Example of the steady parametric simulation working principle. The values that change in each new calculation are in red.

The steady parametric simulation "EngineData_FlightMission_CODE" was performed for the all possible combinations of the following values:

- the z $[m]$ values considered are 0, 489.5, 979, 980, 1469.5, 1959, 1960, 2449.5, 2939, 2940, 3924.5, 3919, 3920, 4409.5, 4899, 4900, 5389.5, 5879, 5880, 6369.5, 6859, 6860, 7349.5, 7839, 7840, 8329.5, 8819, 8820, 9309.5, 9799, 9800, 10289.5, 10779, 10781, 11270.5, 11760;
- the M $[-]$ values considered are 0, 0.17, 0.34, 0.51, 0.68, 0.85;
- the $\dot{m}_f$ $[\frac{kg}{s}]$ considered are 0, 0.025, 0.040, 0.065, 0.090, 0.115, ..., 1.6.

The total off-design calculations performed are $36 \cdot 6 \cdot 65 = 14040$ and for each of them are associated different engine quantities. If for example the values saved for each combination of z, M and $\dot{m}_f$ are the values of L_c and $\dot{m}_{corr}$ of the all turbofan components, it is possible to obtain the Figures 4.5, 4.6, 4.7, 4.8 and 4.9. In these performance maps are reported the design point (black plus), the take-off point (green cross), the off-design points (red)

and the off-design points in which the engine is in idle condition (green). Note that all these points come only from calculations that converged. Moreover, since the points that are in the performance map proximity can be considered valid (for more detail see Sub-section 3.2.1), these maps were filtered from points that are too far from the map borders. From Figures 4.5, 4.8 and and 4.9 it can be seen that all the HP compressor, HP and LP turbine off-design points are inside the map and are also well distributed along a defined path. Instead from Figures 4.6, 4.7 it can be seen that the fan and LP compressor off-design points have an opposite trend and are not confined in a clear path. This is probably due to a non perfect balance between the two components, which are mounted on the same shaft.
The points that generate more problems are the ones associated to the idle condition. In fact, this simple model has difficulties in simulate this particular situation.

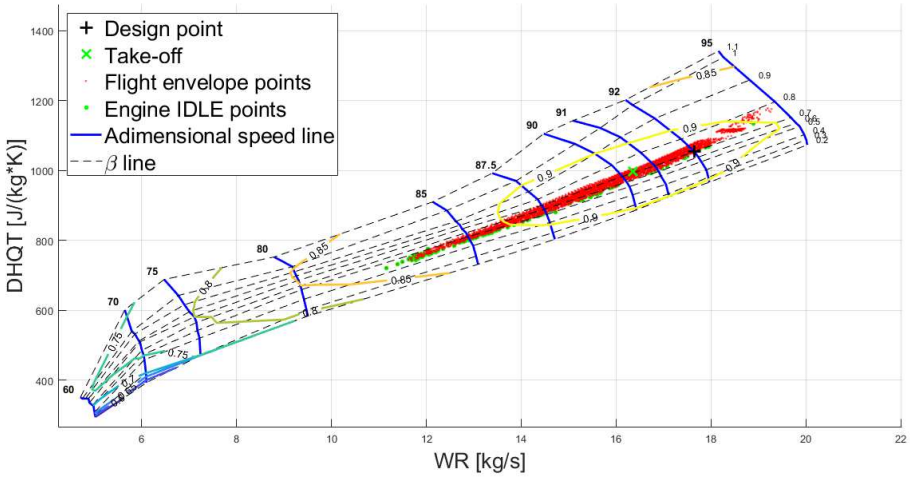

Figure 4.5: CFM56-7B24 HP compressor performance map.

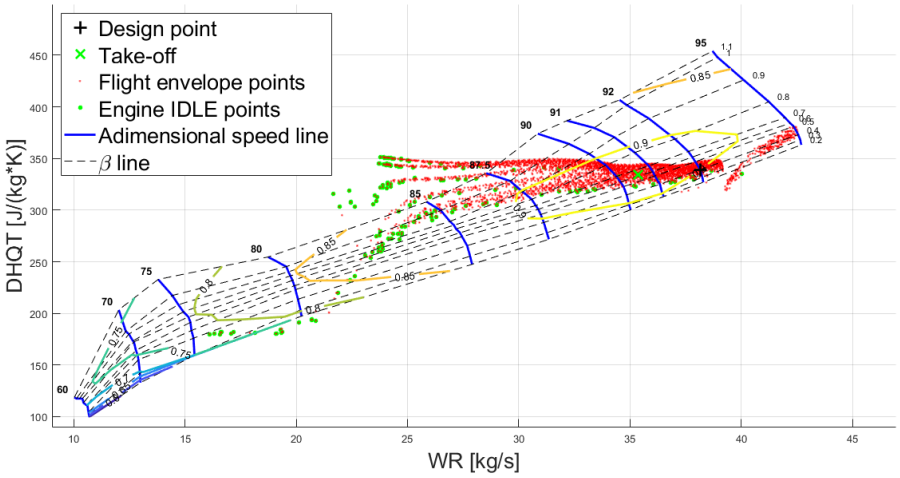

Figure 4.6: CFM56-7B24 LP compressor performance map.

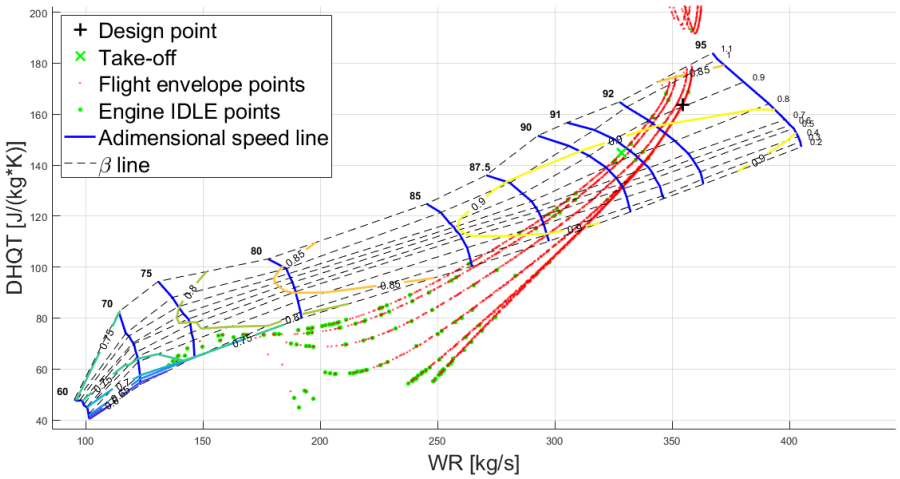

Figure 4.7: CFM56-7B24 Fan performance map.

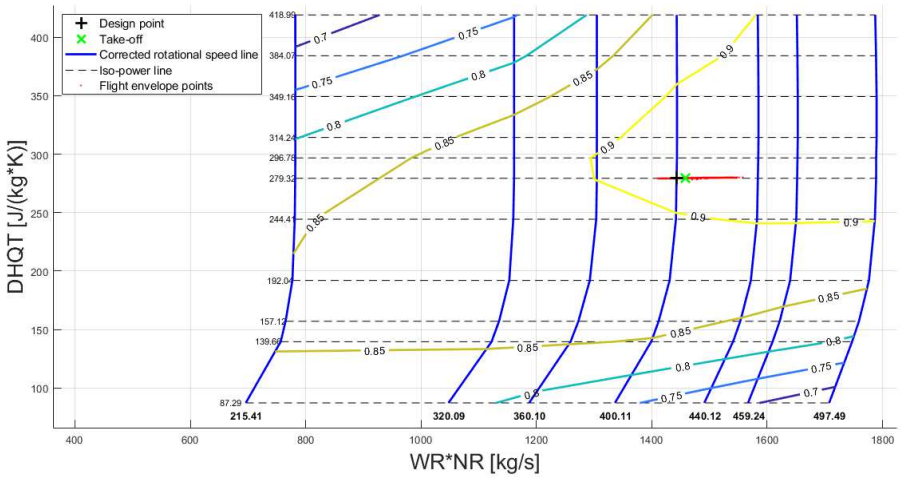

Figure 4.8: CFM56-7B24 HP turbine performance map.

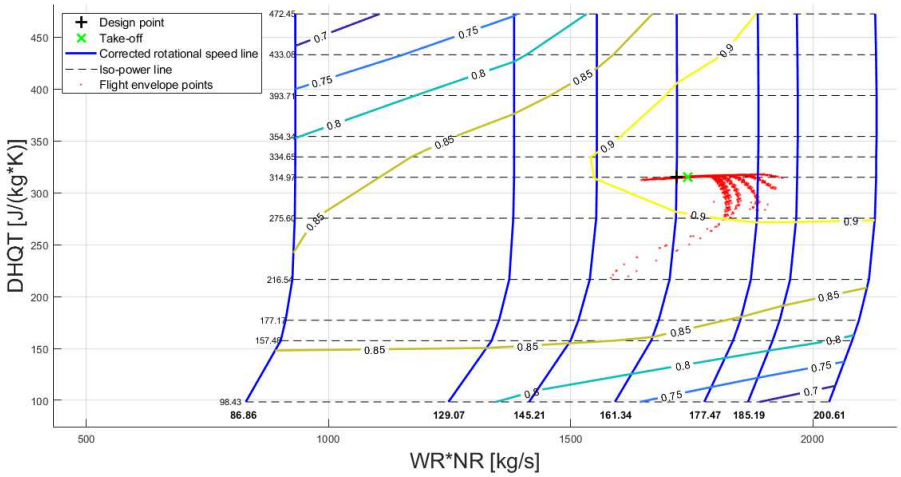

Figure 4.9: CFM56-7B24 LP turbine performance map.

In Figure 4.10 is represented the CFM56-7B24 engine map. The points are the all possible combinations of z, M and $\dot{m}_f$, but depending on their color it is possible to identify:

- black points, which represent combinations in which the calculations did not converge. Usually they are called invalid points;
- red points, which represent combinations in which the calculations converged. These points are outside of at least one engine performance map. Usually they are called wrong results;
- green points, which represent combinations in which the calculations converged.

These points are inside in all the performance maps and usually are called valid results.

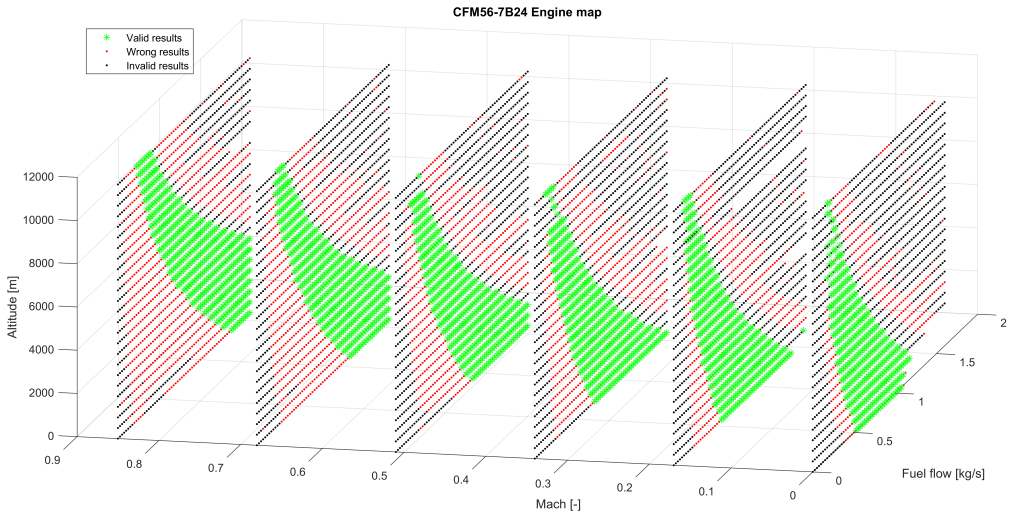

Figure 4.10: CFM56-7B24: Engine map with no extended results.

The engine map represented in Figure 4.10 can't be used in Matlab as engine model, because the engine rangeability is too low. The main problem is that the idle conditions have values of thrust too high. To solve it also the points outside the maps, but near the border, were considered. The result is an engine map with extended rangeability. This map is depicted in Figure 4.11. Remember that in this figure is represented a 3D plot in which each point is identified by its coordinates X (z), Y (M) and Z ($\dot{m}_f$), but each point has also saved inside the values of T_h, SFC, etc... .

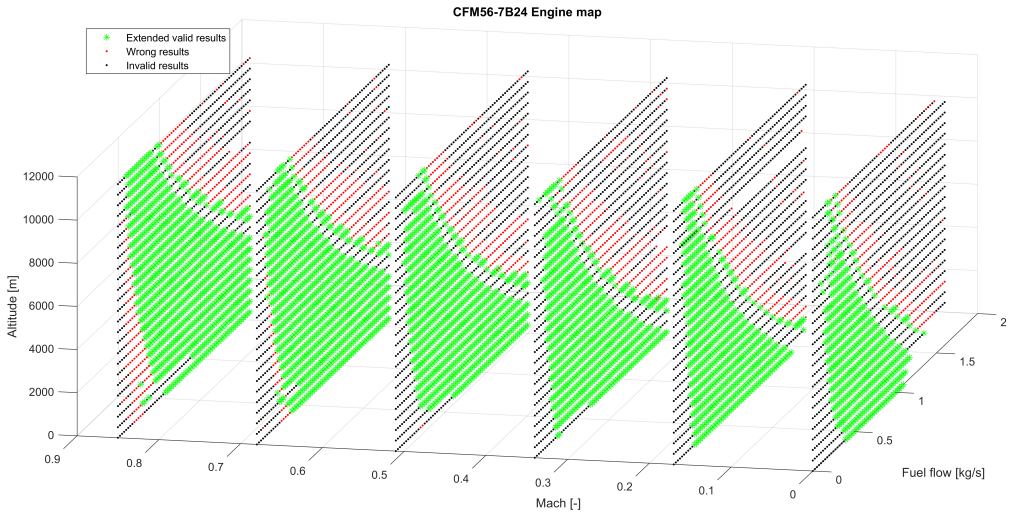

Figure 4.11: CFM56-7B24: Engine map with extended results.

To check and validate the results obtained, the plots in Figures 4.12 were created. These plots are for different values of z and each line is for different values of M. In the plots are represented the values of T_h vs $\dot{m}_f$. As expected from theory, the trend is not linear and in particular at high values of T_h to increase slightly T_h a huge increase of $\dot{m}_f$ is required. Moreover, increasing M at fix $\dot{m}_f$, T_h decreases, because ΔV in the thrust equation decreases. Note that for certain values of z and M the results are not so good, even if in general they are. This can be explained in two ways:

- the first explanation si connected to the fact that the initial variables provided to these groups of calculations were too far from the solution searched by the non-linear solver and so the calculation did not converge. Fortunally, this is not a big problem, because in Matlab the engine map is transofrmed in a cloud of interpolated values, so these values can be computed through interpolation;
- the second explanation is connected to the fact that CFM56-7B24 is an engine developed for short/medium range missions, so it is expected that it does not work well at high altitude. This is the case of Figure 4.12f.

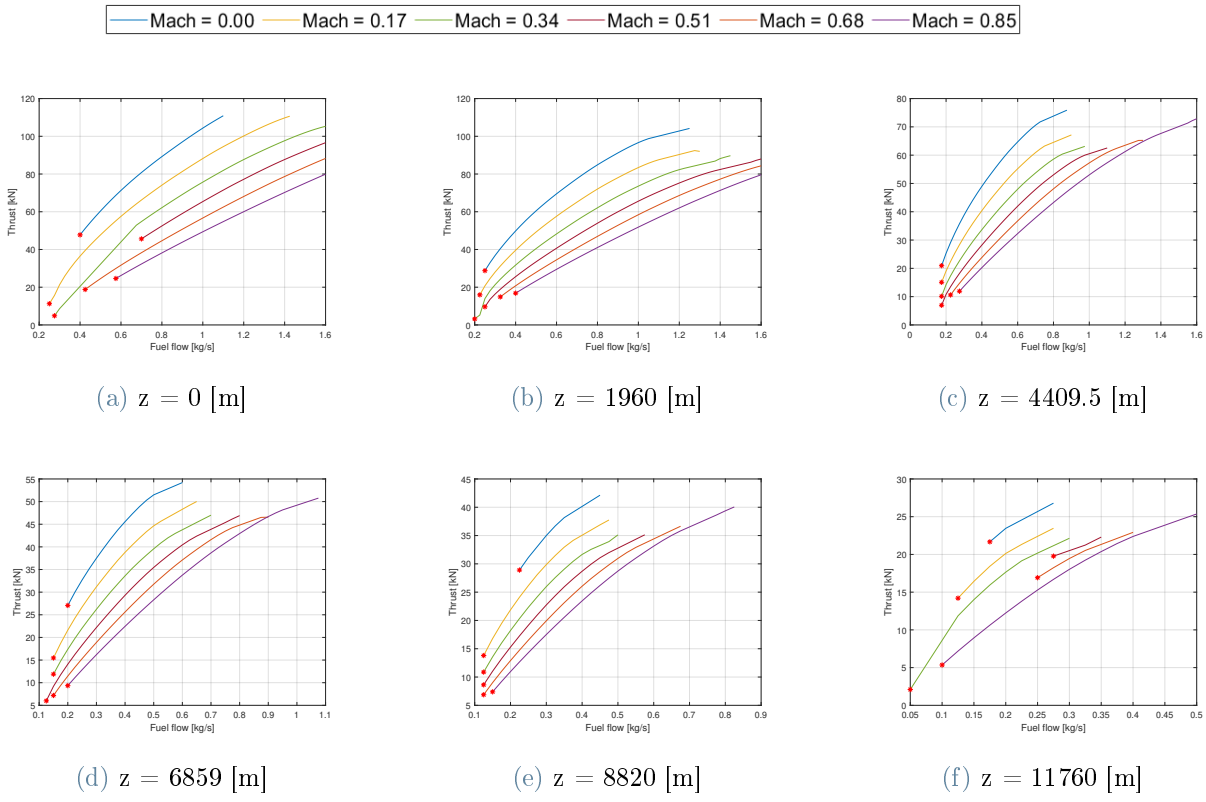

(a) z = 0 [m] (b) z = 1960 [m] (c) z = 4409.5 [m]

(d) z = 6859 [m] (e) z = 8820 [m] (f) z = 11760 [m]

Figure 4.12: Thrust vs Fuel flow plots of CFM56-7B24.

To validate the model also in off-design, from the engine map the values associated to take-off were extracted. Then, in the same way as what was done to validate the model in design condition (Sub-section 4.1.1) the results obtained from EcosimPro are compared to the ones obtained from Stefano's code [23]. The thermodynamic cycle obtained through his code is depicted in Figure 4.13, instead the results comparison can be seen in Figure 4.7.

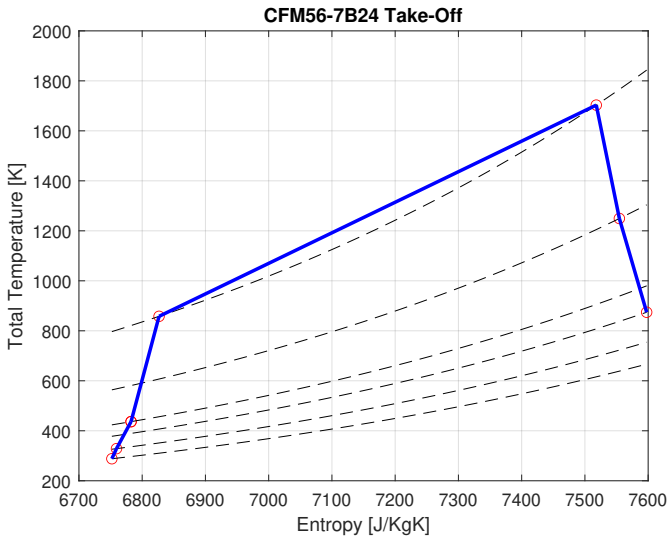

Figure 4.13: CFM56-7B24 thermodynamic cycle in take-off condition.

Component	EcosimPro Value	Matlab Value	Error [%]
Fan	13.51 [MW]	13.31 [MW]	+1.5
LP compressor	5.55 [MW]	5.44 [MW]	+2
HP compressor	21.83 [MW]	21.20 [MW]	+2.9
HP turbine	21.83 [MW]	23.29 [MW]	−6.7
LP turbine	19.06 [MW]	19.26 [MW]	−1.2

Table 4.7: CFM56-7B24 comparison between power components computed with EcosimPro and Matlab in take-off condition.

Also in off-design the model is validated, since the max absolute error is less than 7 % and the thermodynamic cycle has the typical shape of a turbofan cycle.

4.2. GEnx-1B64

Figure 4.14: GEnx-1B64.

The engine used as reference for the long mission range is GEnx-1B64. This is a turbofan engine developed and produced by General Electric aviation, which is a subsidiary of General Electric (GE). GE, which was founded in 1917, has the headquartered in Evendale, Ohio, and it is one of the major aeroengine producer in the world. The GEnx turbofan family is an advanced dual rotor, axial flow, high-bypass turbofan jet engine and it is the successor of the CF6 family [36]. These turbofans were chosen because are largely used by civil intercontinental aircrafts and also because its EcosimPro schematic (Figure 4.15) is identical to the one of CFM56. In this way, all the work done for the CFM56 in Section 4.1 can be recycled. From the all GEnx family, GEnx-1B64 was chosen because is the turbofan mounted on Boeign 787-800, which is the long range reference aricraft in this thesis. Moreover, in literature are present a lot of data [7] [36].

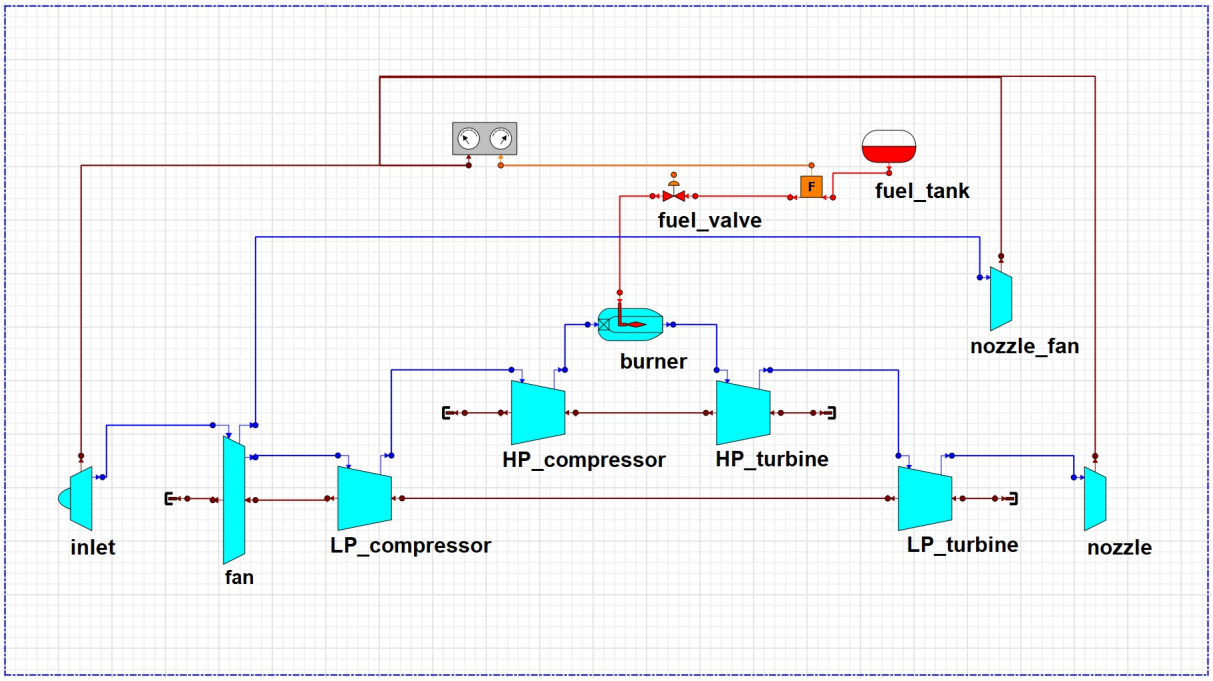

Figure 4.15: GEnx-1B64 schematic.

4.2.1. Engine design

The engine design procedure is identical to the one presented for CFM56-7B24 in Section 4.1, therefore in this section only the main aspects will be highlighted.
The main differences from the previous engine are the values of the boundary conditions and dynamic variables, which can be found respectively in Table 4.8 and 4.9. As before, the chosen design condition is the cruise also because this engine is designed for long range missions, so for sure its design point coincide with the cruise. With respect to CFM56-7B24 the GEnx-1B64 works at higher altitude and Mach, its BPR value is higher and since it is a bigger and more powerful engine also $\dot{m}_{in}$ and the overall pressure ratio are higher. Since GEnx-1B64 has a bigger fan, it has to rotate to a lower rotational speed in order to limit the transonic phenomena that occurs at the fan blade periphery.

Component	Variable	Value	Unit
Aircraft	z	12000	m
	M	0.85	-
Fan	BPR	8.53	-
	$\dot{N}$	0	$\frac{\text{rpm}}{\text{s}}$
	η_{is}	0.925	-
	N_{ad}	93	%
	β_c	1.45	-
	$beta$	0.9	-
LP compressor	η_{is}	0.925	-
	N_{ad}	92.5	%
	β_c	2.4	-
	$beta$	0.3	-
HP compressor	$\dot{m}_{in}$	45.7	$\frac{\text{kg}}{\text{s}}$
	$\dot{N}$	0	$\frac{\text{rpm}}{\text{s}}$
	η_{is}	0.925	-
	N_{ad}	92	%
	β_c	15	-
	$beta$	0.7	-
Burner	AL	3.5	$\frac{\text{kg}}{\text{s}\cdot\text{m}^3}$
	β_c	0.96	-
	$p_{T_{in}}$	2100000	Pa
	$T_{T_{in}}$	880	K
HP turbine	$L_{e_{NS}}$	1	$\frac{\text{J}}{\text{kg}\cdot\text{K}}$
	η_{is}	0.93	-
	N_{corr}^{NS}	1	$\frac{\text{r}}{\text{s}}$
	$T_{T_{in}}$	1480	K
LP turbine	L_e^{NS}	1	$\frac{\text{J}}{\text{kg}\cdot\text{K}}$
	η_{is}	0.93	-
	N_{corr}^{NS}	1	$\frac{\text{r}}{\text{s}}$

Table 4.8: GEnx-1B64 design: Boundary conditions. The blue values are known from literature [7] [35], instead the green ones are due to the fact that the simulation is steady.

Component	Variable	Value	Unit
LP compressor	N	2560	$\frac{\text{r}}{\text{min}}$
HP compressor	N	11377	$\frac{\text{r}}{\text{min}}$

Table 4.9: GEnx-1B64 design: Dynamic variables. The blue values are known from literature [36].

Once the engine design simulation is performed, it is possible to verify that the values of T_h and SFC obtained are very close to the real ones. These values are reported in Table 4.10. As expected from theory, with respect to CFM56-7B24 the value of T_h is higher and the value of SFC lower.

Variable	EcosimPro Value	Real engine Value	Error [%]
T_h	56.98 [kN]	56.80 [kN]	+0.3
SFC	$1.447e^{-05}$ $[\frac{\text{kg}}{\text{N·s}}]$	$1.369e^{-05}$ $[\frac{\text{kg}}{\text{N·s}}]$	+5.7

Table 4.10: GEnx-1B64 global performances comparison between the model and the real engine [7] in cruise condition.

At this point also the GEnx-1B64 schematic is designed, hence all the components data computed, so the off-design analysis can be performed.

4.2.2. Off-design analysis

To perform the off-design analysis and obtain the GEnx-1B64 engine map, the same procedure and codes used for the CFM56-7B24 were implemented. Hence, all the considerations done in Sub-section 4.1.2 are still valid. The main difference from the previous case is that now the input of the off-design simulation is the GEnx-1B64 model. Another important difference is that the values of z, M and $\dot{m}_f$, in which the engine is tested, are different, since the engine can reach higher altitude and Mach and it consumes more fuel. The GEnx-1B64 steady parametric simulation was performed for the all possible combinations of the following values:

- the z $[m]$ values considered are 0, 489.5, 979, 980, 1469.5, 1959, 1960, 2449.5, 2939, 2940, 3924.5, 3919, 3920, 4409.5, 4899, 4900, 5389.5, 5879, 5880, 6369.5, 6859, 6860,

7349.5, 7839, 7840, 8329.5, 8819, 8820, 9309.5, 9799, 9800, 10289.5, 10779, 10780, 11269.5, 11759, 11761, 12250.5, 12740;

- the M $[-]$ values considered are 0, 0.18, 0.36, 0.54, 0.72, 0.9;
- the $\dot{m}_f$ $[\frac{\text{kg}}{\text{s}}]$ values considered are 0, 0.0595, 0.1190, 0.1785, 0.2380, 0.2975, ..., 3.808.

The total off-design calculations performed are $39 \cdot 6 \cdot 65 = 15210$ and, as before, some of them converged instead other did not converge.

The results of the off-design simulation, in terms of points in the component performance maps, are reported in Figures 4.16, 4.17, 4.18, 4.19 and 4.20. It can be seen that the point trends are very similar to the ones of CFM56-7B24. Also in this case the problems arise in idle condition.

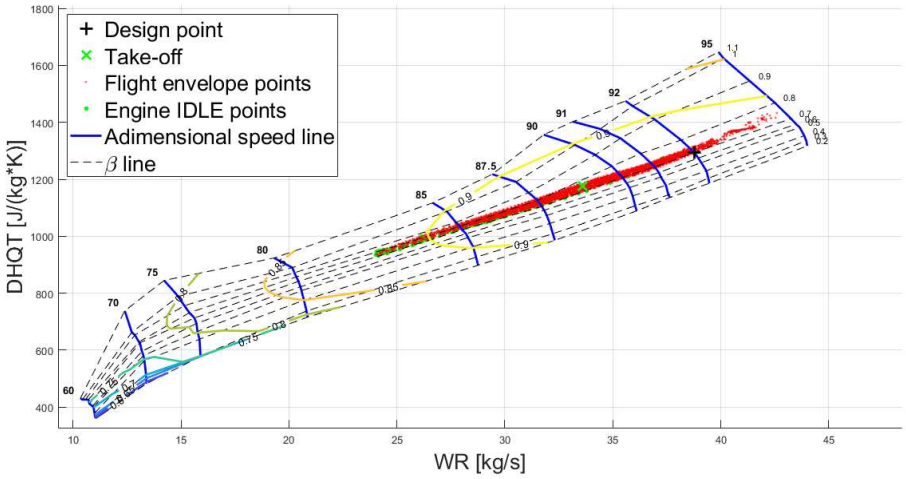

Figure 4.16: GEnx-1B64 HP compressor performance map.

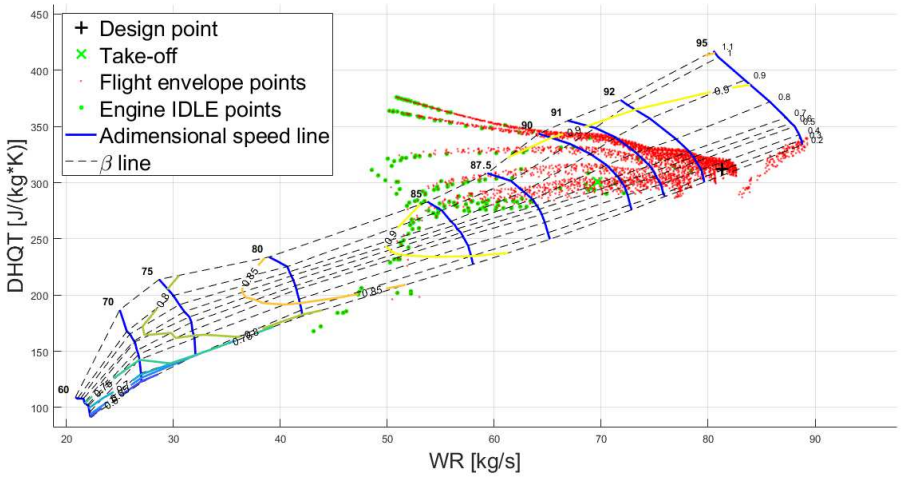

Figure 4.17: GEnx-1B64 LP compressor performance map.

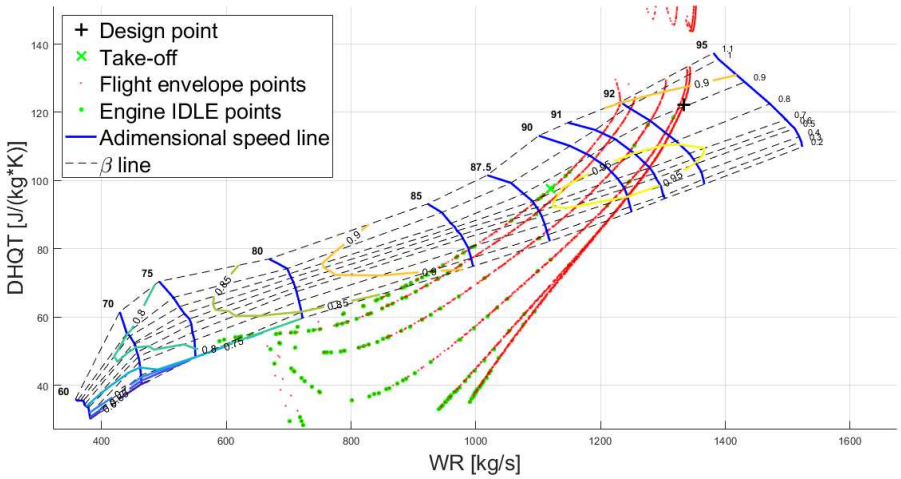

Figure 4.18: GEnx-1B64 Fan performance map.

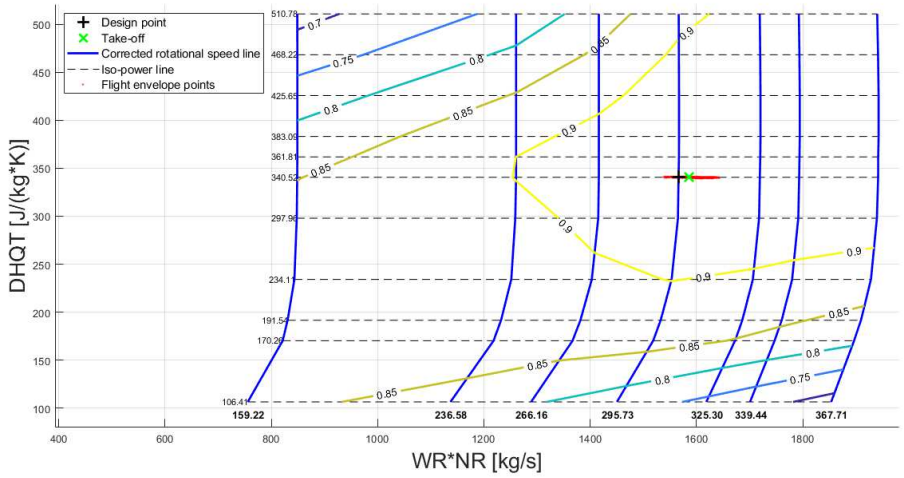

Figure 4.19: GEnx-1B64 HP turbine performance map.

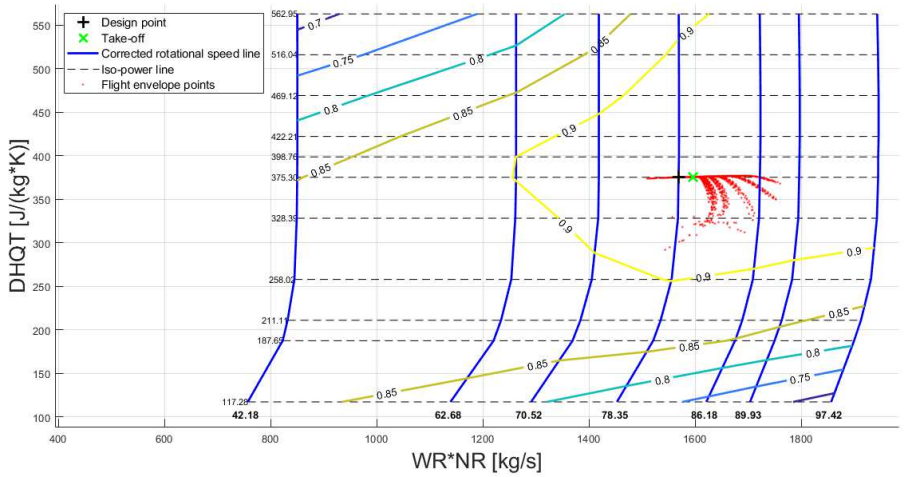

Figure 4.20: GEnx-1B64 LP turbine performance map.

Also the GEnx-1B64 engine map is similar to the one of the CFM56-7B24 (Figure 4.21), even if now the rangeability at low altitude and mach is worst. This fact could be explained knowning that this engine is designed to work mainly in cruise condition, hence it is reasonable to have a lower rangeability in off-design.

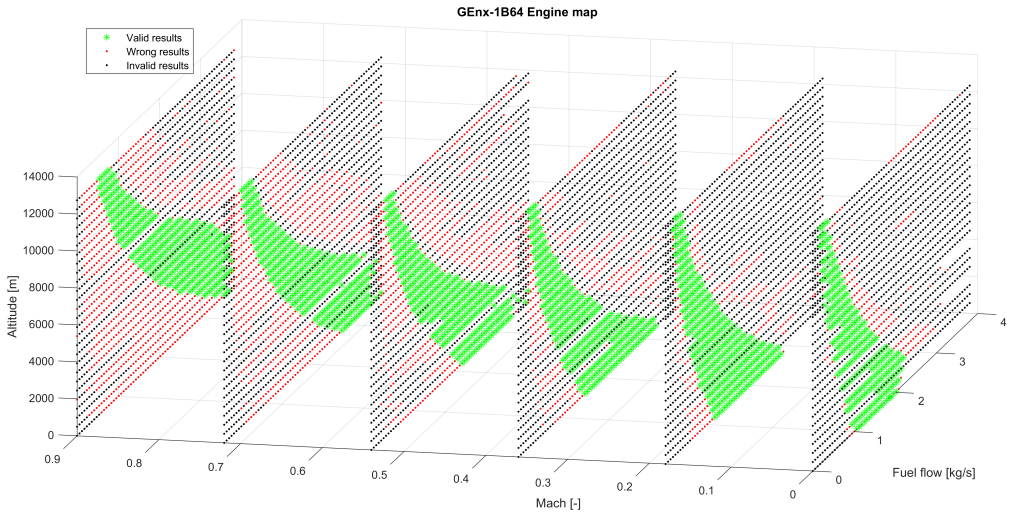

Figure 4.21: GEnx-1B64: Engine map with no extended results.

As before, in order to extend the rangeability, also the points outside the performance maps are considered valid. The result is shown in Figure 4.22.

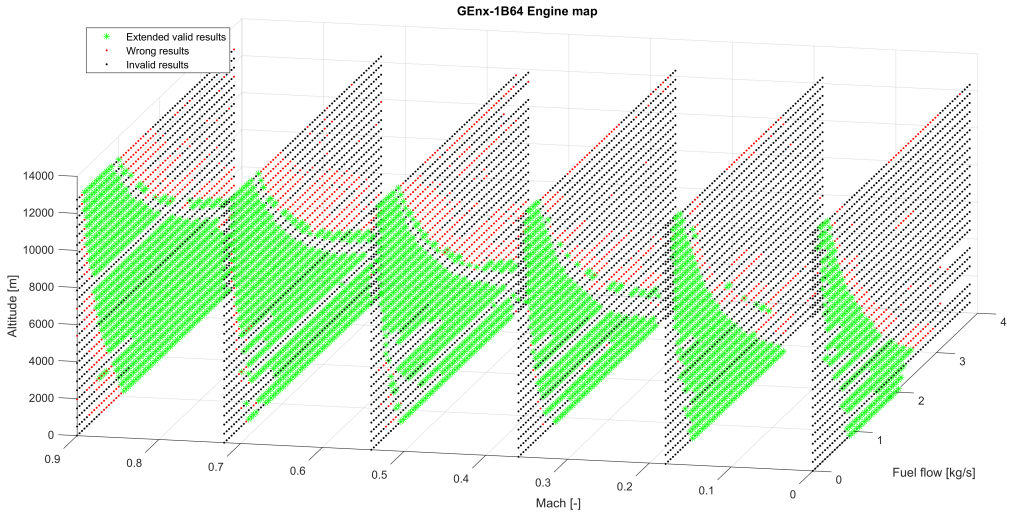

Figure 4.22: GEnx-1B64: Engine map with extended results.

Finally, the plots that show the T_h vs SFC at different values of z and M are reported in Figure 4.23. As expected, since this engine is designed for long range missions, the model converge easily at high z and M, instead at low z and M the results are less good.

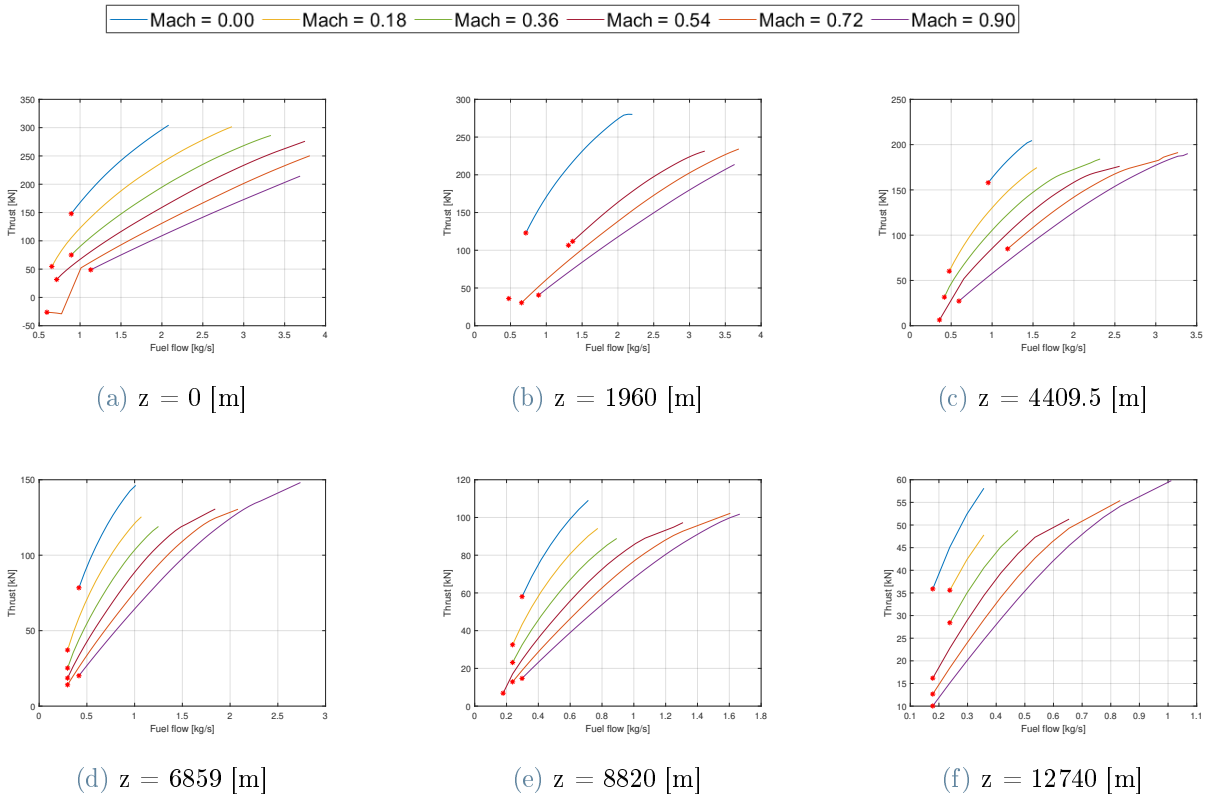

(a) z = 0 [m] (b) z = 1960 [m] (c) z = 4409.5 [m]

(d) z = 6859 [m] (e) z = 8820 [m] (f) z = 12740 [m]

Figure 4.23: Thrust vs Fuel flow plots of GEnx-1B64.

Now, both the reference turbofan engines are modeled and their model verified. In the engine maps are saved all the engine performances for a wide range of flight conditions. At this point the two engine maps, in form of tables, are added in Matlab. In the following chapter will be presented the same design and off-design analysis procedure, but applied to the CR fan engine.

5 | Electric counter-rotating fans modelling on EcosimPro

The aim of this chapter is to present the same modelling procedure described in Chapter 4, but applied to the electric CR fan case. All the concepts regarding the schematic, the design and off-design partitions generation, the design and off-design simulations, etc... are still valid and they will be used at first to design the electric CR fan schematics and then to obtain the engine maps.

Since this is a new engine typology, different models were modeled and for each of them an engine map obtained. In this way, it will be possible to test all these engine models in the various flight missions, hence obtain a comparison between them. The schematic used is the same for each model because the engine scheme is the same. The first subdivision is between the engine models designed for short and medium range missions, called HYB-CF1, and the engine models designed for long range missions, called HYB-CF2. The name is the abbreviation of hybrid (HYB) counter-rotating fan (CF) modeled for short and medium range missions (1) or long range missions (2). The second subdivision regards if these engines are designed in 2 engines configuration (2eng) or 10 engines configuration (10eng). So, for example there are the HYB-CF1-2eng and HYB-CF1-10eng engine models. The last subdivision regards the choice of the design point condition. Since the main electric CR fan paramters are the N_{ratio} and the P_{ratio}, the engine was designed for different combinations of these parameters. The different design points (DP) chosen are called DPref, DP1, DP2, DP3 and DP4 and are itemized in Table 5.1. So, for example, the models inside the group HYB-CF1-2eng are: HYB-CF1-2eng-DPref, HYB-CF1-2eng-DP1, HYB-CF1-2eng-DP2, HYB-CF1-2eng-DP3, HYB-CF1-2eng-DP4. All the possible electric CR fan models are 20 and are listed in Figure 5.1. Note that not all of them will be considered, but the reason will be explained later.

Variable	DPref	DP1	DP2	DP3	DP4
N_{ratio}	1	0.9	1.1	1	1
P_{ratio}	1	1	1	0.9	1.1

Table 5.1: Different design point conditions for the electric CR fan design.

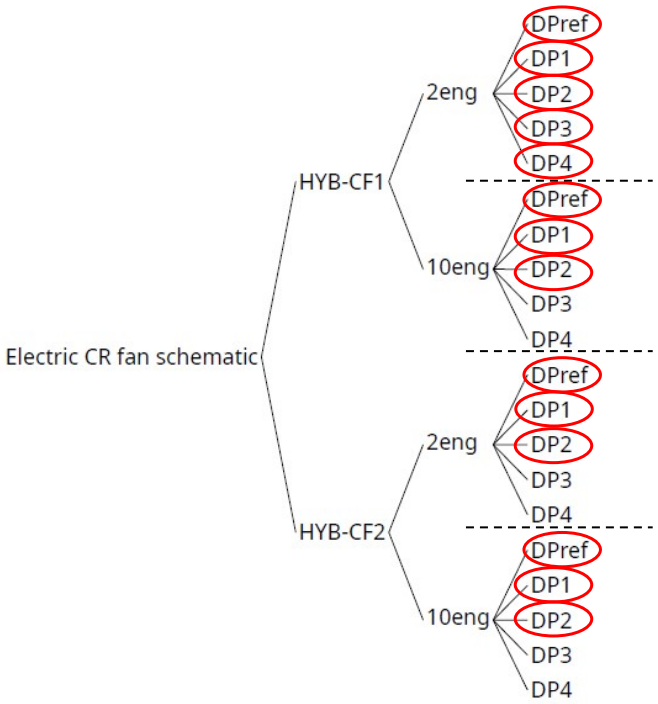

Figure 5.1: Scheme of the all possible electric CR fan models. Only the engine models inside the red circle will be analyzed in this chapter.

Component	Value	Unit
CR fan	$CG1$	-
	$CG2$	-
	$CG4$	-
	$CG5$	-
	$N_{D,FR}$	-
	N_{ratio}	-
Nozzle	$A_{CRN_{out}}$	m^2

Table 5.2: Electric CR fan data transformed in unknowns.

5.1. HYB-CF1

In Figure 5.2 is depicted the HYB-CF1 schematic. This engine is extremely simple, in fact the components are: inlet, electric CR fan, two electric engines (one for each shaft) and the outlet. Due to its simplicity, the components data transformed in unknowns in the design partition are only the ones in Table 5.2. As for the reference turbofan cases, these variables are mainly the performance map scaling factors and the nozzle area.

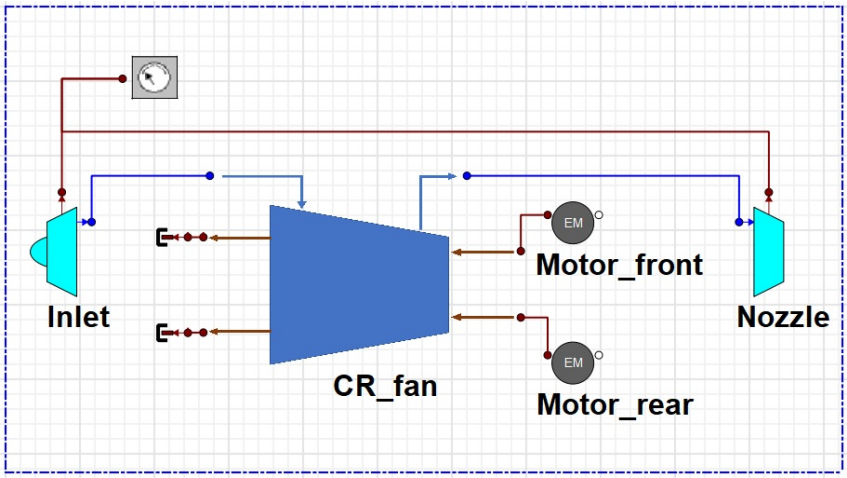

Figure 5.2: HYB-CF1 schematic.

5.1.1. Engine design: 2 engines configuration

The boundary conditions used for the five engines in the group HYB-CF1-2eng are reported in Table 5.3. All these engines were designed around the cruise point, in fact the values of z and M are the same of the CFM56-7B24 case. The value of $N_{D,FR}$ was chosen depending on what was found in the literature and the same was done for η_{is}. Instead, the values of β_c and $\dot{m}_{in}$ were selected in order to provide the same value of T_h of CFM56-7B24 in that flight condition. Note that, in order to reduce the power needed for a certain T_h, it was chosen a low value of β_c and so an high value of $\dot{m}_{in}$. This is in line with modern turbofans trend. Only N_{ratio} and P_{ratio} are different among these five design point conditions. In fact, changing N_{ratio} changes the perfomance map and torque ratio map selected, instead changing P_{ratio} changes the power split between the two shafts.

Component	Variable	DPref value	DP1 value	DP2 value	DP3 value	DP4 value	Unit
Aircraft	z	10668	10668	10668	10668	10668	m
	M	0.8	0.8	0.8	0.8	0.8	-
CR fan	η_{is}	0.92	0.92	0.92	0.92	0.92	-
	$N_{D,FR}$	5000	5000	5000	5000	5000	$\frac{\text{rpm}}{\text{s}}$
	N_{ratio}	1	0.9	1.1	1	1	-
	$N_{ad,FR}$	98	98	98	98	98	%
	β_c	1.2	1.2	1.2	1.2	1.2	-
	P_{ratio}	1	1	1	0.9	1.1	-
	$\dot{m}_{in}$	508	508	508	508	508	$\frac{\text{kg}}{\text{s}}$
	$beta$	0.7	0.7	0.7	0.7	0.7	-

Table 5.3: HYB-CF1-2eng: Boundary conditions for the five different design points.

The same approach used for the reference turbofans is now used to perform the design experiment of these five engine models. The results of these experiments are the components data.

The design experiment was already validated for CFM56-7B64 in Sub-section 4.1.1, instead the electric CR fan component needs to be validated. To do that, the compression power obtained from EcosimPro can be compared to the one computed with the adiabatic compressor power equation

$$P = \frac{\gamma \cdot p_{T_{in}} \cdot \dot{m}_{in}}{\rho_{in} \cdot (\gamma - 1)} \left[\beta_c^{\left(\frac{\gamma-1}{\gamma}\right)} - 1 \right]. \tag{5.1}$$

The results obtained, which are referred to the DPref design point, are reported in Table 5.4.

Component	EcosimPro Value	Equation Value	Error [%]
Electric CR fan	7.34 [MW]	6.74 [MW]	+8.9

Table 5.4: HYB-CF1-2eng-DPref: electric CR fan component validation through compression power comparison in cruise condition.

Even if the error is around 9%, the electrc CR fan can be considered validated, because

the equation used is referred to a simple adiabatic case. The error is attributed to the higher compression power needed in the case of a more realistic compressor. Moreover, another proof that this new component works, is given by the CFM56-7B24 fan power in the design (i.e. cruise) condition. In a turbofan most of the thrust is provided by the fan. Therefore the fan power should be less, but in the same order of magnitude of the one of the CR fan. As expected the fan power is 5.58 [MW], instead the CR fan power is 7.34 [MW].

Now, the five engine models HYB-CF1-2eng-DPref, HYB-CF1-2eng-DP1, HYB-CF1-2eng-DP2, HYB-CF1-2eng-DP3, HYB-CF1-2eng-DP4 are designed, so they can be used for the next step that is the off-design analysis.

5.1.2. Parametric off-design analysis: 2 engines configuration

The off-design analysis was performed in analogy with the one of CFM56-7B24. The steps to follow in order to obtain the engine maps for these five models are the same and the experiments were implemented in the same way. The values of z and M, in which these models were tested, are the ones of the CFM56-7B24 case. In fact, in both cases the flight missions considered are the short and medium. The main difference is that now the energy source is not the fuel, but the electricity, hence instead of $\dot{m}_f$ the other parameter is the total electric power (P) provided by the two electric engines.

The different values of P, in [MW], are 0, 0.1, 0.2, 0.3, 0.4, ..., 16. Therefore, the total number of the off-design calculations performed are $36 \cdot 6 \cdot 161 = 34776$. Remember that these off-design calculations were performed for each one of the five models considered. The results obtained in terms of performance points in the performance maps, are depicted in Figure 5.4. Remember also that each point in this map is the result of a single off-design calculation at a certain z, M and P. The results are reported only for HYB-CF1-2eng-DPref, HYB-CF1-2eng-DP1 and HYB-CF1-2eng-DP2, because the results obtained for HYB-CF1-2eng-DP3 and HYB-CF1-2eng-DP4 are identical to the ones of HYB-CF1-2eng-DPref. This fact was somehow exptected since the considered performance and torque ratio map change only between DPref, DP1 and DP2. The case DP3 and DP4 use the same DPref maps (the ones with $N_{ratio} = 1$) and boundary conditions, hence it is correct to have the same results. The only difference between DPref, DP3 and DP4 is the P_{ratio} value that is respectively 1, 0.9 and 1.1. Hence, even if for these three cases the torque ratio map used is the same, the off-design points are different, because the load in the two shafts is different (Figures 5.3). From these observations two important conclusions can be drawn:

- the first one is that from the electric CR fan model point of view, with the other boundary conditions fixed, the global performances depends only on N_{ratio} because is the variable that select which performance and torque ratio maps use;
- the second one is that, considering the same boundary conditions, the P_{ratio} modifies only the load distribution between the two shafts and not the value of the total P needed. Hence, considering the electric CR fan components like a black box described by inputs, maps and outputs, if the other boundary conditions and the maps used are the same also the results will be the same. The P_{ratio} parameter becomes useful when the electric engines have to be designed. In fact, knowing the values of power, torque and rotational speed in each shaft, it is possible to choose the correct electric engine and also understand if a gearbox is needed or not. This last part will not be analyzed in this thesis.

In order to confirm these two observations, in Sub-section 7.1.2 the short range flight mission will be performed also with the engines HYB-CF1-2eng-DP3 and HYB-CF1-2eng-DP4. It will be seen that the results obtained are identical to the ones obtained with the engine HYB-CF1-2eng-DPref. Therefore, except in that sub-section, the DP3 and DP4 cases will be not analyzed anymore.

Coming back to the analysis of Figures 5.4 and 5.3 it can be seen that the off-design points are well distributed inside both the performance and torque ratio maps. In the all cases the design point is in the region of higher efficiency. Like in the reference turbofan cases, also now the points that are outside the map border are the ones referred to the idle conditions. An important aspect to note is that the performance map of the DP1 case, so with $N_{ratio} = 0.9$, is scaled at higher efficiency values. This means that probably the CR fan engine HYB-CF1-2eng-DP1 will provide better results among the other CR fan engines during the flight missions.

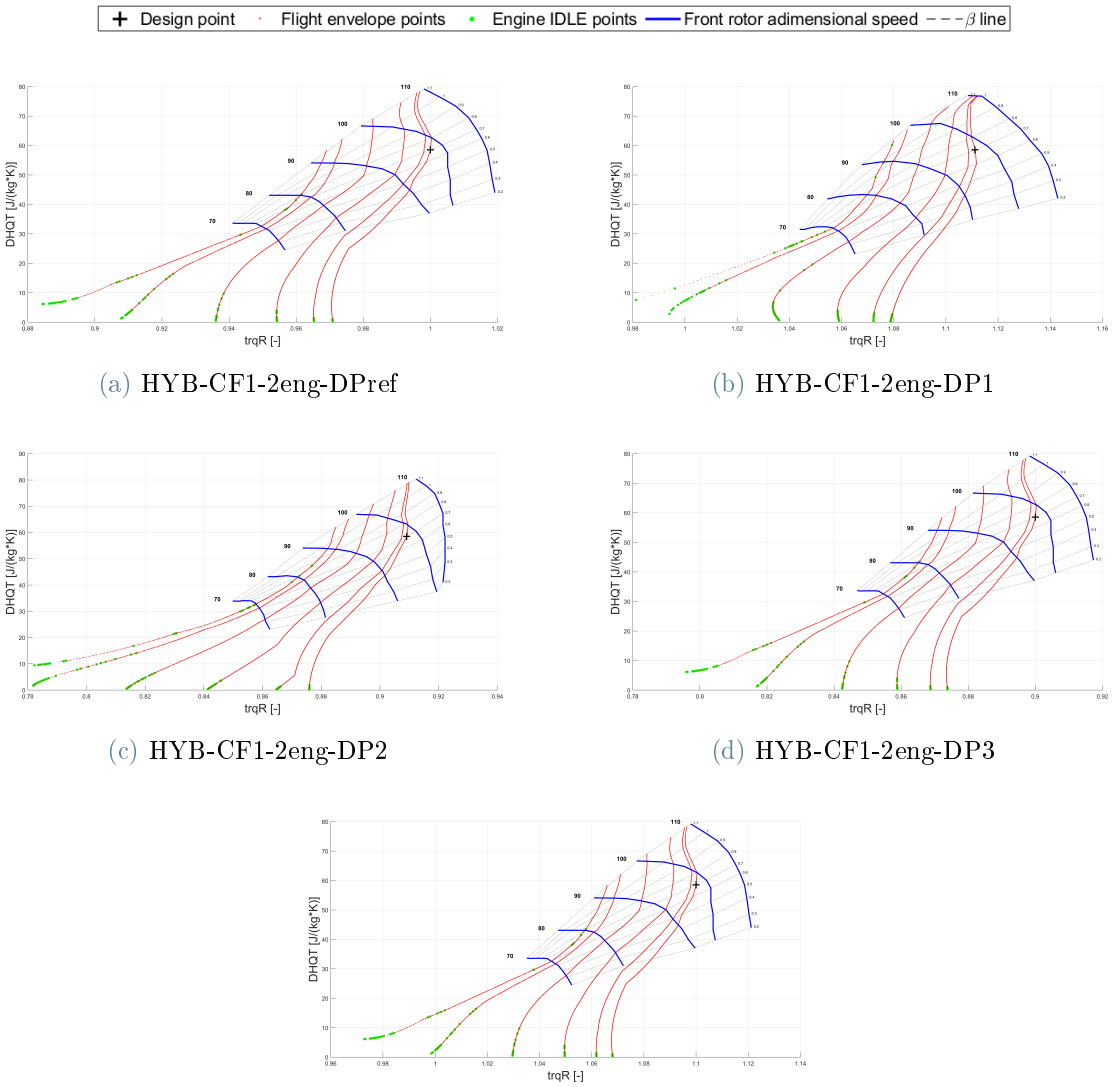

(a) HYB-CF1-2eng-DPref

(b) HYB-CF1-2eng-DP1

(c) HYB-CF1-2eng-DP2

(d) HYB-CF1-2eng-DP3

(e) HYB-CF1-2eng-DP4

Figure 5.3: CR fan engines HYB-CF1-2eng: torque ratio maps.

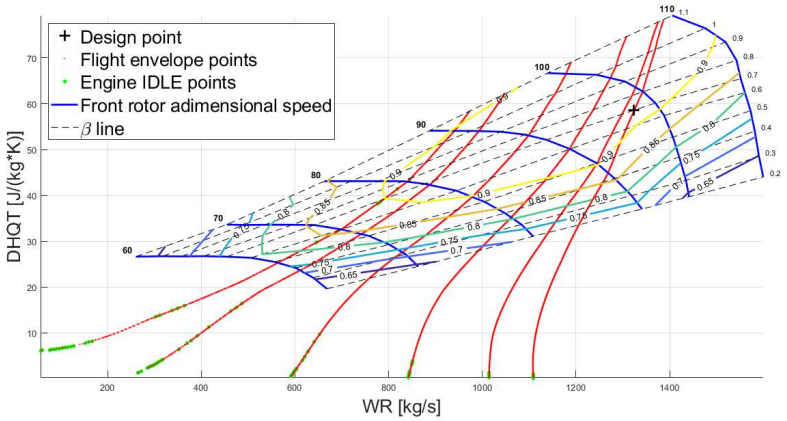

(a) HYB-CF1-2eng-DPref

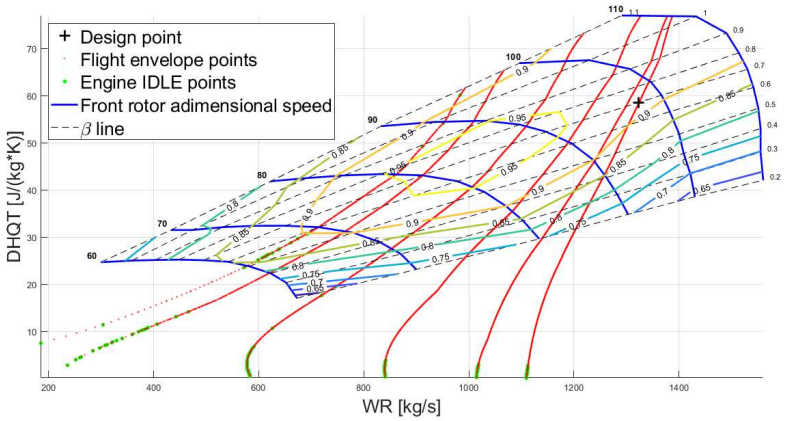

(b) HYB-CF1-2eng-DP1

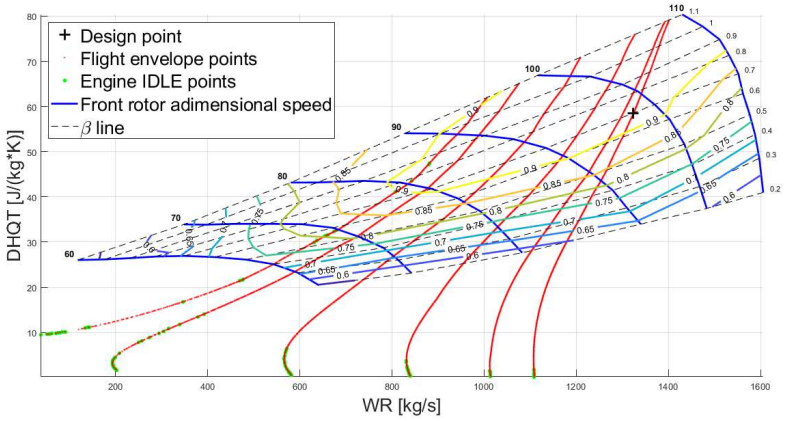

(c) HYB-CF1-2eng-DP2

Figure 5.4: CR fan engines HYB-CF1-2eng: performance maps. The performance maps of the CR fan engines HYB-CF1-2eng-DP3 and HYB-CF1-2eng-DP4 are not reported because they are identical to the one of the CR fan engine HYB-CF1-2eng-DPref.

In analogy with what was done for the reference turbofans, also in this case the engine maps are generated. In Figure 5.5 are represented the engine maps of HYB-CF1-2eng-DPref, HYB-CF1-2eng-DP1 and HYB-CF1-2eng-DP2. In can be noted that, in general, the CR fan rangeability is very high and this fact is confirmed also from the literature. Another important aspect is that, maybe due to the schematic simplicity, almost all the off-design calculations converged. For reasons not very well understood, but probably due to an internal problem in the EcosimPro solver, the invalid points are concentrated in the HYB-CF1-2eng-DP1 engine map at low M.

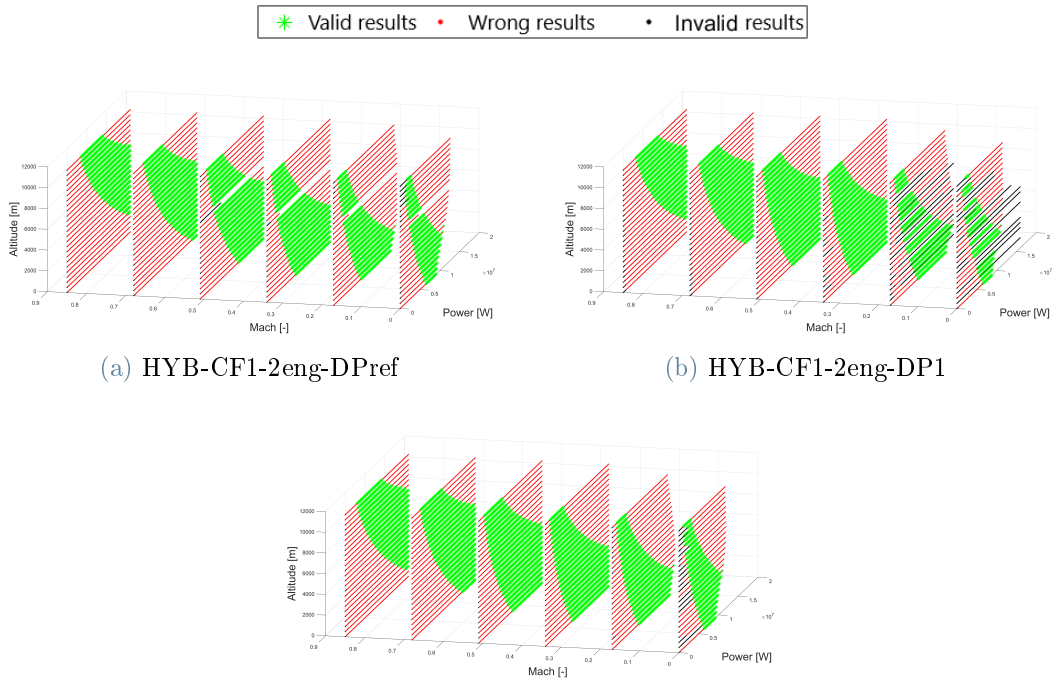

(a) HYB-CF1-2eng-DPref

(b) HYB-CF1-2eng-DP1

(c) HYB-CF1-2eng-DP2

Figure 5.5: HYB-CF1-2eng engine maps with no extended results.

For the same reason explained in the turbofan cases, it is possible to consider valid also points outside the maps. Since the CR fan rangeability is very high this passage is not mandatory. These extended engine maps were considered only because in some points of the flight mission the engine power is imposed equal to zero, therefore from these extended engine maps Matlab can compute the engine drag.

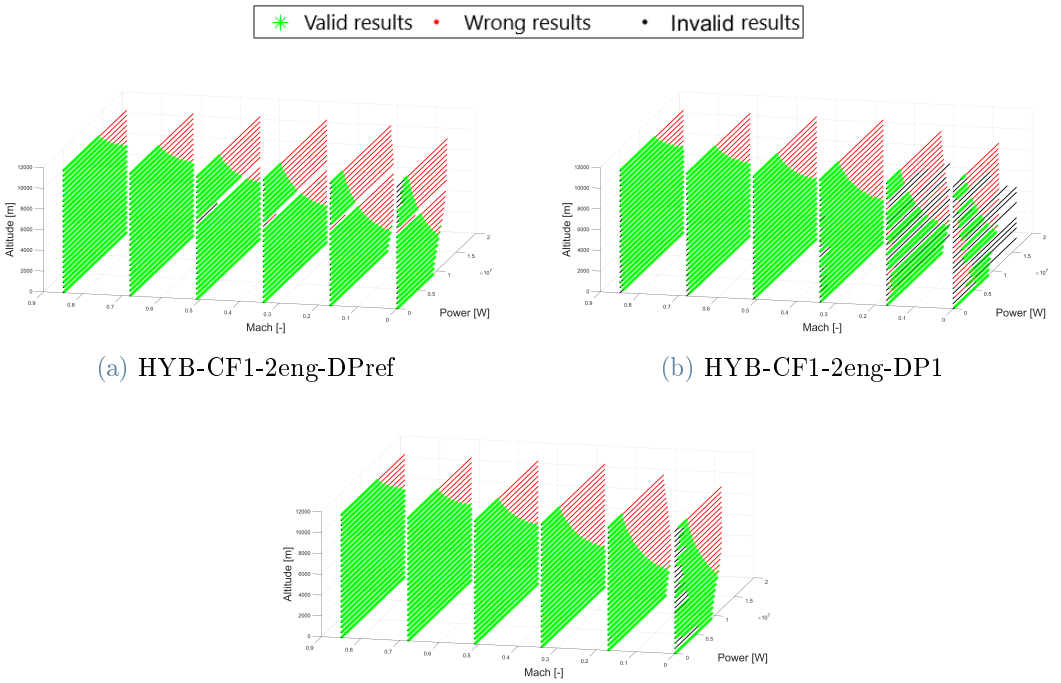

(a) HYB-CF1-2eng-DPref

(b) HYB-CF1-2eng-DP1

(c) HYB-CF1-2eng-DP2

Figure 5.6: HYB-CF1-2eng engine maps with extended results.

In order to validate in another way the electric CR fan component, the plots T_h vs P were generated for different values of z and M. To avoid useless complications, in Figure 5.7 only the results for the CR fan engine HYB-CF1-2eng-DPref were reported. The trend is as expected, in fact T_h reduces if z and M increase and this is an another proof that the CR fan component is well coded.

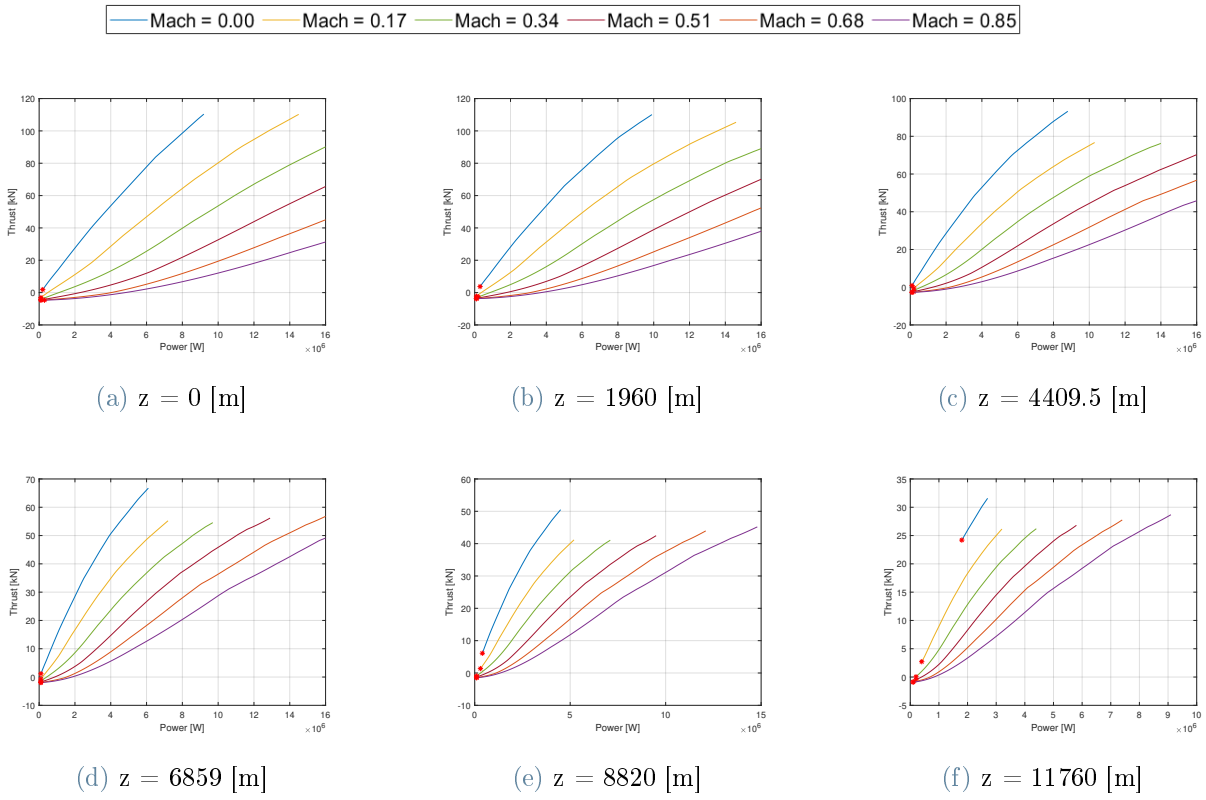

(a) z = 0 [m] (b) z = 1960 [m] (c) z = 4409.5 [m]

(d) z = 6859 [m] (e) z = 8820 [m] (f) z = 11760 [m]

Figure 5.7: HYB-CF1-2eng-DPref: Thrust vs Power plots.

To make a final check, as before, the CR fan compression power obtained in EcosimPro is compared to the one obtained with the Equation (5.1). The result is reported in Table 5.5. As expected, the compression power is lower in the adiabatic case, hence the electric CR fan component can be finally considered validated.

Component	EcosimPro Value	Equation Value	Error [%]
Electric CR fan	8.96 [MW]	8.1 [MW]	+9.6

Table 5.5: HYB-CF1-2eng-DPref: electric CR fan component validation through compression power comparison in take-off condition.

5.1.3. Engine design: 10 engines configuration

The same procedure used for the engine models HYB-CF1-2eng is applied now. The goal is to generate the engine maps for the engines HYB-CF1-10eng-DPref, HYB-CF1-10eng-DP1 and HYB-CF1-10eng-DP2 (Figure 5.1). As before, these engines are modeled in cruise condition and they will be used for short and medium range missions. The difference is

that the HYB-CF1-10eng are smaller because they will be mounted on the aircraft in a distributed propulsion configuration, with 10 engines in total. In order to highlight how the performances change by modifing only the engine numbers, the boundary conditions used are the same as in the HYB-CF1-2eng case. The only parameter that has to be changed is $\dot{m}_{in}$, because now the single engine generates less thrust.

The boundary conditions used are reported in Table 5.6. Note that, for the reasons explained in Sub-section 5.1.2, the HYB-CF1-10eng-DP3 and HYB-CF1-10eng-DP4 will be not analyzed.

Component	Variable	DPref value	DP1 value	DP2 value	Unit
Aircraft	z	10668	10668	10668	m
	M	0.8	0.8	0.8	-
CR fan	η_{is}	0.92	0.92	0.92	-
	$N_{D,FR}$	5000	5000	5000	$\frac{\text{rpm}}{\text{s}}$
	N_{ratio}	1	0.9	1.1	-
	$N_{ad,FR}$	98	98	98	%
	β_c	1.2	1.2	1.2	-
	P_{ratio}	1	1	1	-
	$\dot{m}_{in}$	101.8	101.8	101.8	$\frac{\text{kg}}{\text{s}}$
	$beta$	0.7	0.7	0.7	-

Table 5.6: HYB-CF1-10eng: Boundary conditions for the three different design points.

5.1.4. Parametric off-design analysis: 10 engines configuration

Once the engine models HYB-CF1-10eng-DPref, HYB-CF1-10eng-DP1 and HYB-CF1-10eng-DP2 are designed, the off-design analysis for each of them can be performed. The off-design calculations will be done for the same values of z and M of the CR fan engines HYB-CF1-2eng, since the associated flight missions are the same, but with different values of P because the engines are less powerful. The P values considered for that case, in [MW], are 0, 0.1, 0.2, 0.3, ..., 3.2. Therefore, the total number of calculations is less and its number is $36 \cdot 6 \cdot 33 = 7128$.

The results in terms of performance maps and torque ratio maps are reported respectively in Figures 5.9 and 5.8. These results are very similar to ones obtained for the HYB-CF1-2eng engine models, even if now the map scaling factors are different. Also in this case

it is confirmed the fact that the perfromance map of the engine HYB-CF1-10eng-DP1 presents higher values of efficiency.

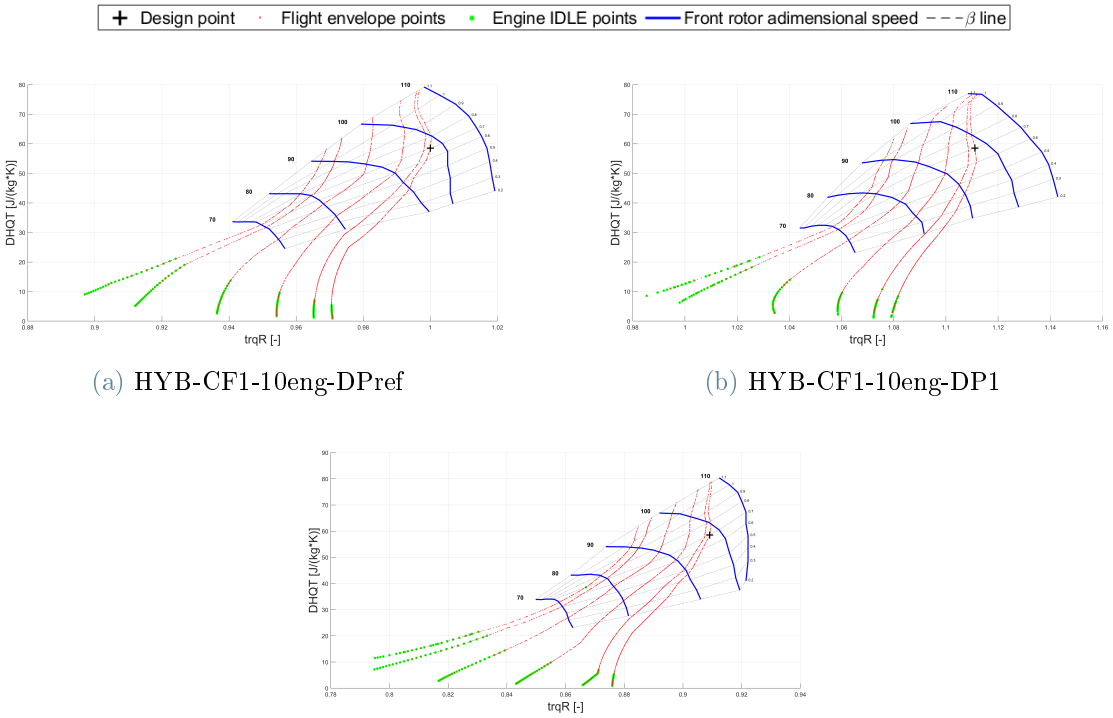

(a) HYB-CF1-10eng-DPref

(b) HYB-CF1-10eng-DP1

(c) HYB-CF1-10eng-DP2

Figure 5.8: CR fan engines HYB-CF1-10eng: torque ratio maps.

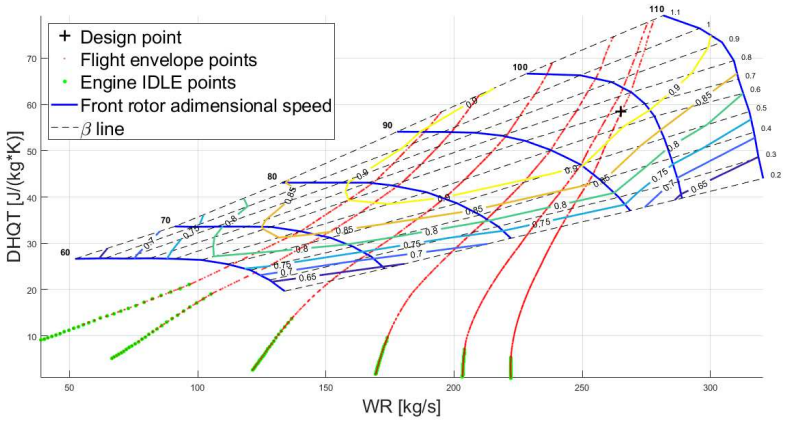

(a) HYB-CF1-10eng-DPref

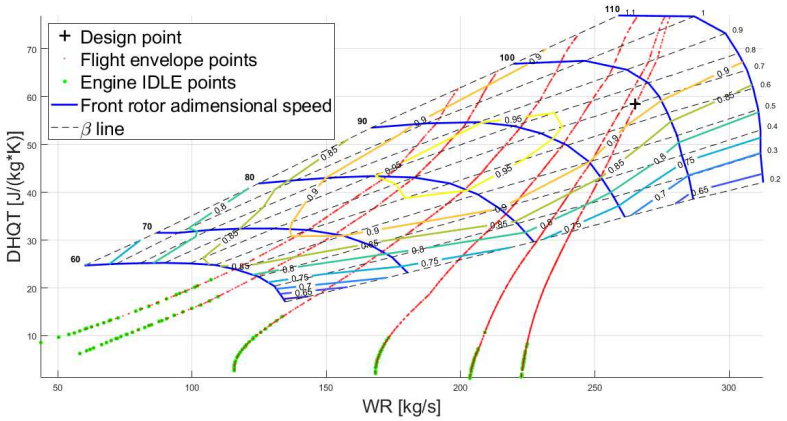

(b) HYB-CF1-10eng-DP1

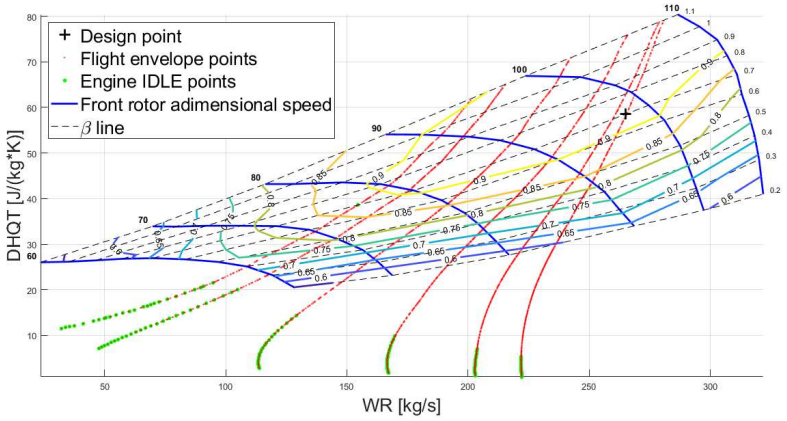

(c) HYB-CF1-10eng-DP2

Figure 5.9: CR fan engines HYB-CF1-10eng: performance maps.

In Figures 5.10 are represented the engine maps of HYB-CF1-10eng-DPref, HYB-CF1-10eng-DP1 and HYB-CF1-10eng-DP2. This are similar to the ones obtained for the CR

fan engines HYB-CF1-2eng. The main difference is that now the number of the off-design calculations that did not converge is less.

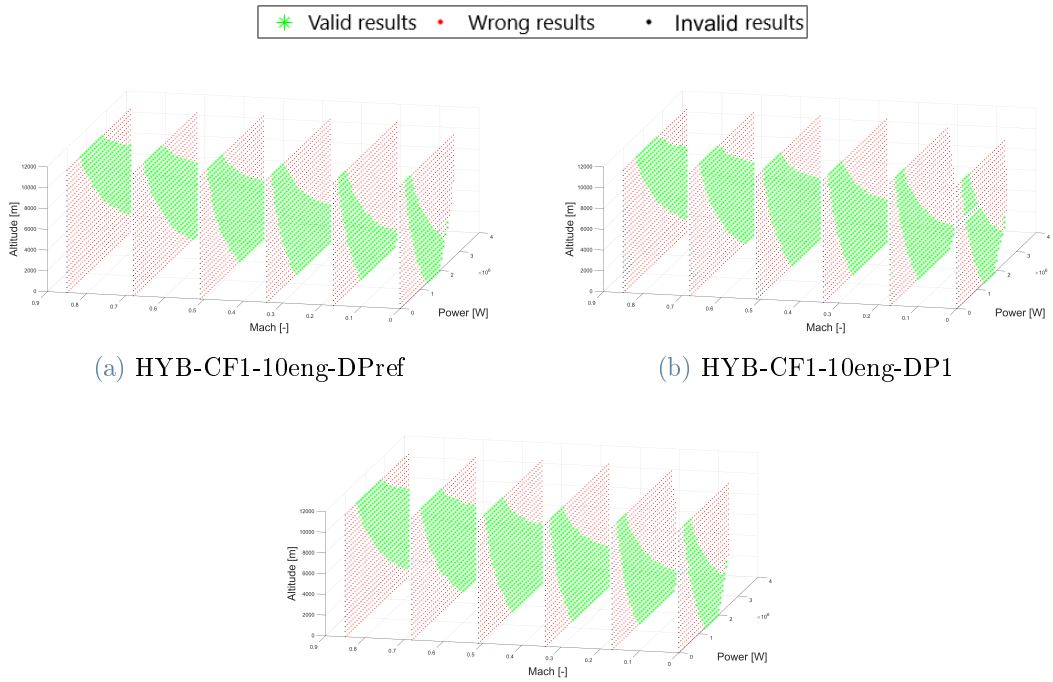

(a) HYB-CF1-10eng-DPref

(b) HYB-CF1-10eng-DP1

(c) HYB-CF1-10eng-DP2

Figure 5.10: HYB-CF1-10eng engine maps with no extended results.

5.2. HYB-CF2

In this section the design and off-design results obtained for the engine models HYB-CF2 will be presented. This section is structured in the same way as Section 5.2 and also the same procedures to design the models and test them in off-design conditions are used. In the HYB-CF2 group there are all the engine models designed for long range missions (Figure 5.1). Therefore, in this case the reference turbofan is the GEnx-1B64. The engine schematic is the same as HYB-CF1 and it is depicted in Figure 5.11. As before, initially the CR fan engines HYB-CF2 will be designed and tested in 2 engines configuration (Sub-sections 5.2.1 and 5.2.2) and then in 10 engines configuration (Sub-sections 5.2.3 and 5.2.4). At the end of this section the engine maps of the CR fan engines HYB-CF2-2eng-DPref, HYB-CF2-2eng-DP1, HYB-CF2-2eng-DP2, HYB-CF2-10eng-DPref, HYB-CF2-10eng-DP1 and HYB-CF2-10eng-DP2 will be obtained.

The reader should have noted that in this thesis the structure of the design/off-design partitions and the implementation of the design/off-design simulations is the same for all the engines analyzed (CFM56-7B24, GEnx-1B64, HYB-CF1-2eng-DPref, ..., HYB-CF1-

10eng-DPref, ..., HYB-CF2-2eng-DPref, ..., HYB-CF2-10eng-DPref,..., HYB-CF2-10eng-DP2). The idea was to develop a general procedure to follow in order to perform different engine design and off-design analysis, changing only the boundary conditions and the schematic (if needed).

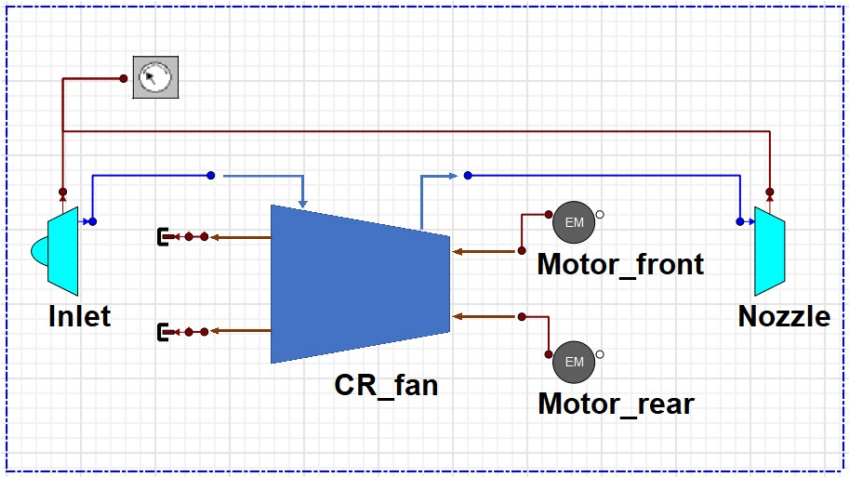

Figure 5.11: HYB-CF2 schematic.

5.2.1. Engine design: 2 engines configuration

The design point condition is still the cruise and the boundary conditions used to design the CR fan engines HYB-CF2-2eng-DPref, HYB-CF2-2eng-DP1 and HYB-CF2-2eng-DP2 are reported in Table 5.7. The values of z and M are equal to the ones used for GEnx-1B64, because the flight mission is the same (long range). The values of η_{is} and $N_{D,FR}$ were imposed equal to ones of the HYB-CF1 case, since there is no a specific reason to change them. Instead, after some tests, it was chosen to change the $N_{ad,FR}$ value to obtain better results in terms of calculation convergences. β_c and $\dot{m}_{in}$ were selected in order to provide the same thrust of GEnx-1B64. The phylosophy to have an engine with an high value of $\dot{m}_{in}$ and a low value of β_c is applied also in this case, even if the value of β_c is higher with respect the HYB-CF1 case. This choice is due to the fact that the thrust that this engine has to provide is very high. Therefore, to limit the engine size, since the value of $\dot{m}_{in}$ can't be too high, an higher value of β_c was chosen.

Component	Variable	DPref value	DP1 value	DP2 value	Unit
Aircraft	z	12000	12000	12000	m
	M	0.85	0.85	0.85	-
CR fan	η_{is}	0.92	0.92	0.92	-
	$N_{D,FR}$	5000	5000	5000	$\frac{\text{rpm}}{\text{s}}$
	N_{ratio}	1	0.9	1.1	-
	$N_{ad,FR}$	95	95	95	%
	β_c	1.4	1.4	1.4	-
	P_{ratio}	1	1	1	-
	$\dot{m}_{in}$	680	680	680	$\frac{\text{kg}}{\text{s}}$
	$beta$	0.7	0.7	0.7	-

Table 5.7: HYB-CF2-2eng: Boundary conditions for the three different design points.

The three engine design simulations can be performed, hence the CR fan engine models HYB-CF2-2eng-DPref, HYB-CF2-2eng-DP1 and HYB-CF2-2eng-DP2 are obtained.

5.2.2. Parametric off-design analysis: 2 engines configuration

At this point, the off-design analysis for these three engines can be performed, hence the engine map for each of them obtained. The off-design calculations were performed for values different from the HYB-CF1 case, because the flight mission considered is different. The values of z and M are the same used for the GEnx-1B64 case, instead the values of P, in [MW] are 0, 0.406250, 0.8125, 1.21875, ..., 65. Therefore the total number of calculations done for each steady parametric simulation is $39 \cdot 6 \cdot 161 = 37674$.

From Figures 5.12 and 5.13 it can be seen that in this case the off-design points follow a more clear path and most of them are located in the high efficiency region. Note that, again, the HYB-CF2-2eng-DP1 performance map is the one with the higher values of efficiency.

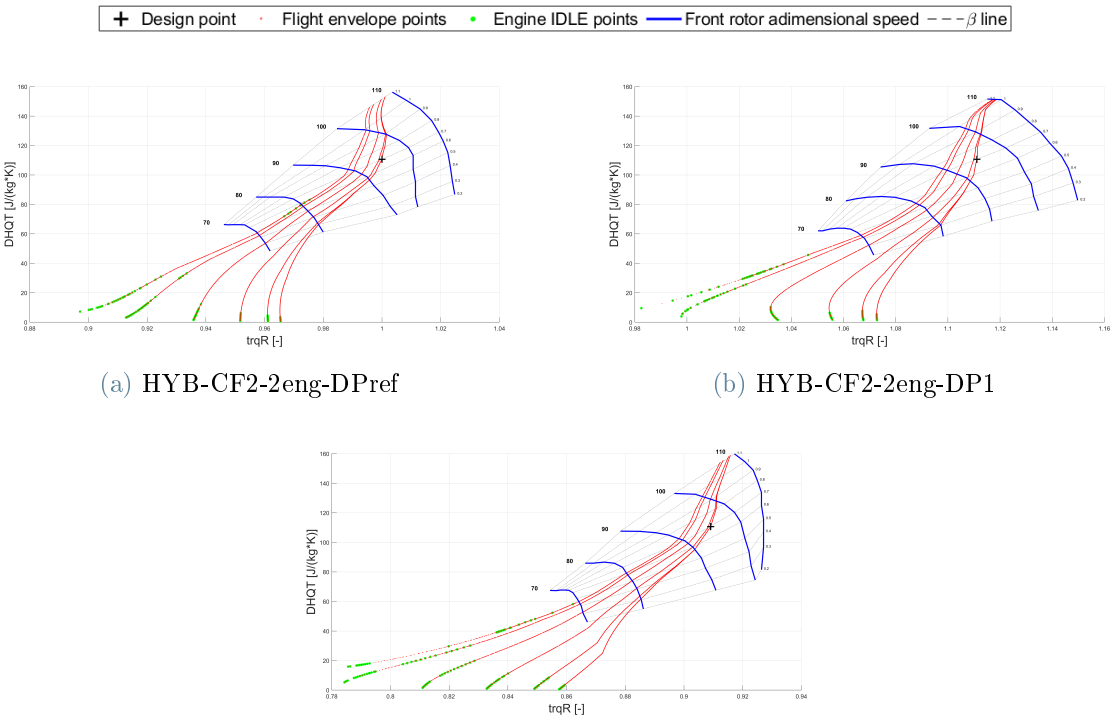

(a) HYB-CF2-2eng-DPref

(b) HYB-CF2-2eng-DP1

(c) HYB-CF2-2eng-DP2

Figure 5.12: CR fan engines HYB-CF2-2eng: torque ratio maps.

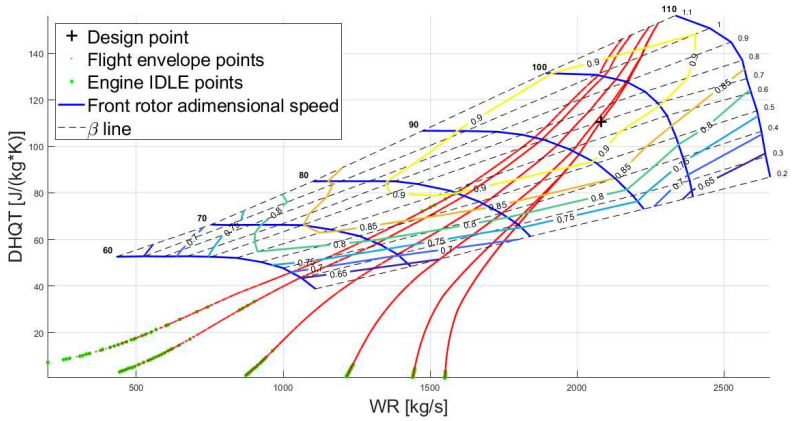

(a) HYB-CF2-2eng-DPref

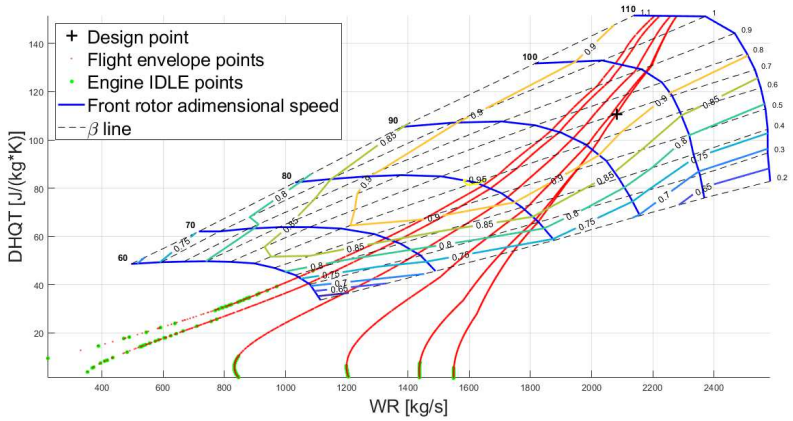

(b) HYB-CF2-2eng-DP1

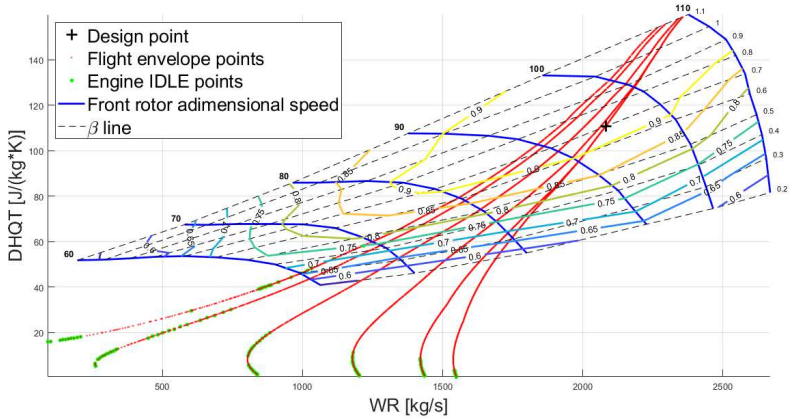

(c) HYB-CF2-2eng-DP2

Figure 5.13: CR fan engines HYB-CF2-2eng: performance maps.

The engine maps obtained for these three engines present a very high rangeability, confirming also in this case one of the main advantages of CR fans.

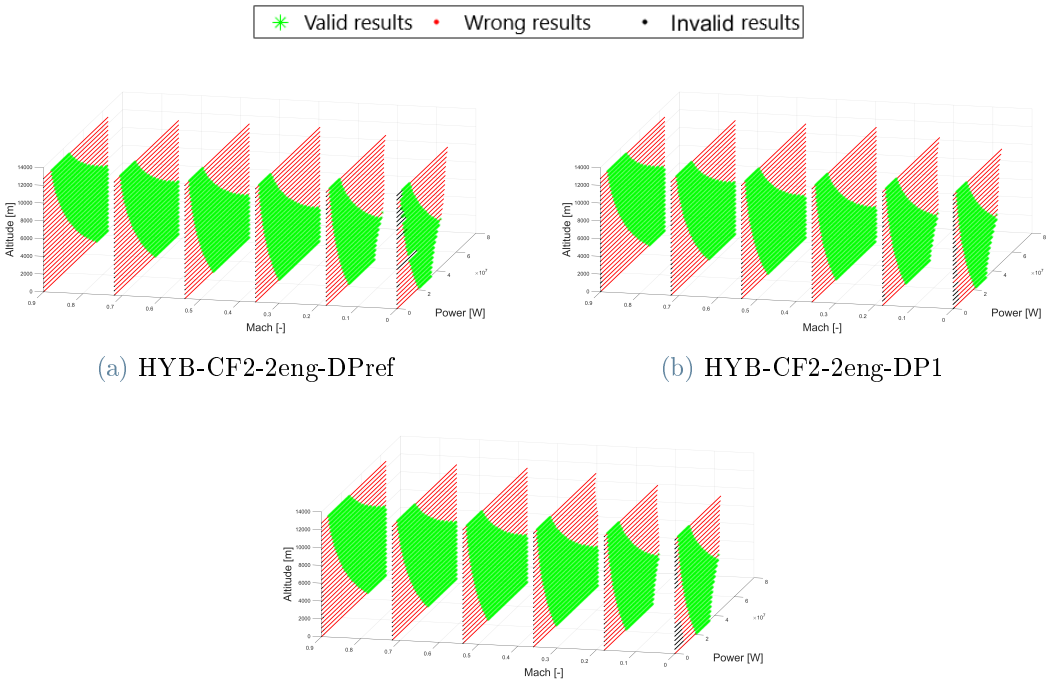

(a) HYB-CF2-2eng-DPref

(b) HYB-CF2-2eng-DP1

(c) HYB-CF2-2eng-DP2

Figure 5.14: HYB-CF2-2eng engine map with no extended results.

5.2.3. Engine design: 10 engines configuration

The last CR fan engines modeled are HYB-CF2-10eng-DPref, HYB-CF2-10eng-DP1 and HYB-CF2-10eng-DP2. The boundary conditions chosen are the ones in Table 5.8. As for the engines HYB-CF2-2eng, also these ones are designed for long range missions, hence the values of z and M are the same as before. The difference is that these engines are smaller because they will be mounted in the aircraft in a distributed propulsion configuration. Therefore, the values of β_c and $\dot{m}_{is}$ has to be changed with respect the HYB-CF2-2eng case. β_c was chosen as small as possible in order to have the highest propulsive efficiency, but at the same time big enough to limit $\dot{m}_{in}$, hence the engine size.

Component	Variable	DPref value	DP1 value	DP2 value	Unit
Aircraft	z	12000	12000	12000	m
	M	0.85	0.85	0.85	-
CR fan	η_{is}	0.92	0.92	0.92	-
	$N_{D,FR}$	5000	5000	5000	$\frac{\text{rpm}}{\text{s}}$
	N_{ratio}	1	0.9	1.1	-
	$N_{ad,FR}$	95	95	95	%
	β_c	1.3	1.3	1.3	-
	P_{ratio}	1	1	1	-
	$\dot{m}_{in}$	170	170	170	$\frac{\text{kg}}{\text{s}}$
	$beta$	0.7	0.7	0.7	-

Table 5.8: HYB-CF2-10eng: Boundary conditions for the three different design points.

Once the boundary conditions are added to the design experiments, the three CR fan engine models can be designed, hence their components data obtained.

5.2.4. Parametric off-design analysis: 10 engines configuration

Also for these three CR fan engines the steady parametric simulations were performed. The values of z and M considered are the same as before, but now the engines are less powerful. Therefore the new values of P, in [MW], considered are 0, 0.156250, 0.3125, 0.46875, ... 10. The number of the off-design calculations are $39 \cdot 6 \cdot 65 = 15210$. The off-design points obtained are represented in the torque ratio and performance maps respectively in Figures 5.15 and 5.16. The results are very similar to the ones obtained with the 2 engines configuration and as for the previous cases the engine with the highest value of efficiency is the one with $N_{ratio} = 0.9$. The conclusion that can be drawn is that the map associated to $N_{ratio} = 0.9$ is the one that provides the best performances. This conclusion will be confirmed also in Chapter 7, when the flight missions will be analyzed.

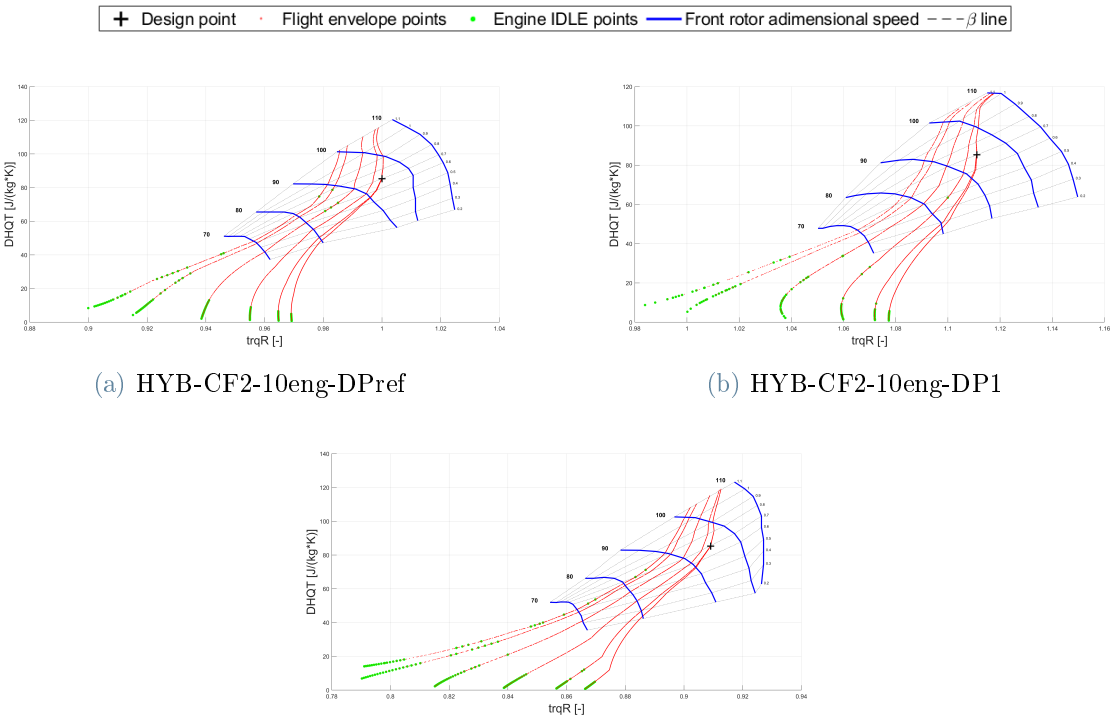

(a) HYB-CF2-10eng-DPref

(b) HYB-CF2-10eng-DP1

(c) HYB-CF2-10eng-DP2

Figure 5.15: CR fan engines HYB-CF2-10eng: torque ratio maps.

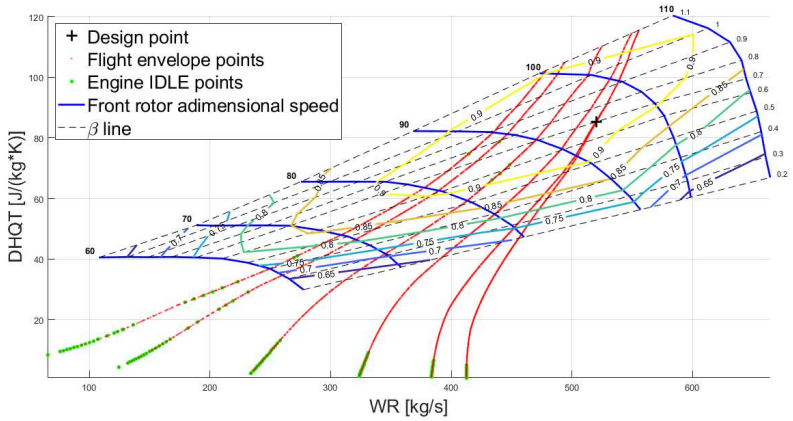

(a) HYB-CF2-10eng-DPref

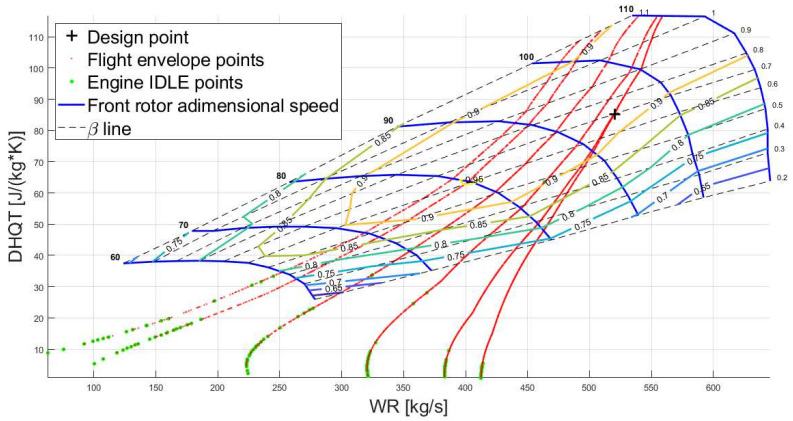

(b) HYB-CF2-10eng-DP1

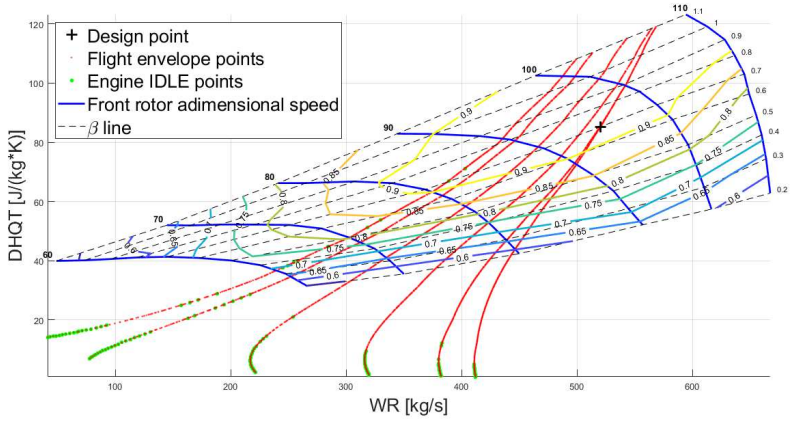

(c) HYB-CF2-10eng-DP2

Figure 5.16: CR fan engines HYB-CF2-10eng: performance maps.

Finally, the last engine maps presented in this thesis are ones depicted in Figure 5.17. Also in this case the rangeability is high, hence it can be concluded that the CR fan engine, in

general, presents higher values of rangeability with respect the turbofan. In general most of the calculations converged, even if the engine HYB-CF2-10eng-DP1 at low M and z presents an high concentration of not converged calculations. The same thing happened also with the CR fan engine HYB-CF1-2eng-DP1 (Sub-section 5.1.2).

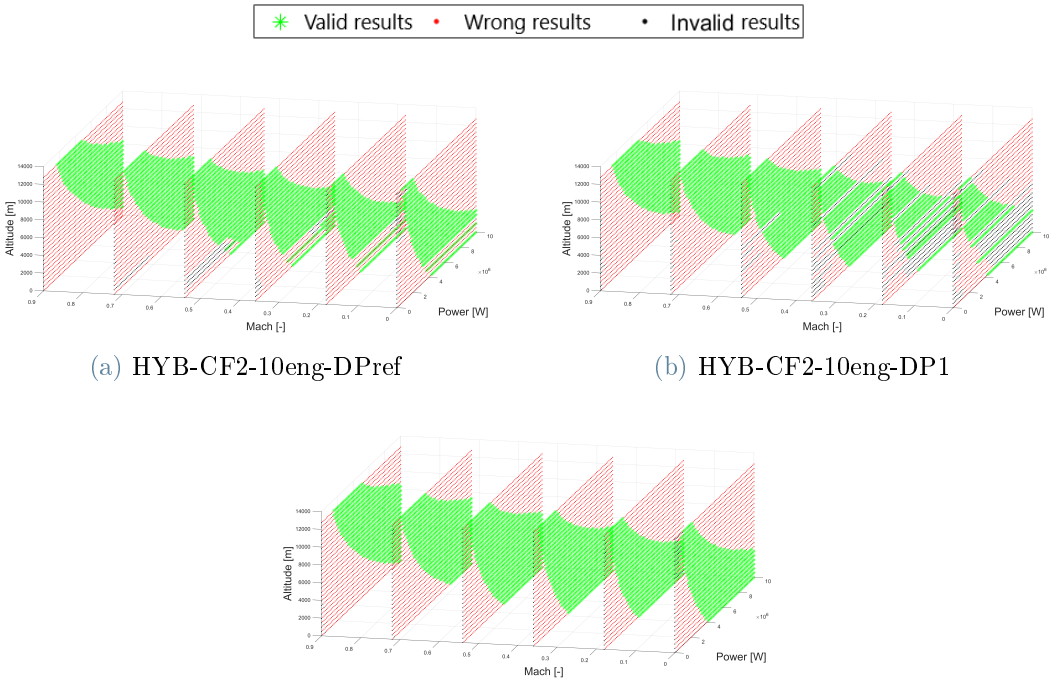

(a) HYB-CF2-10eng-DPref

(b) HYB-CF2-10eng-DP1

(c) HYB-CF2-10eng-DP2

Figure 5.17: HYB-CF2-10eng engine maps with no extended results.

6 | Flight Mission

The aim of this chapter is to describe how the flight mission analysis is implemented in Matlab and what are the data needed as input. To simulate the aircraft performances during a flight, several informations are needed. These informations regard the atmosphere, the flight path, the aircraft model, the propulsive system model, the aircraft data and the propulsive system data. The Matlab code used is structured in a general way, hence it can be used to analyze all the different missions with all the possible combinations of aircraft and engines by simply changing the inputs. This code can be seen as a block diagram, in which the diagrams can be subdivided in:

- input blocks, that are the ones that can be changed by the user. This blocks are four and are:
  - aircraft data, which will be described in Section 6.1. This data are for example the number of engines mounted on the aircraft, the aircraft mass and others data useful to compute the aircraft aerodynamic;
  - engines data, which will be described in Section 6.2. These data are referred only to the hybrid configuration;
  - flight mission data, which will be described in Section 6.3. These data are the values of altitude, velocity and rate of climb for each flight phase. The flight missions considered are short, medium and long range.
  - engine model, which was described in Chapters 4 and 5. The engine models are the engine maps created in EcosimPro, that in Matlab are added in the form of tables. An example of engine map in form of a table is provided in Figure 6.1. Rememeber that the total number of the engine maps is 16. 2 are the ones of CFM56-7B24 and GEnx-1B64, instead the other 14 are for the CR fans (Figure 5.1);
- fixed blocks, that can't be changed and are the same for all the calculations. These blocks are two and are:

– aircraft model, that is well described in Sub-section 2.4.2. Substantially the aircraft is modeled with the point mass approach;

– atmoshpere model, that is the ISA model and it is described in Sub-section 2.4.1.

The schematization of the Matlab code in blocks is depicted in Figure 6.2. In the following sections the aircraf, engine and flight mission data will be presented.

	1	2	3	4	5	6	7	8	9
Name	Electric_CrFan.Power (W)	Monitor_FORCE.thrust.F (N)	TURBOJET.Altitude (m)	TURBOJET.Mach (-)	Electric_CrFan.WR (kg/s)	Electric_CrFan.DHQT (J/(kg·K))	Electric_CrFan.NR (-)	Electric_CrFan.PQ (-)	Electric_C
Alias	--	--	--	--	--	--	--	--	--
0	0	0	0	0	0	73.7433884	1	1.192572	0
1	-100000	552.793716	0	0	56.8351577	6.16404095	1	1.01068628	-299.3848
2	-200000	1860.36062	0	0	104.255623	6.7206781	1	1.01207162	-563.5175
3	-300000	3377.0266	0	0	140.443908	7.48343401	1	1.0136802	-803.1730
4	-400000	4905.06324	0	0	169.233436	8.28049698	1	1.01530269	-1026.395
5	-500000	6398.9198	0	0	193.261898	9.06371724	1	1.01689067	-1237.526
6	-600000	7852.56099	0	0	214.05772	9.81980671	1	1.01843761	-1439.141
7	-700000	9269.7422	0	0	232.538852	10.5459353	1	1.01994736	-1632.933
8	-800000	10656.1595	0	0	249.288863	11.242676	1	1.02142588	-1820.095
9	-900000	12017.2954	0	0	264.698247	11.9117077	1	1.02287893	-2001.520
10	-1000000	13357.8856	0	0	279.039676	12.5549973	1	1.02431149	-2177.896
11	-1100000	14748.5326	0	0	293.180934	13.144363	1	1.02579906	-2349.368
12	-1200000	16199.6897	0	0	307.251312	13.6826458	1	1.02735299	-2516.190
13	-1300000	17643.5109	0	0	320.638109	14.2040044	1	1.02890074	-2679.111
14	-1400000	19080.2446	0	0	333.426172	14.7099411	1	1.03044254	-2838.457
15	-1500000	20510.1668	0	0	345.684557	15.2017598	1	1.03197867	-2994.510
16	-1600000	21933.5588	0	0	357.470292	15.6805977	1	1.03350941	-3147.514
17	-1700000	23350.6956	0	0	368.831065	16.1474524	1	1.03503503	-3297.681
18	-1800000	24761.8399	0	0	379.807203	16.6032036	1	1.03655579	-3445.199
19	-1900000	26167.2388	0	0	390.433148	17.0486307	1	1.03807195	-3590.235
20	-2000000	27567.1236	0	0	400.738573	17.4844282	1	1.03958373	-3732.938
21	-2100000	28961.7092	0	0	410.749249	17.9112173	1	1.04109135	-3873.440
22	-2200000	30351.1953	0	0	420.487715	18.3295564	1	1.04259502	-4011.863

Figure 6.1: Example of engine map in the form of table. In this figure is shown a piece of the CR fan HYB-CF1-2eng-DPref engine map.

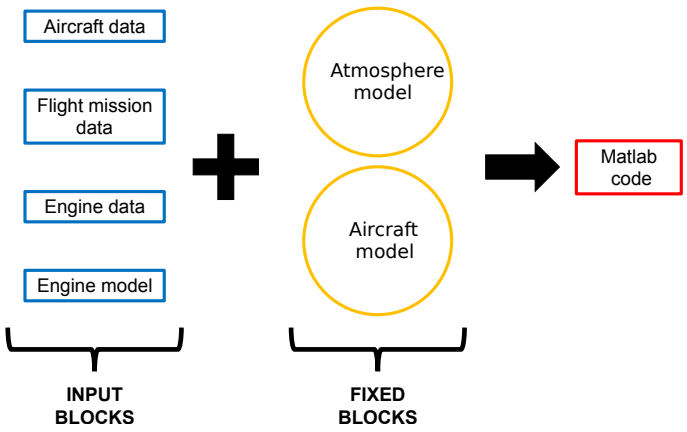

Figure 6.2: Matlab code structure.

6.1. Aircraft data

The two aircrafts considered in this thesis are:

- Boeing 737-800, that is a tyical narrow-body aircraft. It is a very common civil aircraft used for both short and medium range missions;
- Boeing 787-800, that is a wide body aircraft. Also in this case, it is a very common civil aircraft, but used for long range missions.

The choice of these two aircrafts was done for several reasons. First of all, as said in the previous lines, since they are very common aircrafts they can be used as reference for the all narrow body and wide body aircraft classes. In other words, the results obtained can be considered valid also for other aircrafts. Due to the fact that are very common, in literature it was easy to find the data needed. Moreover, these aircrafts are compatible with the reference turbofans analyzed in this thesis. Note that the choice of the aircraft depends on the turbofan and viceversa. Hence, their choice was a trade-off depending on the data available in literature for both aircraft and turbofan.

Since the aircraft is modeled as a point mass, the data needed are:

- N_{eng}, that is the number of engines mounted on the aircraft. This data is needed in order to compute the correct values of T_h, $\dot{m}_f$, etc... since the engine maps added on Matlab are referred only to a single engine;
- $\hat{S}$, that is the wing surface. This value is needed to compute L and D;
- m_{MTOW}, that is the maximum aircraft weight at take-off;
- m_{PAY}, that is the maximum payload mass. Note that in general the aircrafts do not fly always with the maximum payload. Instead, for this thesis it was chosen to fix the payload mass at its maximum value, because in that way it will be easier to compare the results between the reference and hybrid aircrafts;
- m_{OEW} is the overall empty weight of the aircraft. This value is the sum of the aircraft weight when is empty plus the crew weight plus their baggage. This value include also the engines weight and the weight of the all working fluids. Note that in this thesis it was assumed that in the hybrid configuration the weight of the CR fan blades plus the GT is equal to the weight of the associated reference turbofan. In other words, in the hybrid cases, inside the value of m_{OEW} is included the weight of the CR fan blades and the one of the GT;
- C_{D0}, $C_{D0_{IC}}$ and C_{D0_A} are different values of the zero-lift drag coefficient. These values depend on the flight phase. In cruise condition the wing is clear and the landing gear is retracted, hence the value used is C_{D0}. During the initial climb phase the landing gear is retracted, but there are the flaps, hence the value used is

$C_{D0_{IC}}$. Instead, during the approach phase, the landing gear is down and the flaps are used also to slow down the aircraft, hence the value used is C_{D0_A}. The value of C_{D0_A} is bigger than $C_{D0_{IC}}$ that is bigger than C_{D0};

- k is the parameter that takes in account the lift contribution inside the C_D. In this thesis the C_D is computed as $C_D = C_{D_0} + k \cdot C_L^2$.

6.1.1. Boeing 737-800

The Boing 737-800 data were found both on the internet [33] and in the work of Junzi at al. [4]. These data are represented in Table 6.1. The engines that can be mounted on that aircraft are the CF56-7B24 in 2 engines configuration, the CR fans HYB-CF1-2eng and the CR fans HYB-CF1-10eng. Depending on which engine is used the value of N_{eng} could be 2 or 10.

Variable	Value	Unit
N_{eng}	2/10	-
$\hat{S}$	124.6	m^2
m_{MTOW}	78245	kg
m_{PAY}	20276	kg
m_{OEW}	41413	kg
C_{D0}	0.021	-
$C_{D0_{IC}}$	0.041	-
C_{D0_A}	0.051	-
k	0.0365	-

Table 6.1: Boeing 737-800 specifications.

6.1.2. Boeing 787-800

Similar considerations can be done for Boeing 787-800. Also in this case the data were found both on the internet [34] and in the work of Junzi et al. [4]. These data are represented in Table 6.2. In this aircraft is possible to mount the GEnx-1B24 in 2 engines configuration, the CR fans HYB-CF2-2eng and the CR fans HYB-CF2-10eng . As expected, the values of C_{D0_A}, $C_{D0_{IC}}$, C_{D0} and k are very similar to the ones of the Boeing 737-800, in fact these aircrafts are very similar even if the size is different.

Variable	Value	Unit
N_{eng}	2/10	-
$\hat{S}$	377	m^2
m_{MTOW}	227930	kg
m_{PAY}	43318	kg
m_{OEW}	119950	kg
C_{D0}	0.022	-
$C_{D0_{IC}}$	0.042	-
C_{D0_A}	0.052	-
k	0.0361	-

Table 6.2: Boeing 787-800 specifications.

6.2. Engines data

The engines data are needed only for the hybrid configurations, in particular these data are the initial values of SFC (SFC_{init}) for the GTs and the values of efficiency, SP and SE for the electric components.

Remember from Sub-section 2.3.1 that the two hybrid configurations analyzed are tu-el pc and hy-el se. The principal unknown of these systems are the GTs SFC. In fact, the GT was not modeled in this thesis, hence it hasn't its engine map. Note that one of the main scope of the engine map is to provide the value of $\dot{m}_f$ for a certain value of T_h in a certain flight condition. But, there is a reason why the GT was not modeled. Since the electric components are modeled simple as black boxes defined by their efficiency, SP and SE, a more sofisticated model for the GT it would have been useless and also not correct. Moreover, it is more interesting to leave the GT SFC as unknown and then, in the flight mission analysis, compute the target value needed in order to obtain an hybrid system that performs better with respect the reference case. This last part will be explained in detail in the Chapter 7. To compute the SFC target the code needs SFC_{init}. Since there are two rerefence turbofans engines, the CFM56-7B24 and the GEnx-1B64, and two groups of electric CR fan engines, HYB-CF1 and HYB-CF2, therefore there are also two GTs. These GTs are called: GT1, if it is mounted in the hybrid system with the HYB-CF1 engines, and GT2, if it is mounted in hybrid system with the HYB-CF2 engines. In other words:

- GT1 is mounted when the mission is short or medium, hence GT1 can be mounted

only on Boeing 737-800;

- GT2 is mounted when the mission is long, hence GT2 can be mounted only on Boeing 787-800.

The values of SFC_{init} for these two GTs are reported in Table 6.3. These values were chosen looking in the GE aeroderivative gas turbine catalogue [13]. Since in the short or medium range missions the max power needed by the electric CR fans is in the order of 30 [MW], the SFC_{init} of GT1 was chosen similar to an aeroderivative gas turbine designed for that level of power. In the same way, the value of GT2 SFC_{init} was chosen. As expected, bigger is the GT and lower is the value of SFC.

Turbogas generator	Variable	Value	Unit
GT1	SFC_{init}	$5.9444e^{-8}$	$\frac{kg}{s \cdot W}$
GT2	SFC_{init}	$5.2733e^{-8}$	$\frac{kg}{s \cdot W}$

Table 6.3: Turbogas generators: Initial values of SFC.

The electric components data are reported in Table 6.4. These values were taken from the work of Hendrik et al. [15] and they can be considered fine even if this is a work done in 2017. Only the battery SP was changed, because in the last years its value increased a lot (Figure 6.3).

Component	Variable	Value	Unit
Battery	η	0.99	-
	SP	1000	$\frac{W}{kg}$
	SE	720000	$\frac{J}{kg}$
Electric generator	η	0.95	-
	SP	9500	$\frac{W}{kg}$
Electric motor	η	0.95	-
	SP	9500	$\frac{W}{kg}$
Power electronics	η	0.98	-
	SP	62000	$\frac{W}{kg}$

Table 6.4: Electric components efficiency, SP and SE.

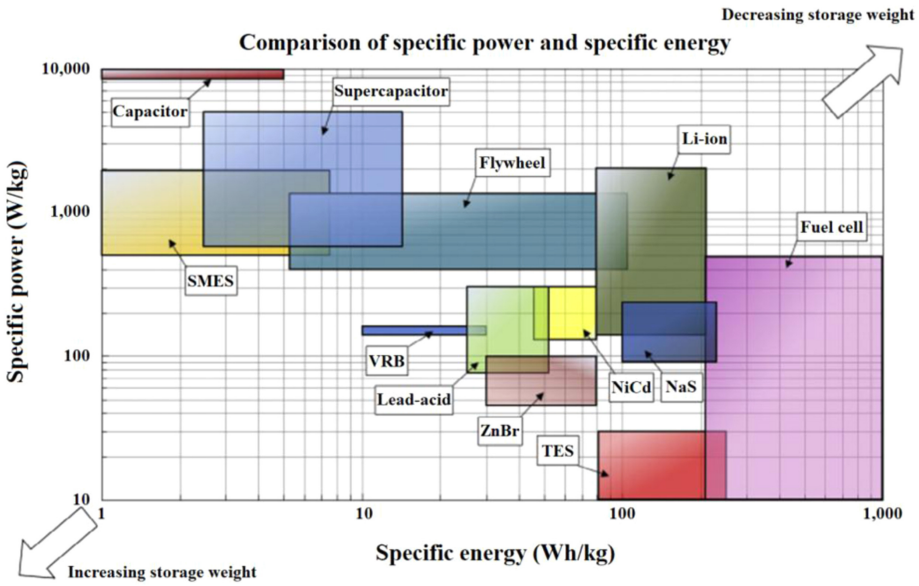

Figure 6.3: Li-ion battery state of the art [41].

6.3. Flight Mission data

Until this point, the flight missions have never been defined in detail. Depending on the range, in this thesis the flight missions were subdivided in:

- short range mission, which is a mission of ~ 500 [km];
- medium range mission, which is a mission of ~ 2000 [km];
- long range mission, which is a mission of ~ 6500 [km];

Each mission is divided in different flight phases, which are reported in Table 6.5. Each flight phase is defined by its initial and ending values of altitude and velocity. Moreover, except for the cruise, also the value of the rate of climb is imposed. Note that the climb phase is divided in two parts only for the long range mission case. The flight phases and the respectively values of z, V (or M) and RC come from Eurocontrol. The values for the short/medium range missions are referred to Boeing 737-800 [8] and the ones of the long range mission are referred to Boein 787-800 [9]. All these values were also corrected depending on real data found on Flightradar24 [10].

Flight phase	Variable	Short range value	Medium range value	Long range value	Unit
Take-off	t_{TO}	30	30	30	s
Initial climb	z_{start}	0	0	0	m
	z_{end}	1524	1524	1524	m
	V_{start}	84.88	84.88	97.74	$\frac{m}{s}$
	V_{end}	149.189	149.189	149.189	$\frac{m}{s}$
	RC	10.7	10.7	9.8	$\frac{m}{s}$
Climb 1	z_{start}	1524	1524	1524	m
	z_{end}	7315.2	7315.2	4572	m
	V_{start}	149.189	149.189	149.189	$\frac{m}{s}$
	V_{end}	223.8	242.44	180.189	$\frac{m}{s}$
	RC	10.16	10.16	11.5	$\frac{m}{s}$
Climb 2	z_{start}	//	//	4572	m
	z_{end}	//	//	7315.2	m
	V_{start}	//	//	180.189	$\frac{m}{s}$
	M_{end}	//	//	0.85	-
	RC	//	//	5.3	$\frac{m}{s}$
Const. M climb	z_{start}	7315.2	7315.2	7315.2	m
	z_{end}	9800	11000	12000	m
	M_{start}	0.72	0.78	0.85	-
	M_{end}	0.72	0.78	0.85	-
	RC	7.62	5.62	3	$\frac{m}{s}$
Cruise	z_{start}	9800	11000	12000	m
	z_{end}	9800	11000	12000	m
	M_{start}	0.72	0.78	0.85	-
	M_{end}	0.72	0.78	0.85	-
	RC	0	0	0	$\frac{m}{s}$
Initial descent	z_{start}	9800	11000	12000	m
	z_{end}	7315.2	7315.2	7315.2	m
	M_{start}	0.72	0.78	0.85	-
	M_{end}	0.71	0.71	-	-
	RC	-4.064	-4.064	-13.208	$\frac{m}{s}$
Descent	z_{start}	7315.2	7315.2	7315.2	m
	z_{end}	3048	3048	3048	m
	M_{start}	0.71	0.71	0.85	-
	M_{end}	-	-	-	-
	RC	-17.78	-17.78	-14.224	$\frac{m}{s}$
Approach	z_{start}	3048	3048	3048	m
	z_{end}	0	0	0	m
	V_{start}	-	-	-	$\frac{m}{s}$
	V_{end}	128.611	128.611	130	$\frac{m}{s}$
	RC	-7.62	-7.62	-7.62	$\frac{m}{s}$

Table 6.5: Flight mission input data. These data are the same both for the reference and the hybrid cases.

This last part is referred only to the hybrid systems. As said before, the two hybrid configurations considered are tu-el pc and hy-el se. Therefore, each flight mission (short/medium/long) can be performed both in the tu-el pc and hy-el se configurations. In this thesis CASE 1 and CASE 1bis are referred to the hy-el se configuration, instead

CASE 2 and CASE 2 bis are referred to the tu-el pc configuration. Remember that the battery is present only in the hy-el se configuration. The only difference between CASE 1 and CASE 1bis is only on the use of the battery. In CASE 1 the battery is used during the all descent phases, instead in CASE 1bis the battery is used only on the first part of the descent phases. The difference between CASE 2 and CASE 2bis is that in CASE 2bis the weight of the aircraft is imposed equal to one of the reference case. Hence, in CASE 2bis the weight of the all electric components is not considered. CASE 2bis was implemented in order to highlight the performances of the electric CR fan engines. CASE 2bis can be used also to highlight how much the increase in the aircraft weight, due to the electric components, can derate the performances. All these four cases are reported in Table 6.6.

Note that in CASE 1 and 1bis the battery is used only in the descent phases. In fact, from a preliminary analysis, it was found that during the climb phases the power and energy required are so high that the battery can't be used, because its resulting weight would be too high. These results are in line with what can be found in literature. For this reason, in hybrid aircrafts, in general the battery provides only a certain percentage of the total power needed. In this case instead, it was chosen to use the battery during the descent phases, since here the power needed is relatively low. Note that the optimization of the hybrid system is not part of this thesis.

	CASE 1	**CASE 1bis**	**CASE 2**	**CASE 2bis**
Take-off	GT	GT	GT	GT
Initial climb	GT	GT	GT	GT
Climb 1	GT	GT	GT	GT
Climb 2	GT	GT	GT	GT
Const. M climb	GT	GT	GT	GT
Cruise	GT	GT	GT	GT
Initial descent	Battery	Battery	GT	GT
Descent	Battery	Battery	GT	GT
Approach	Battery	GT	GT	GT

Table 6.6: Different hybrid systems used during a certain flight mission.

7 | Results analysis

The aim of this last chapter is to present the results obtained in the different flight missions. For each flight mission, different combinations of aircraft, propulsive system and hybrid system will be considered and the results compared to the ones of the reference cases. Until this point all the ingredients needed to perform a flight mission analysis were presented and these ingredients are for example the aircraft typologies, the engine maps, the four different settings of the hybrid system (CASE 1, CASE 1bis, CASE 2 and CASE 2bis), etc... . About the hybrid system, remember that it can be the tu-el pc (i.e. CASE 2 and 2bis) or the hy-el se (i.e. CASE 1 and 1bis) and that the electric CR fans mounted can be in 2 or 10 engines configuration (i.e. 2eng or 10eng). Therefore, the overall hybrid propulsive systems with the engines can appear in four different configurations, which are depicted in Figures 7.1, 7.2, 7.3 and 7.4.

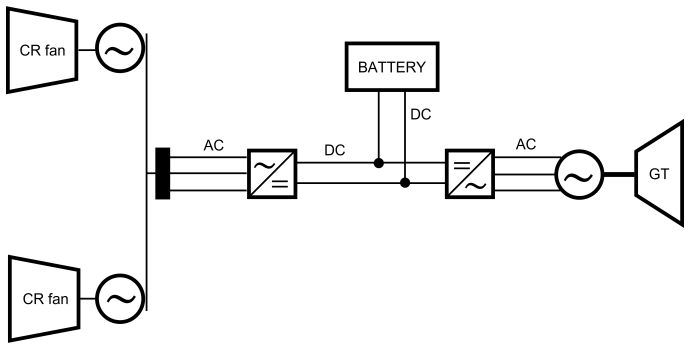

Figure 7.1: Hy-el se with 2 electric CR fan engines. This configuration is used in CASE 1 and CASE 1bis. For each one of these two CASEs the electric CR fan engines can be part of the HYB-CF1-2eng or HYB-CF2-2eng series. Remember that each CR fan engine is propelled by two electric engines, one for each shaft. Therefore, for example, in this case the total number of electric engines is 4.

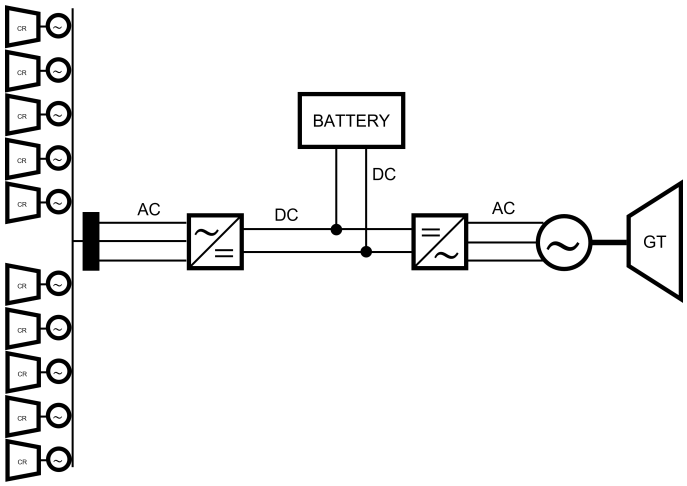

Figure 7.2: Hy-el se with 10 electric CR fan engines. This configuration is used in CASE 1 and CASE 1bis. For each one of these two CASEs the electric CR fan engines can be part of the HYB-CF1-10eng or HYB-CF2-10eng series. The total number of electric engines is 20.

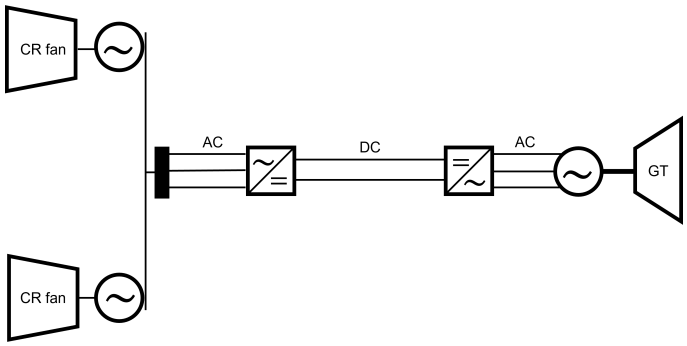

Figure 7.3: Tu-el pc with 2 electric CR fan engines. This configuration is used in CASE 2 and CASE 2bis. For each one of these two CASEs the electric CR fan engines can be part of the HYB-CF1-2eng or HYB-CF2-2eng series. The total number of electric engines is 4.

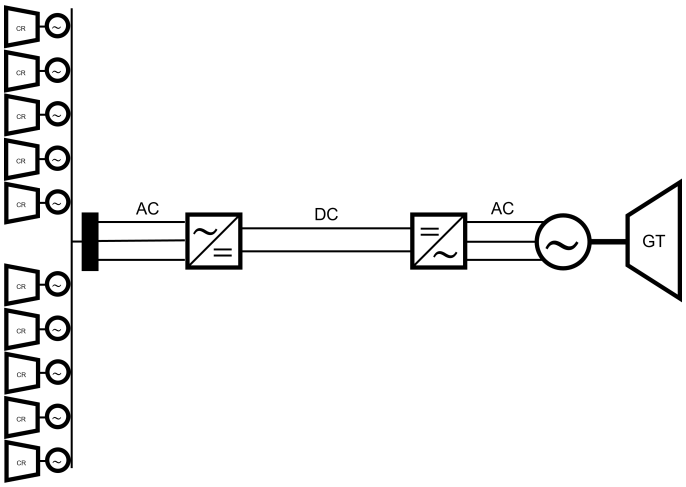

Figure 7.4: Tu-el pc with 10 electric CR fan engines. This configuration is used in CASE 2 and CASE 2bis. For each one of these two CASEs the electric CR fan engines can be part of the HYB-CF1-10eng or HYB-CF2-10eng series. The total number of electric engines is 20.

To help the reader to understand what flight missions will be analyzed in this chapter, a brief summary about them will be done.

First of all, all the flight missions analyzed can be subdivided, depending on the range, in three main groups: short, medium and long. Then, for each group is defined a reference case. The reference flight missions for the short and medium range cases, are the ones performed by the Boeing 737-800 propelled by CFM56-7B24. Instead, the reference flight mission for the long range case, is the one performed by the Boeing 787-800 propelled by GEnx-1B64. In all these three cases, the turbofans mounted are 2. Once these results are obtained, the flight missions with the hybrid systems can be performed and compared to the respective reference cases. Remember that all the CR fan engines in the group HYB-CF1 can be mounted only in the Boeing 737-800, hence used in short/medium range missions, instead the ones in the group HYB-CF2 can be mounted only in the Boeing 787-800, hence used in long range missions. The last subdivision regards the hybrid system. In fact, once the flight mission range (i.e. the aircraft) and the electric CR fans are selected, it is possible to test different hybrid systems. All these possible flight missions are schematized in Figure 7.5. Moreover, remember that the CR fan engines in the groups HYB-CF1 and HYB-CF2 are the ones reported in Figure 5.1.

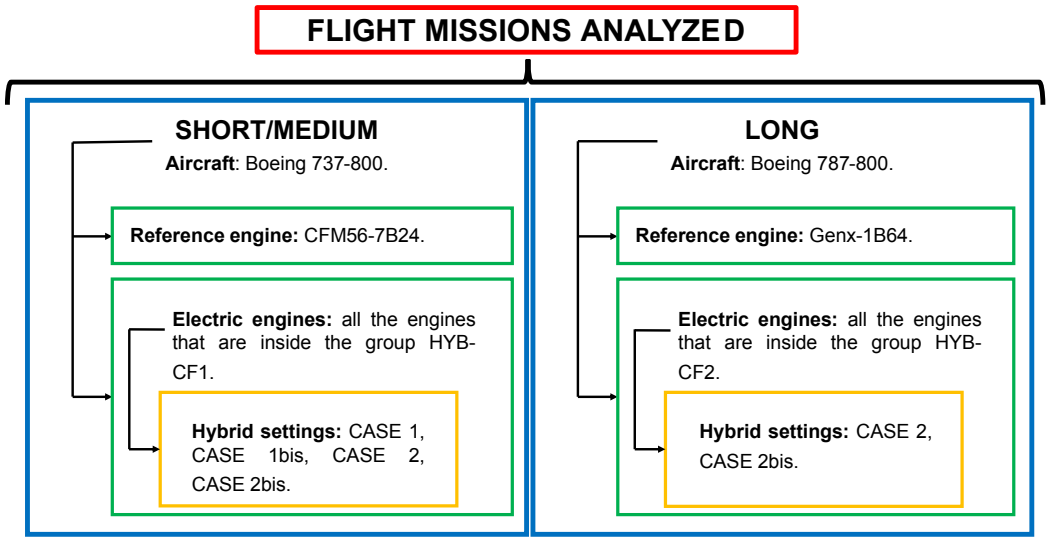

Figure 7.5: All possible cases of flight missions. Note that, for a reason that will be explained later, for the long range case the only possible hybrid settings are CASE 2 and CASE 2bis.

To avoid all the possible misunderstandings, the complete list of the all flight missions analyzed in this chapter is reported in Appendix A.

7.1. Short range mission analysis

In this section are reported all the results for the short range missions. In the first sub-section (Sub-section 7.1.1) the reference case will be analyzed. Instead, in Sub-sections 7.1.2 and 7.1.3 are analyzed the cases in which are mounted, respectively, the electric CR fans in 2 engines configuration (i.e. engines in the group HYB-CF1-2eng) and in 10 engines configuration (i.e. engines in the group HYB-CF1-10eng).

7.1.1. Reference: Boeing 737-800 propelled by CFM56-7B24

The reference case for the short range mission is the one performed by the Boieng 737-800 propelled by CFM56-7B24. The values obtained from this analysis, will be used as comparison for the other short flight missions. In Figures 7.6, 7.7, 7.8, 7.9 and 7.10 are reported the performance points during the different flight phases. These plots are very interesting, because they show how these components behave during the flight mission and a lot of considerations can be done. First of all, as exptected, during the climb phases all the components work at high rotational speed and so at high levels of mass flow and pressure ratio. These are the phases in which is required the highest level of

thrust. Instead, during the descent phases the engines work for most of the time in idle condition, so the levels of pressure ratio and mass flow are the lowest possible. As reported in previous chapters, the points associated to the idle contition are the ones outside the map. Note that the points associated to the climb phase, cruise and take-off are inside the region at highest efficiency. Since the CFM56-7B24 is mainly designed for short/medium range missions, this fact confirms that this engine was correctly modeled in EcosimPro. Moreover, these plots can be used also as a check of the Matlab code that computes the flight missions.

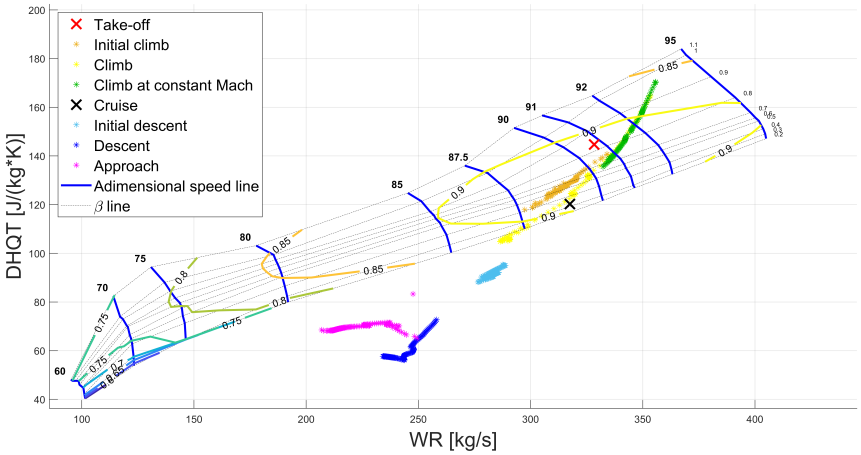

Figure 7.6: Reference short mission: CFM56-7B24 fan performance points during flight.

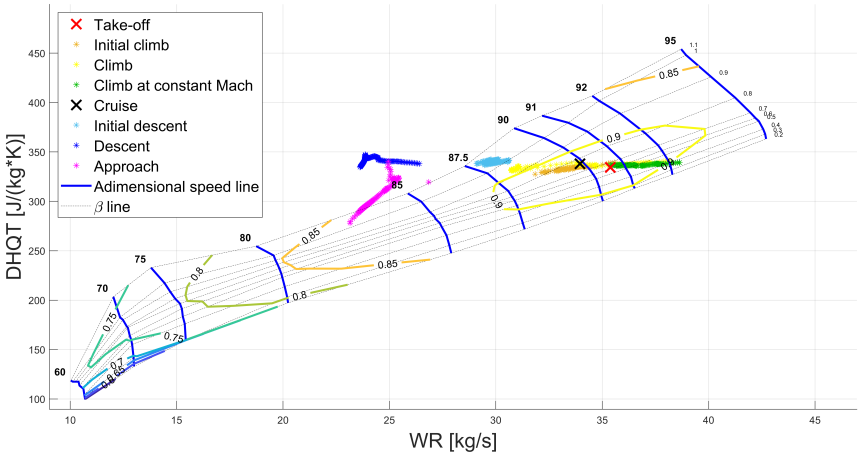

Figure 7.7: Reference short mission: CFM56-7B24 LP compressor performance points during flight.

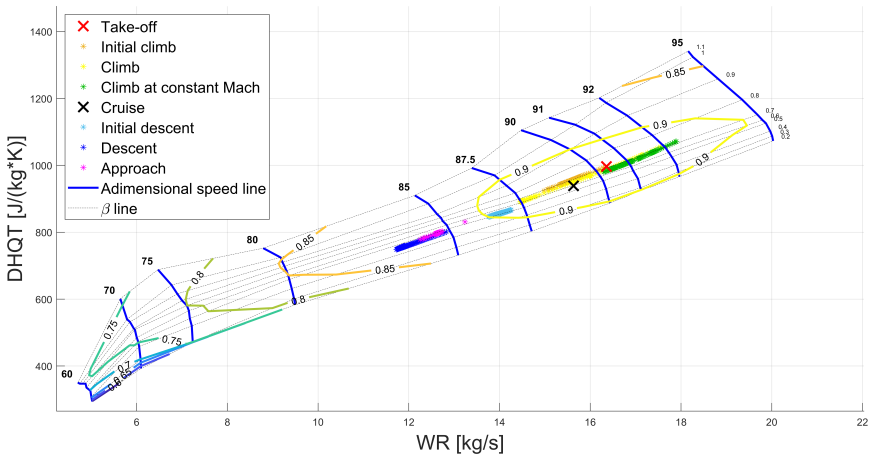

Figure 7.8: Reference short mission: CFM56-7B24 HP compressor performance points during flight.

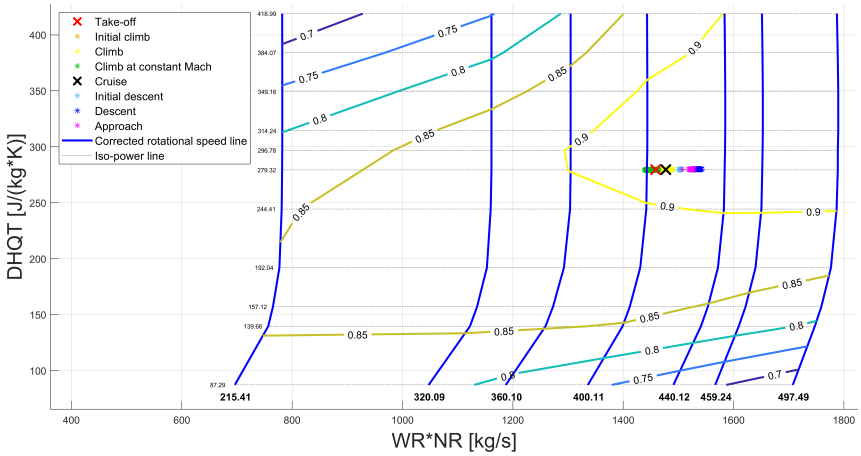

Figure 7.9: Reference short mission: CFM56-7B24 HP turbine performance points during flight.

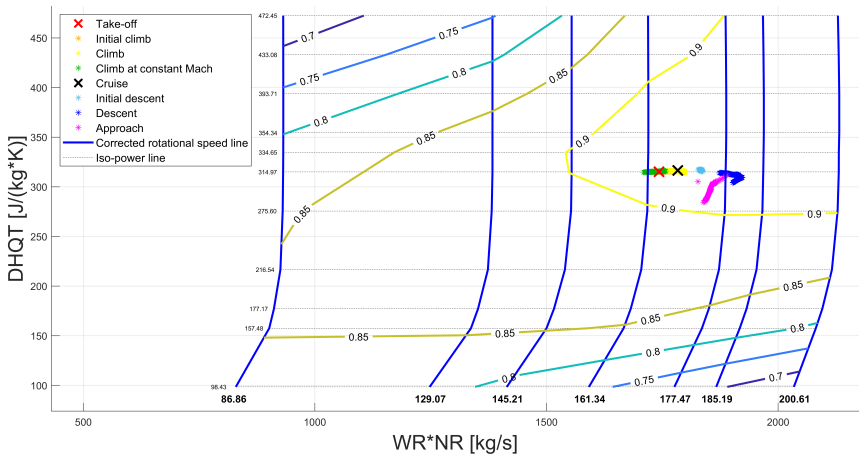

Figure 7.10: Reference short mission: CFM56-7B24 LP turbine performance points during flight.

The values of the total fuel consumed, the time of flight and the flight distance are reported in Table 7.1. The value of total fuel consumed is in line with what can be found in literature, even if since this value is very sensitive to a lot of variables, like the flight path, the aircraft weight, the weather, etc..., it is impossible to identify a unique real value. Instead, the values of time of flight and flight distance can be compared to the real ones found on Flightradar24 [10]. In this case, it can be found a strong similarity between estimated and real values. Note that from the value of the total fuel consumed is possible to compute the aircraft mass at take-off. In fact, the total aircraft mass (m_{TOT}) can be computed as:

$$m_{TOT} = m_{OEW} + m_{PAY} + m_{FUEL}; \tag{7.1}$$

hence $m_{TOT} = 63822$ [kg], which is less than m_{MTOW}. All these checks provide another proof regarding the validity of the codes used, both on EcosimPro and Matlab, to perform the flight mission.

	Value	**Unit**
Total fuel consumed	2133	kg
Time of flight	41	min
Flight distance	477	km

Table 7.1: Reference short range mission analysis final results.

In the following plots are shown how parameters like T_h, $\dot{m}_f$, M, etc... change during the

flight mission. Moreover, these plots are another way to validate the Matlab code.

In Figure 7.11 is reported the flight path followed by the aircraft. This is a short range mission and it can be seen that the cruise is only a short part of the overall mission. Instead in Figure 7.12 is shown the M trend during the mission. The overspeed present at the beginning of the descent is confirmed also from real data [10]. This overspeed can be explained through the fact that during this phase the air density is so low that, even if the engines are at idle, the aircraft increases its speed.

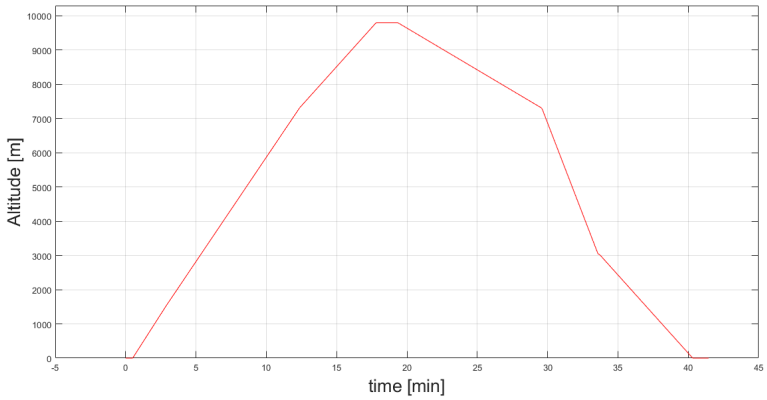

Figure 7.11: Reference short mission: Altitude vs time of flight.

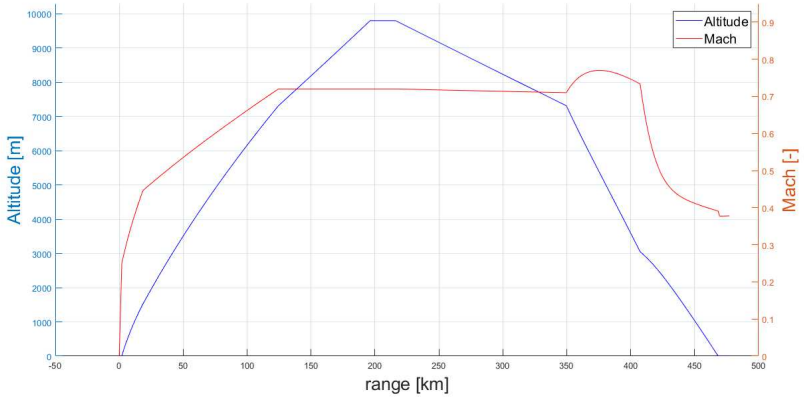

Figure 7.12: Reference short mission: Altitude and Mach vs range.

In Figures 7.13 and 7.14 are depicted the trends of T_h and $\dot{m}_f$. Since T_h is linked to $\dot{m}_f$, these two trends are similar and, as expected, the highest values are during the climb phases. It is interesting to note that during this phase $\dot{m}_f$ is more than two times the fuel flow consumed during the cruise. The same considerations are valid also for T_h.

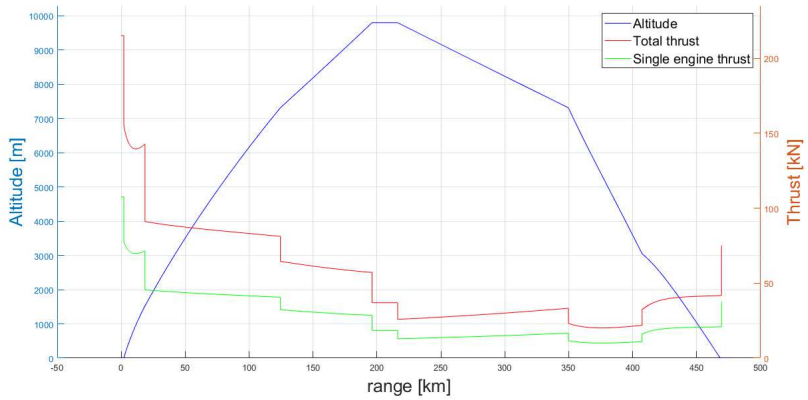

Figure 7.13: Reference short mission: Altitude and Thrust vs range.

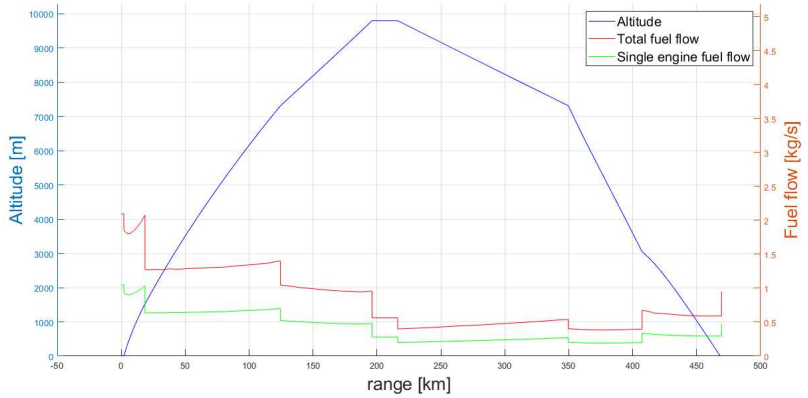

Figure 7.14: Reference short mission: Altitude and Fuel flow vs range.

In this last plot, depicted in Figure 7.15, it can be noted that the aircraft mass remains almost constant during the flight mission. In particular, the mass reduction is around 3.3 %, hence also an hypothesis of constant mass during the flight would have been correct.

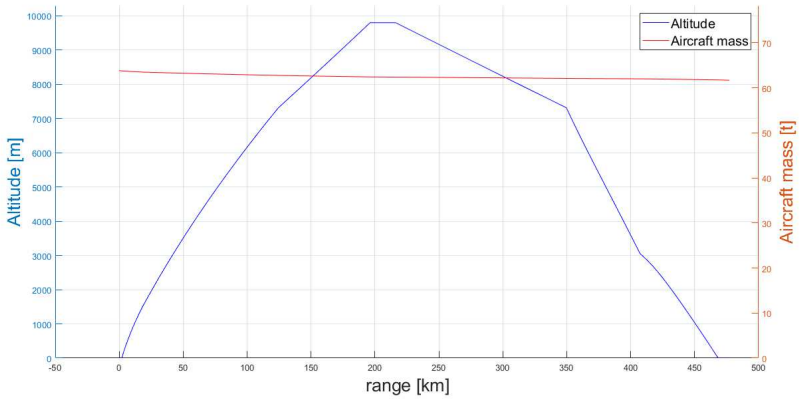

Figure 7.15: Reference short mission: Altitude and Aircraft mass vs range.

All these results confirm once again the correct implementation of the flight mission analysis. Very similar trends of T_h, M, etc... can be found also in the following flight missions. Therefore, in order to avoid confusion in this chapter, these plots will be presented only if necessary. From now on, the main focus will be only on the comparison between the reference and the others flight missions.

7.1.2. Sensitivity analysis: Boeing 737-800 propelled by HYB-CF1 with 2 engines configuration

The different flight missions analyzed in this sub-section are the ones from 1 to 15 of Appendix A. These are the ones performed by Boeing 737-800 in which are alternatively mounted the CR fan engines HYB-CF1-2eng-DPref, HYB-CF1-2eng-DP1, HYB-CF1-2eng-DP2, HYB-CF1-2eng-DP3 and HYB-CF1-2eng-DP4. The hybrid systems tested are CASE 1 and CASE 1bis with the layout hy-el se, and CASE 2 and CASE 2bis with the layout tu-el pc.

In Figure 7.16 is represented how this sub-section is structured. First of all, from that tree diagram, it can be understood that now the missions analyzed are the short ones and that the electric CR fans are in 2 engines configuration. Then, in order to highlight how the global flight mission performances change depending on both the engine and the hybrid system used, four tables were created. These tables are one for each hybrid system considered (CASE 1, CASE 1bis, CASE 2 and CASE 2bis) and in each table are compared the results obtained with the different CR fan engines.

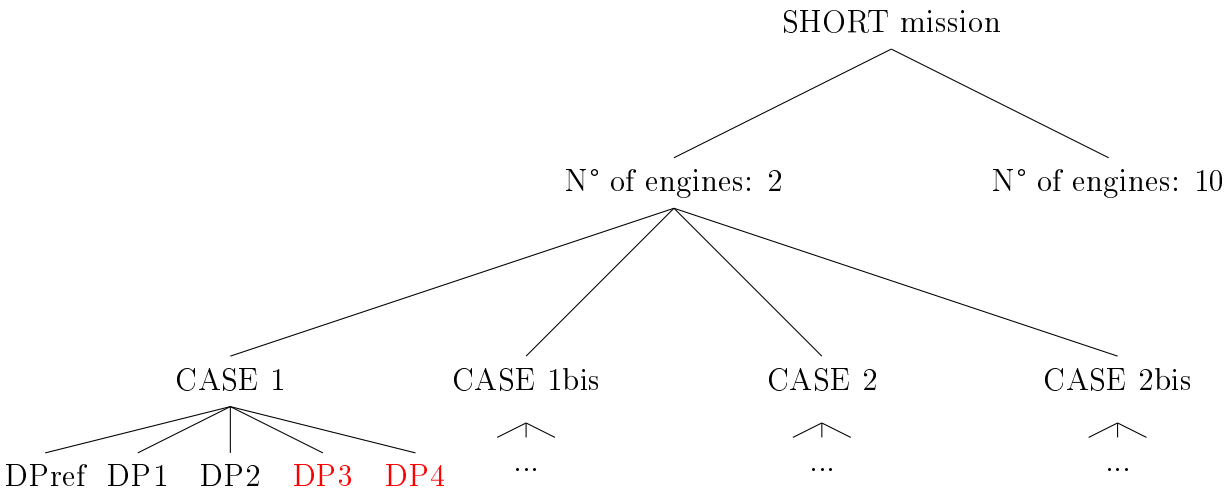

Figure 7.16: Tree diagram that describes the sensitivity analysis procedure in the case of short mission range in 2 engines configuration.

In figure 7.16 the electric engines HYB-CF1-2eng-DP3 and HYB-CF1-2eng-DP4 are in red because they will be analyzed only for the hybrid configuration CASE 1. Then, these engines will be no longer used in this manuscript. The reason of that choice was introduced in Chapter 5, but it will be more clear after the explanation of Table 7.2.

Note that for CASE 1 and CASE 1bis the hybrid system is the hy-el se and so the electric components considered are: the battery, the electric motors, the electric generator and the power electronics. Their weight values are computed through an iterative code. Therefore, in this case, the total mass of the aircraft is computed as:

$$m_{TOT} = m_{OEW} + m_{FUEL} + m_{PAY} + m_{Batt} + m_{ElecMot} + m_{PElec} + m_{ElecGen}.$$

Note that:

- m_{OEW} is imposed identical to the one of the reference case. This value can't be changed;
- m_{PAY}, in the first iteration of the code, is imposed identical to the one of the reference case. During the iterations this value can be reduced;
- m_{FUEL}, m_{Batt}, $m_{ElecMot}$, m_{PElec} and $m_{ElecGen}$, are initialized in the code equal to zero and when these values reach convergence the iterations stop. Note that reducing the value of SFC the value of m_{FUEL} is reduced. In analogy, increasing the electric components η, SP and SE the values of m_{Batt}, $m_{ElecMot}$, m_{PElec} and $m_{ElecGen}$ are reduced.

Instead, in CASE 2 and CASE 2bis the hybrid system is the tu-el pc and so the electric components are: the electric motors, the electric generator and the power electronics. As before, their weight values are computed through the same iterative code, with the only difference that now the total mass of the aircraft is:

$$m_{TOT} = m_{OEW} + m_{FUEL} + m_{PAY} + m_{ElecMot} + m_{PElec} + m_{ElecGen}.$$

Before starting to analyze Table 7.2 is necessary to explain how the flight mission code works. The value of m_{TOT} has to be less then m_{MTOW}. In the code there are two parameters that, if needed, can "adjust" the value of m_{TOT} and are: the GT SFC and m_{PAY}. Moreover, even if $m_{TOT} < m_{MTOW}$, the code search the condition in which m_{FUEL} of the hybrid case is less than m_{FUEL} of the reference case. In fact, one scope of this thesis is to define what is the GT SFC value, called SFC_{target}, that permits to save fuel and, if m_{PAY} has to be reduced, what is the penalty in terms of payload.

Hence, in the hybrid flight mission code, four possibilities are considered:

1. the first possibility is when at take-off $m_{TOT} < m_{MTOW}$. From that situation, the code can continue in four different ways:

   (a) the aircraft with the hybrid configuration consumes less fuel with respect the reference one. In this case $SFC_{target} = SFC_{init}$, even if the real target value of SFC is for sure bigger. The value of m_{PAY} remains unchanged;

   (b) the aircraft with the hybrid configuration consumes more fuel with respect the reference one. Since SFC is an unknown, the code starts to reduce this value until the point in which m_{FUEL} is less than the reference one is reached. The value of SFC obtained is called SFC_{target} and its meaning is simple: it is the maximum value of SFC that the GT should have in order that the fuel consumed in the hybrid case is less with respect the reference one. Starting from that value, the hybrid configuration permits to save fuel. In that case m_{PAY} remains unchanged;

   (c) the aircraft with the hybrid configuration consumes more fuel with respect the reference one. The code starts to reduce SFC until its limit value is reached. This limit is reached when SFC is 38 % lower with respect SFC_{init}. At this point the code starts to reduce m_{PAY}, in fact the idea is that a lighter aircraft consumes less fuel. When the condition m_{FUEL} less than reference is reached, the code stops. The value of m_{PAY} found defines the payload penalty;

(d) the aircraft with the hybrid configuration consumes more fuel with respect the reference one. The code starts to reduce at first SFC, until its limit, and then m_{PAY}. Also m_{PAY} can't be reduced beyond a certain value. Its limit value is reached when m_{PAY} is 90 % lower with respect its initial value. At this point the code stops. A condition in which m_{FUEL} is less than the reference one can't be reached;

2. the second possibility is when at take-off $m_{TOT} > m_{MTOW}$. In that condition the value of m_{TOT} has to be reduced. The code starts to reduce the value of SFC, hence m_{FUEL}. If the condition $m_{TOT} < m_{MTOW}$ is reached, then the code can continue in the four different ways previously analyzed (i.e. (a), (b), (c) and (d)).

3. the third possibility is when at take-off $m_{TOT} > m_{MTOW}$ and the limit value of SFC is reached. At this point the code starts to reduce m_{PAY} until m_{TOT} becomes less than m_{MTOW}. If this condition is reached and if m_{FUEL} is less than reference, the code stops, and the limit value of SFC is equal to SFC_{target}. The payload penalty is defined by the reduction in m_{PAY}. Instead, if m_{FUEL} is bigger than reference, the code can continue like (c) or (d).

4. the fourht possibility is when at take-off $m_{TOT} > m_{MTOW}$ and the limit values of SFC and m_{PAY} are reached. In this case an error appears in the code and the flight mission can't be performed.

Now should be more clear how the code works. This code was used to analyze all the possible flight missions with all the hybrid propulsive systems.

CASE 1

	DPref	DP1	DP2	DP3	DP4	Unit
SFC_{init} **reduction**	-38	-38	-38	-38	-38	%
SFC_{target}	$3.69e^{-8}$	$3.69e^{-8}$	$3.69e^{-8}$	$3.69e^{-8}$	$3.69e^{-8}$	$\frac{kg}{s \cdot W}$
m_{PAY}	9926	11516	9106	9926	9926	kg
m_{PAY} **reduction**	-10350	-8760	-11170	-10350	-10350	kg
	-51	-43.2	-55.1	-51	-51	%
Battery P_{max}	17.4	15.8	18.2	17.4	17.4	MW
GT P_{max}	37.2	37.3	37.2	37.2	37.2	MW
Battery energy used	3234	3068	3368	3234	3234	kWh
m_{FUEL}	1142	1131	1154	1142	1142	kg
Fuel saved wrt reference	+991	+1002	+980	+991	+991	kg

Table 7.2: Short range mission analysis, 2 engines configuration: CASE 1 results. From left to right the flight missions analyzed are the ones with number 2, 6, 10, 14 and 15 of Appendix A.

In Table 7.2 is reported the comparison betweeen the flight missions results, obtained with the hybrid layout depicted in Figure 7.1, of the five Cr fan engines HYB-CF1-2eng-DPref, HYB-CF1-2eng-DP1, HYB-CF1-2eng-DP2, HYB-CF1-2eng-DP3 and HYB-CF1-2eng-DP4. First of all, it can be noted that the results obtained with the engines HYB-CF1-2eng-DPref, HYB-CF1-2eng-DP3 and HYB-CF1-2eng-DP4 are identical. This confirms what was written in Chapter 5. Since the engines HYB-CF1-2eng-DP3 and HYB-CF1-2eng-DP4 do not provide useful results, from now on will be not considered anymore. Then, it can be noted that in all these cases both SFC and m_{PAY} were reduced. Moreover, SFC reached its limit value. The code reduced these two terms in order to respect the condition $m_{TOT} < m_{MTOW}$. In fact, looking in Table 7.3, it can be noted that m_{TOT} of the hybrid aircraft is just a little lower than m_{MTOW}. Coming back to Table 7.2, the engine highlighted in yellow is the one that has the better performances. This engine is the HYB-CF1-2eng-DP1, in fact it can save more fuel while reducing less m_{PAY}. This fact can be seen also by looking the energy consumed by the battery, the max power required by the battery and the max power required by the GT. Since the GT P_{max} is more or less the same for all the electric engines, it means that during the climb phases, hence when is required max thrust, their performances are identical. Instead, the HYB-CF1-2eng-DP1 gain can be seen from both the battery energy used and the

battery max power, hence when the engine works at lower level of thrust. This result was expected and confirms what was seen in Chapter 5. In fact, in that chapter was pointed out that the highest value of efficiency is reached when $N_{ratio} = 0.9$ (i.e. the design point condition DP1). Moreover the scaled performance map with $N_{ratio} = 0.9$ has the largest high efficiency area.
These results have both positive and negative aspects. The positive one is the fact that, even if the payload is 43.2 % less, the fuel saved is almost 50 % of the reference value. This means that to bring all the original payload to the final destination, two hybrid aircrafts are needed. Therefore, globally, the fuel consumed is more or less the same and this is a positive aspect. In fact, these results show that could be possible to develop an hybrid system that permits to save at least some % of fuel while trasporting the same payload. Unfortunately, there is also a negative aspect. In fact, these results are obtained considering a strong reduction of SFC. This is a critical aspect, because SFC_{init} is already low since it comes from real aeroderivative gas turbines. A possible solution should be to add a nozzle to the GT in order to produce thrust, hence recover energy from the gas flow. This solution is not so strange, in fact the same thing happen in the turbofans where the core produces mainly mechanical power, but also thrust. That value of thrust is computed in order to obtain the condition of minimum fuel consumption.

From Table 7.3 it can be seen that the main problem is the battery mass, which is the main cause of the huge increase in the aircraft mass.

Mass [kg]

Variable	Ref	DP1
m_{OEW}	41413	41413
m_{Batt}	-	15765 (SP)[1]
m_{PAY}	20276	11516
m_{FUEL}	2133	1131
Total $m_{ElecMot}$	-	3365
m_{PElec}	-	1125
$m_{ElecGen}$	-	3922
m_{tot}	63822	78237
Difference m_{tot} from Ref	-	+14415

Table 7.3: Short range mission, 2 engines configuration, CASE 1: Comparison between the reference component masses and the component masses of the best result between DPref, DP1 and DP2.

In Figure 7.17 are reported the performance and torque ratio maps for the three CR fan engines HYB-CF1-2eng-DPref, HYB-CF1-2eng-DP1 and HYB-CF1-2eng-DP2. These plots can be used as a further check of the flight mission code when an hybrid propulsive system is used. As expected, during the climb phase are reached the highest values of rotiational speed, pressure ratio and mass flow, instead the opposite happens during the descent phase.

[1]SP corresponds to Specific Power $[\frac{W}{kg}]$. It means that the weight of the battery is due to the power that has to deliver. Therefore, the battery dimensional parameter is the "Specific Power". The opposite case is when the weight of the battery is due to the energy that has to store. In that case, the battery dimensional parameter is the Specific Energy $[\frac{W}{kg}]$, and so SE.

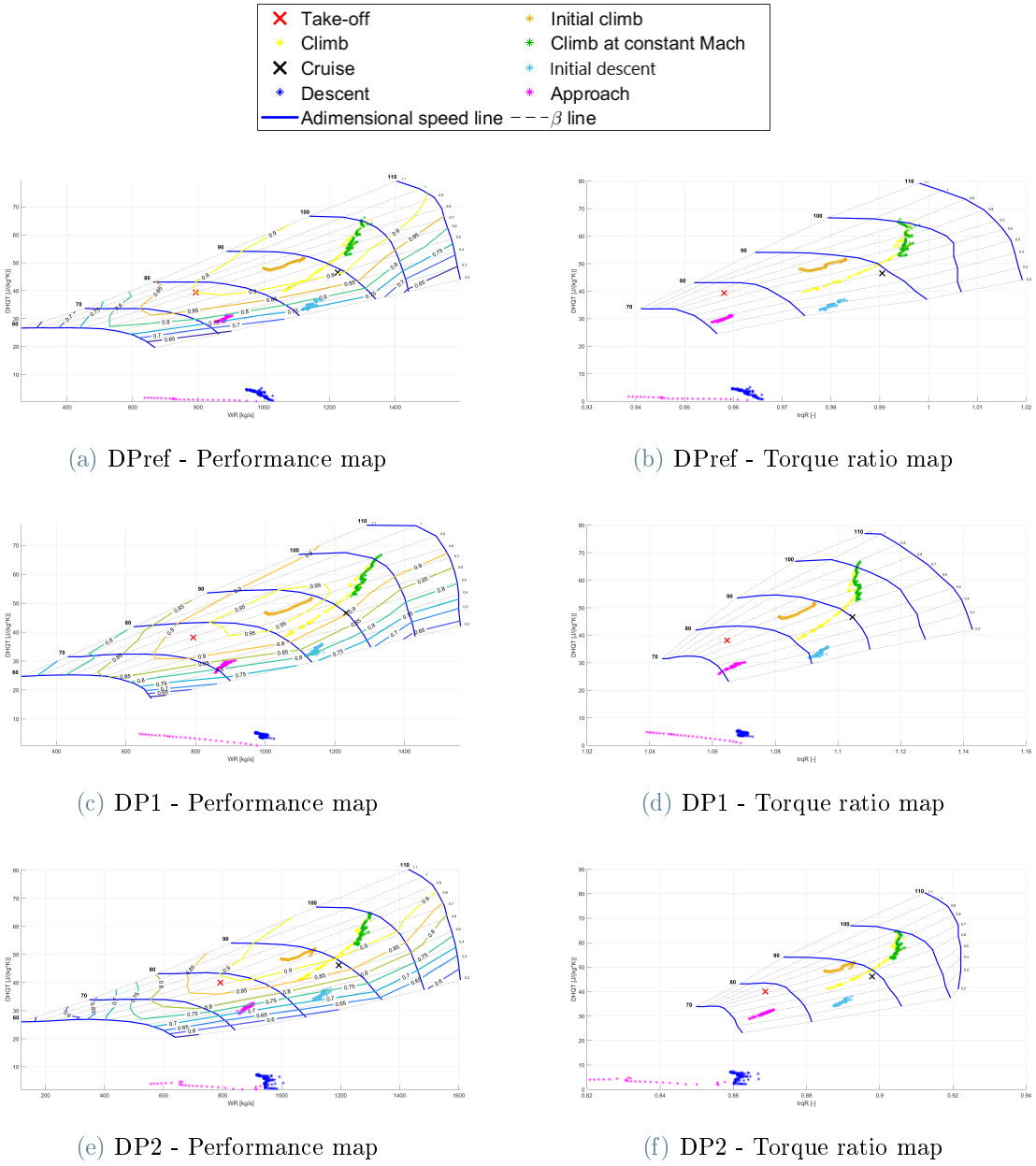

(a) DPref - Performance map

(b) DPref - Torque ratio map

(c) DP1 - Performance map

(d) DP1 - Torque ratio map

(e) DP2 - Performance map

(f) DP2 - Torque ratio map

Figure 7.17: CR fan engines HYB-CF1-2eng in a short range mission, CASE 1: CR fan performance points during flight.

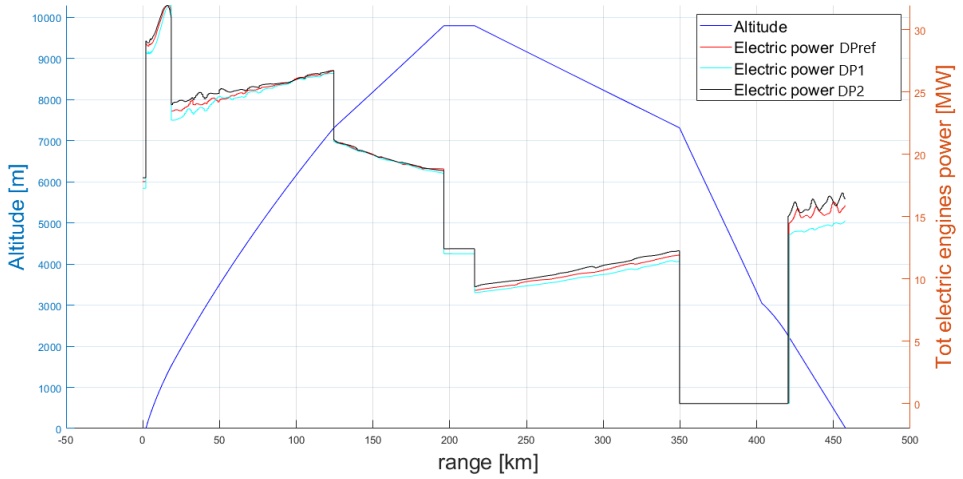

Figure 7.18: Short range mission CASE 1 in 2 engines configuration: Altitude and Tot electric motors power vs Range, results comparison between the CR fan engines HYB-CF1-2eng-DPref, HYB-CF1-2eng-DP1 and HYB-CF1-2eng-DP2.

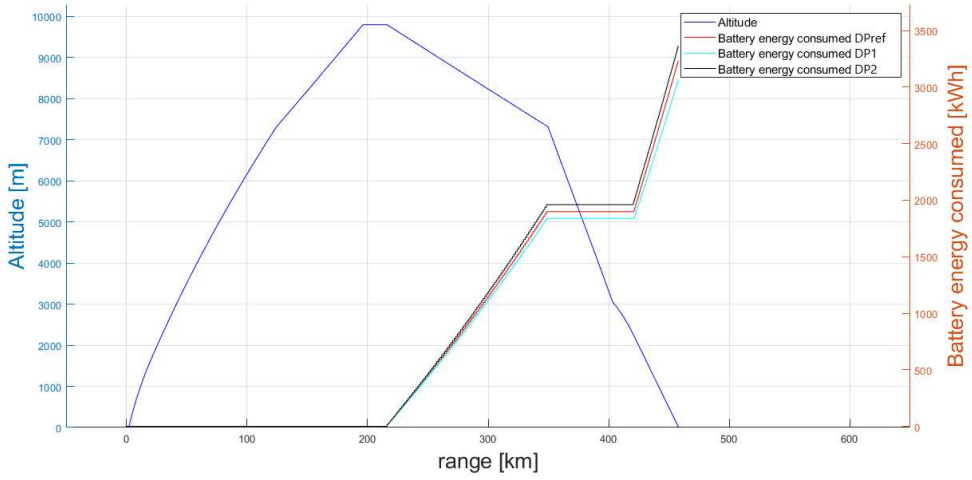

Figure 7.19: Short range mission CASE 1 in 2 engines configuration: Altitude and Battery energy consumed vs Range, results comparison between the CR fan engines HYB-CF1-2eng-DPref, HYB-CF1-2eng-DP1 and HYB-CF1-2eng-DP2.

CASE 1bis

	DPref	DP1	DP2	Unit
SFC_{init} **reduction**	-38	-38	-38	%
SFC_{target}	$3.69e^{-8}$	$3.69e^{-8}$	$3.69e^{-8}$	$\frac{kg}{s \cdot W}$
m_{PAY}	14296	14796	13906	kg
m_{PAY} **reduction**	-5980	-5480	-6370	kg
	-29.5	-27	-31.4	%
Battery P_{max}	12.8	12.3	13.2	MW
GT P_{max}	37.3	37.3	37.2	MW
Battery energy used	1899	1840	1961	kWh
m_{fuel}	1334	1308	1356	kg
Fuel saved wrt reference	+799	+826	+777	kg

Table 7.4: Short range mission analysis, 2 engines configuration: CASE 1bis results. From left to right the flight missions analyzed are the ones with number 3, 7 and 11 of Appendix A.

CASE 1bis is identical to CASE 1, the only difference is that now the approach phase is performed with the GT instead of the battery. The idea is to use the battery only in the phases in which the power and energy required are very low, in order to have a battery pack lighter. From Figures 7.18 and 7.19 of CASE 1 it can be seen that these phases are the initial descent and the descent. Looking the CASE 1bis results in Table 7.5, now the battery mass is almost 3 tons less with respect CASE 1. Therefore, as can be seen in Table 7.4, it is possible to bring more payload, even if also in this case m_{PAY} is less than reference. Obviously, the fuel saved is less than CASE 1. Similar considerations done for CASE 1 can be done also for CASE 1bis, so for example also for CASE 1bis the engine that performs better is the one designed with $N_{ratio} = 0.9$. Unfortunately, the problem of the battery weight is not solved, because the fuel saved does not compense the increase of mass.

Mass [kg]		
Variable	**Ref**	**DP1**
m_{OEW}	41413	41413
m_{Batt}	-	12309 (SP)
m_{PAY}	20276	14796
m_{FUEL}	2133	1308
Total $m_{ElecMot}$	-	3365
m_{PElec}	-	1125
$m_{ElecGen}$	-	3922
m_{tot}	63822	78237
Difference m_{tot} from Ref	-	+14415

Table 7.5: Short range mission, 2 engines configuration, CASE 1bis: Comparison between the reference component masses and the component masses of the best result between DPref, DP1 and DP2.

CASE 2

	DPref	**DP1**	**DP2**	**Unit**
SFC_{init} **reduction**	-12	-9	-13	%
SFC_{target}	5.23e^{-8}	5.41e^{-8}	5.17e^{-8}	$\frac{kg}{s \cdot W}$
m_{PAY}	20276	20276	20276	kg
m_{PAY} reduction	0	0	0	kg
	0	0	0	%
GT P_{max}	35.9	35.5	35.9	MW
m_{FUEL}	2116	2132	2127	kg
Fuel saved wrt reference	+17	+1	+6	kg

Table 7.6: Short range mission analysis, 2 engines configuration: CASE 2 results. From left to right the flight missions analyzed are the ones with number 4, 8 and 12 of Appendix A.

In CASE 2 the electric CR fan engines considered are the same as before, but the hybrid system is different. In fact, the hybrid layout is the one depicted in Figure 7.3. Now the battery is not present, therefore the GT has to remain on for all the flight. In this case m_{PAY} is not reduced, even if the total weight of the aircraft is increased due to the weight

of the electric components (Table 7.7). Again, the better performances are obtained with the engine designed at $N_{ratio} = 0.9$. In fact, it is true that the fuel saved is less with respect the other two engines, but the key parameter is SFC_{target}, which is higher. This means that the required reduction in the GT SFC is less, hence the electric CR fan engine HYB-CF1-2eng-DP1 is more efficienct with respect the others.

Mass [kg]

Variable	Ref	DP1
m_{OEW}	41413	41413
m_{PAY}	20276	20276
m_{FUEL}	2133	2132
Total $m_{ElecMot}$	-	3306
m_{PElec}	-	544
$m_{ElecGen}$	-	3738
m_{tot}	63822	71410
Difference m_{tot} from Ref	-	+7588

Table 7.7: Short range mission, 2 engines configuration, CASE 2: Comparison between the reference component masses and the component masses of the best result between DPref, DP1 and DP2.

CASE 2bis

	DPref	DP1	DP2	Unit
$SFC_{initial}$ **reduction**	-7	-5	-9	%
SFC_{target}	5.53e^{-8}	5.65e^{-8}	5.41e^{-8}	$\frac{kg}{s \cdot W}$
m_{PAY}	20276	20276	20276	kg
m_{PAY} **reduction**	0	0	0	kg
	0	0	0	%
GT P_{max}	33.5	33	34.1	MW
m_{FUEL}	2129	2114	2123	kg
Fuel saved wrt reference	+5	+20	+10	kg

Table 7.8: Short range mission analysis, 2 engines configuration: CASE 2bis results. From left to right the flight missions analyzed are the ones with number 5, 9 and 13 of Appendix A.

CASE 2bis is identical to CASE 2, but now the weight of the electric components are not considered. The assumption done in CASE 2bis is that the aircraft weight at take-off is identical to reference. CASE 2bis is very useful, because permits to compute like a reference value of SFC_{target}. Again, the better performances are reached with HYB-CF1-2eng-DP1. The result obtained is that, starting from a value of $SFC = 5.65e^{-8}$ $\frac{\text{kg}}{\text{s}\cdot\text{W}}$, the combo GT plus electric CR fan engines consumes less fuel with respect CFM56-7B24.

7.1.3. Sensitivity analysis: Boeing 737-800 propelled by HYB-CF1 with 10 engines configuration

The different flight missions analyzed in this sub-section are the ones from 16 to 27 of Appendix A. These are the ones performed by Boeing 737-800 in which are alternatively mounted the CR fan engines HYB-CF1-10eng-DPref, HYB-CF1-10eng-DP1 and HYB-CF1-10eng-DP2. The hybrid systems tested are CASE 1 and CASE 1bis with the layout hy-el se, and CASE 2 and CASE 2bis with the layout tu-el pc.

In Figure 7.20 is represented the structure of this sub-section. This sub-section is analogous to Sub-section 7.1.2, but now the electric CR fans are in distributed propulsion configuration. Remember that these engines were modeled with the same boundary conditions of the ones in 2 engines configuration. The only boundary condition different is $\dot{m}_{in}$, because now the engines are smaller, hence less powerful.

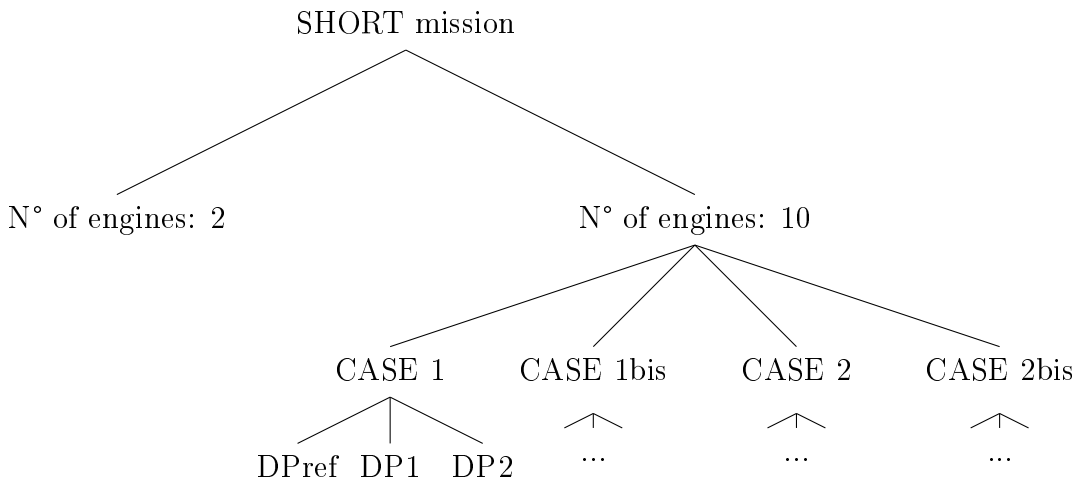

Figure 7.20: Tree diagram that describes the sensitivity analysis procedure in the case of short mission range in 10 engines configuration.

CASE 1

	DPref	DP1	DP2	Unit
SFC_{init} **reduction**	-38	-38	-38	%
SFC_{target}	$3.69e^{-8}$	$3.69e^{-8}$	$3.69e^{-8}$	$\frac{kg}{s \cdot W}$
m_{PAY}	10386	10676	9066	kg
m_{PAY} **reduction**	-9890	-9600	-11210	kg
	-48.8	-47.4	-55.3	%
Battery P_{max}	16.9	16.6	18.2	MW
GT P_{max}	37.3	37.2	37.3	MW
Battery energy used	3214	3169	3351	kWh
m_{FUEL}	1142	1135	1154	kg
Fuel saved wrt reference	+992	+999	+979	kg

Table 7.9: Short range mission analysis, 10 engines configuration: CASE 1 results. From left to right the flight missions analyzed are the ones with number 16, 20 and 24 of Appendix A.

With respect to the case with 2 engines configuration, now the engines HYB-CF1-10eng-DPref and HYB-CF1-10eng-DP1 behave in a very similar way, in fact the results are very similar (Table 7.9). However, between these two the best is still the one that works with $N_{ratio} = 0.9$. Unfortunately, with respect the case of two engines, the global performances are worst, because the fuel saved and m_{PAY} are less. This is explained through the fact that with more engines there are more losses. In fact, now is requested more energy and power from the battery pack, hence it is heavier (Table 7.10). Note that for this preliminary analysis the main advantages of a distributed configuration were not taken in account. However, for future developement of this work they should be taken in account. For example the fact that, from a techonological point of view, in a distributed configuration the power that each electric engine has to deliver is less. So, it is more easy to produce these engines. Another aspect is about the safety, hence the concept of redundancy. Another aspect regards the size of the engine. In order to reduce the energy consumption, $\dot{m}_{in}$ should be high and β_c low. Therefore, in a distributed configuration is easier to achieve higher values of $\dot{m}_{in}$.

Mass [kg]		
Variable	**Ref**	**DP1**
m_{OEW}	41413	41413
m_{Batt}	-	16610 (SP)
m_{PAY}	20276	10676
m_{FUEL}	2133	1135
Total $m_{ElecMot}$	-	3362
m_{PElec}	-	1124
$m_{ElecGen}$	-	3918
m_{tot}	63822	78239
Difference m_{tot} from Ref	-	+14417

Table 7.10: Short range mission, 10 engines configuration, CASE 1: Comparison between the reference component masses and the component masses of the best result between DPref, DP1 and DP2.

CASE 1bis

	DPref	**DP1**	**DP2**	**Unit**
SFC_{init} **reduction**	-38	-38	-38	%
SFC_{target}	3.69e^{-8}	3.69e^{-8}	3.69e^{-8}	$\frac{kg}{s \cdot W}$
m_{PAY}	14256	14826	13906	kg
m_{PAY} **reduction**	-6020	-5450	-6370	kg
	-29.7	-26.9	-31.4	%
Battery P_{max}	12.8	12.3	13.2	MW
GT P_{max}	37.3	37.2	37.3	MW
Battery energy used	1911	1852	1968	kWh
m_{FUEL}	1329	1324	1353	kg
Fuel saved wrt reference	+804	+809	+780	kg

Table 7.11: Short range mission analysis, 10 engines configuration: CASE 1bis results. From left to right the flight missions analyzed are the ones with number 17, 21 and 25 of Appendix A.

In this case, similar considerations can be done. With respect the 2 engines configuration, HYB-CF1-10eng-DPref and HYB-CF1-10eng-DP1 provide very similar results.

Mass [kg]		
Variable	**Ref**	**DP1**
m_{OEW}	41413	41413
m_{Batt}	-	12273 (SP)
m_{PAY}	20276	14826
m_{FUEL}	2133	1324
Total $m_{ElecMot}$	-	3362
m_{PElec}	-	1124
$m_{ElecGen}$	-	3918
m_{tot}	63822	78240
Difference m_{tot} from Ref	-	+14418

Table 7.12: Short range mission, 10 engines configuration, CASE 1bis: Comparison between the reference component masses and the component masses of the best result between DPref, DP1 and DP2.

CASE 2

	DPref	**DP1**	**DP2**	**Unit**
SFC_{init} **reduction**	-12	-10	-14	%
SFC_{target}	5.23e^{-8}	5.35e^{-8}	5.11e^{-8}	$\frac{kg}{s \cdot W}$
m_{PAY}	20276	20276	20276	kg
m_{PAY} **reduction**	0	0	0	kg
	0	0	0	%
GT P_{max}	35.9	35.5	36	MW
m_{FUEL}	2118	2126	2112	kg
Fuel saved wrt reference	+15	+7	+21	kg

Table 7.13: Short range mission analysis, 10 engines configuration: CASE 2 results. From left to right the flight missions analyzed are the ones with number 18, 22 and 26 of Appendix A.

Now the battery is not considered, but the results are slightly worst with respect the case in 2 engines configuration. Instead, the engine designed at DPref shows performance that are more or less the same. It can be concluded that it is better to have two big CR fans

instead ten small CR fans. This conclusion is confirmed also by looking the results of CASE 2bis.

Mass [kg]

Variable	Ref	DP1
m_{OEW}	41413	41413
m_{PAY}	20276	20276
m_{FUEL}	2133	2126
Total $m_{ElecMot}$	-	3308
m_{PElec}	-	544
$m_{ElecGen}$	-	3740
m_{tot}	63822	71407
Difference m_{tot} from Ref	-	+7585

Table 7.14: Short range mission, 10 engines configuration, CASE 2: Comparison between the reference component masses and the component masses of the best result between DPref, DP1 and DP2.

CASE 2bis

	DPref	DP1	DP2	Unit
SFC_{init} **reduction**	-7	-6	-10	%
SFC_{target}	5.53e^{-8}	5.59e^{-8}	5.35e^{-8}	$\frac{kg}{s \cdot W}$
m_{PAY}	20276	20276	20276	kg
m_{PAY} **reduction**	0	0	0	kg
	0	0	0	%
GT P_{max}	33.6	33.1	34.1	MW
m_{FUEL}	2129	2121	2114	kg
Fuel saved wrt reference	+5	+13	+20	kg

Table 7.15: Short range mission analysis, 10 engines configuration: CASE 2bis results. From left to right the flight missions analyzed are the ones with number 19, 23 and 27 of Appendix A.

7.2. Medium range mission analysis

The structure of this section is identical to the one of section Section 7.1. At first will be analyzed the reference case for the medium range missions and then these results will be compared to the ones obtained with the hybrid aircrafts.

7.2.1. Reference: Boeing 737-800 propelled by CFM56-7B24

The reference case for the medium range mission is the one performed by the Boieng 737-800 propelled by CFM56-7B24. The components performance maps are reported in Figures 7.21, 7.22, 7.23, 7.25 and 7.24. The aricraft and the engine mounted are the same used for the short mission. Now the difference is that the cruise is longer and also the values of altitude and Mach are bigger. Therefore, the performance points in the performance maps will be located in different positions. However, the trends are similar, a part from the fact that during the climb phases the values of pressure ratio and mass flow are higher. This can be explained through the fact that the aircraft is heavier (more fuel), hence it needs more thrust.

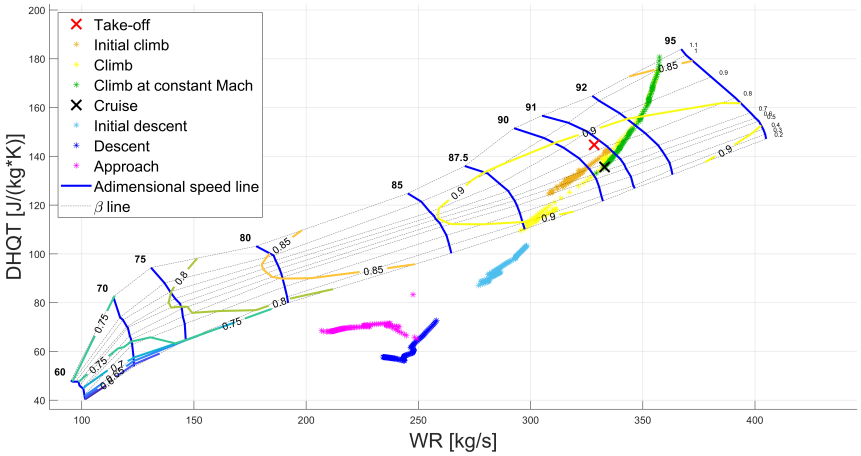

Figure 7.21: Reference medium mission: CFM56-7B24 fan performance points during flight.

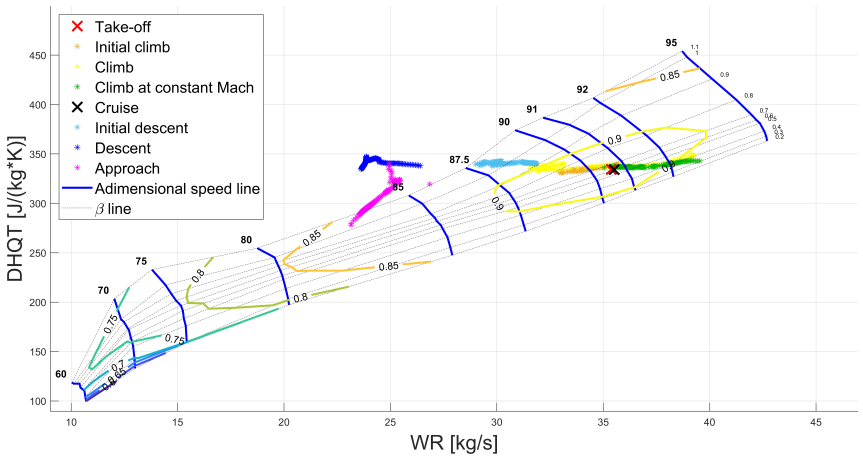

Figure 7.22: Reference medium mission: CFM56-7B24 LP compressor performance points during flight.

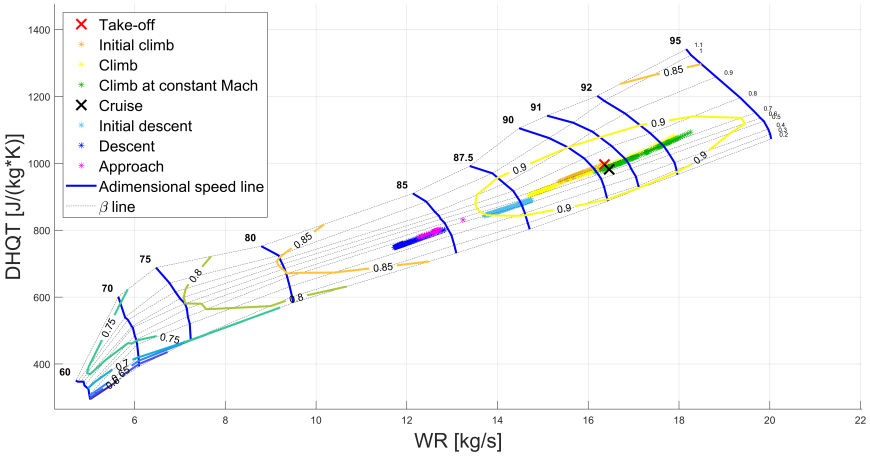

Figure 7.23: Reference medium mission: CFM56-7B24 HP compressor performance points during flight.

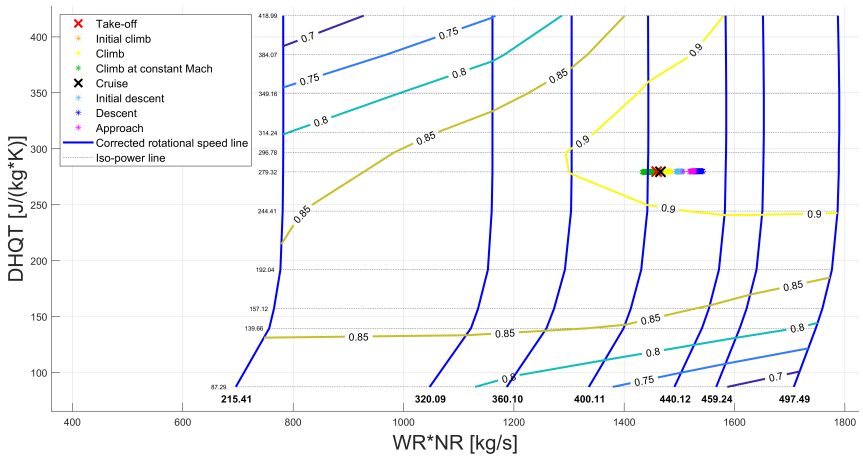

Figure 7.24: Reference medium mission: CFM56-7B24 HP turbine performance points during flight.

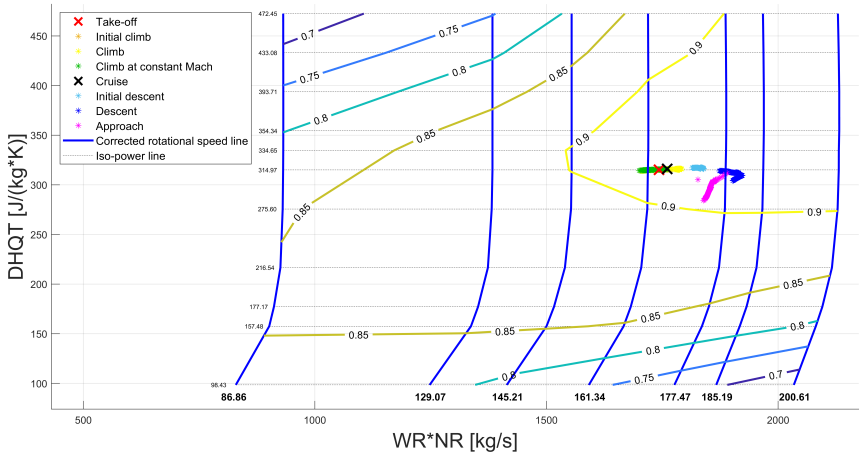

Figure 7.25: Reference medium mission: CFM56-7B24 LP turbine performance points during flight.

The values obtained in Table 7.16 were checked in literature and they will be used as reference for the medium range mission.

	Value	Unit
Total fuel consumed	6223	kg
Time of flight	152	min
Flight distance	2016	km

Table 7.16: Reference medium range mission analysis final results.

In order to have a graphical view of how variables like z, M, $\dot{m}_f$, etc... vary during the flight mission, the following plots are reported (Figures 7.26, 7.27, 7.28, 7.29 and 7.30). Note that now the aircraft flies for most of the time in cruise condition. Hence, if in the analysis of the short missions were pointed out the performance differences during climb and descent between the CFM56-7B24 and the hybrid systems, now these differences will be associated mainly to the cruise.

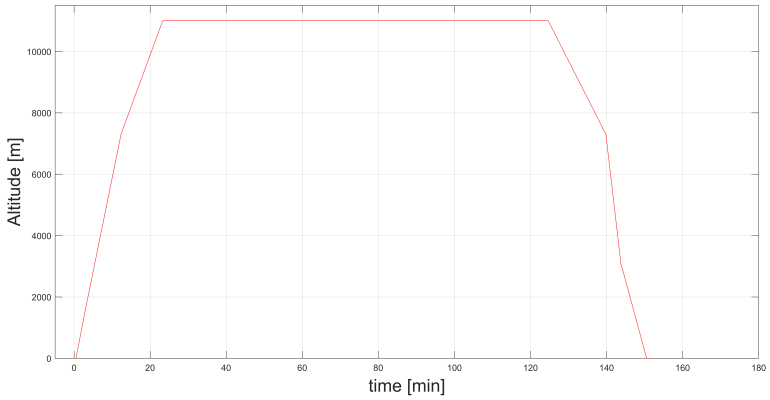

Figure 7.26: Reference medium mission: Altitude vs time of flight.

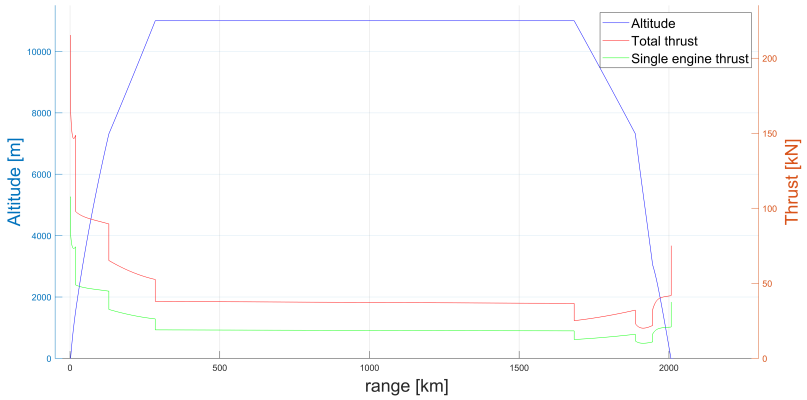

Figure 7.27: Reference medium mission: Altitude and Thrust vs range.

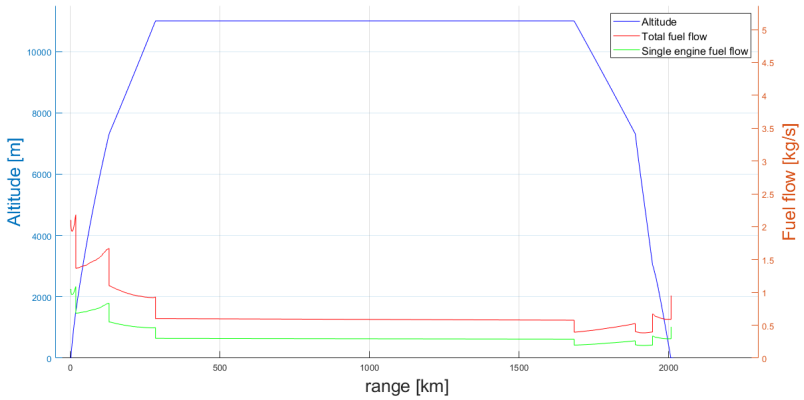

Figure 7.28: Reference medium mission: Altitude and Fuel flow vs range.

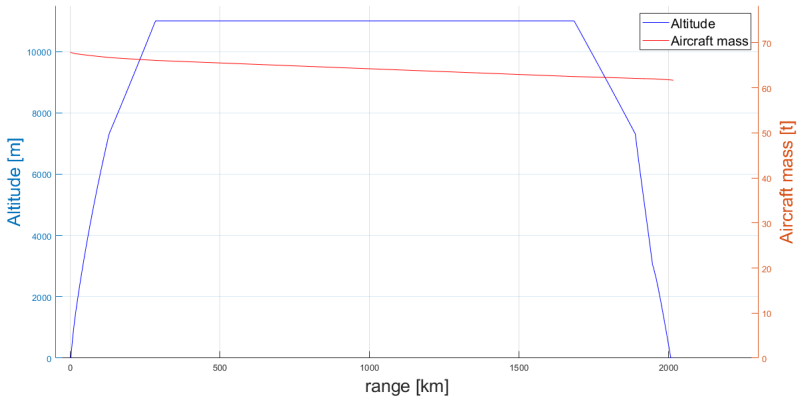

Figure 7.29: Reference medium mission: Altitude and Aircraft mass vs range.

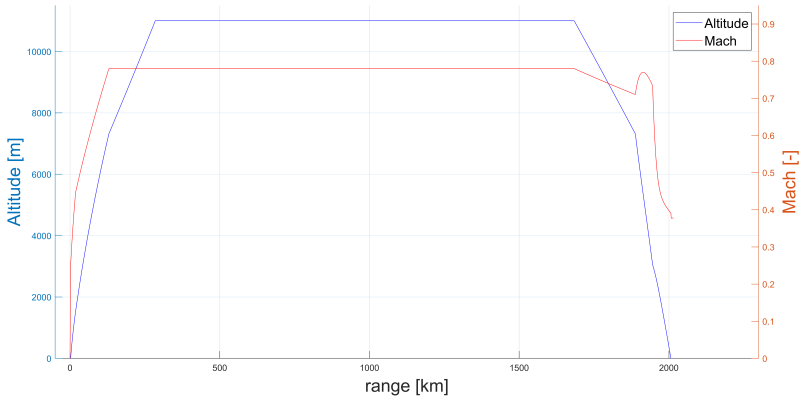

Figure 7.30: Reference medium mission: Altitude and Mach vs range.

7.2.2. Sensitivity analysis: Boeing 737-800 propelled by HYB-CF1 with 2 engines configuration

The different flight missions analyzed in this sub-section are the ones from 29 to 40 of Appendix A. These are the ones performed by Boeing 737-800 in which are alternatively mounted the engines HYB-CF1-2eng-DPref, HYB-CF1-2eng-DP1 and HYB-CF1-2eng-DP2. The hybrid systems tested are CASE 1 and CASE 1bis with the layout hy-el se, and CASE 2 and CASE 2bis with the layout tu-el pc. Note that the electric engines and the CASEs analyzed are the same used in the short missions.

In Figure 7.31 is represented how this sub-section is structured.

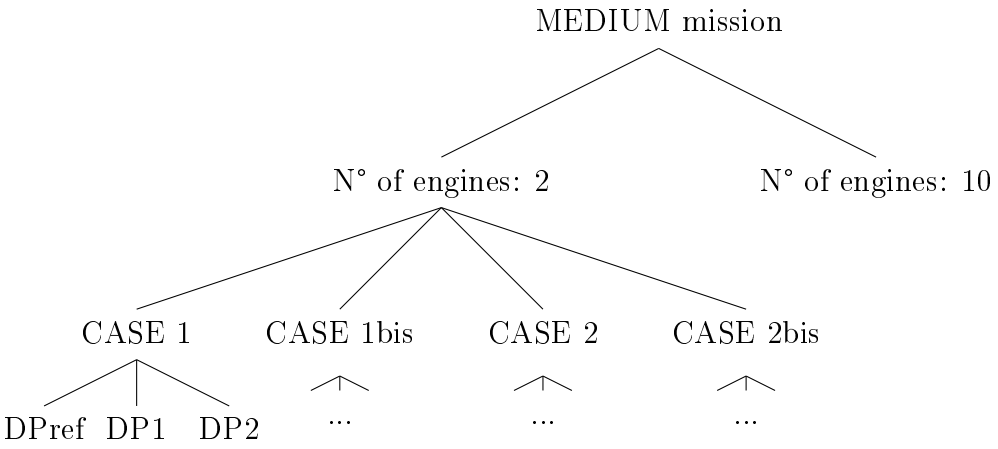

Figure 7.31: Tree diagram that describes the sensitivity analysis procedure in the case of medium mission range in 2 engines configuration.

CASE 1

	DPref	DP1	DP2	Unit
SFC_{init} **reduction**	-38	-38	-38	%
SFC_{target}	$3.69e^{-8}$	$3.69e^{-8}$	$3.69e^{-8}$	$\frac{kg}{s \cdot W}$
m_{PAY}	3496	4436	2686	kg
m_{PAY} **reduction**	-16780	-15840	-17590	kg
	-82.8	-78.1	-86.8	%
Battery P_{max}	17.4	15.6	17.9	MW
GT P_{max}	37.2	37.3	37.2	MW
Battery energy used	4066	3880	4223	kWh
m_{FUEL}	4588	4582	4613	kg
Fuel saved wrt reference	+1635	+1641	+1610	kg

Table 7.17: Medium range mission analysis, 2 engines configuration: CASE 1 results. From left to right the flight missions analyzed are the ones with number 29, 33 and 37 of Appendix A.

From Table 7.17 it can be seen that in general the results are worst with respect the short mission case. The first thing to note is that since the flight mission is longer it is required more fuel. This fuel increment has the consequence to reduce m_{PAY}, in fact the condition $m_{TOT} < m_{MTOW}$ has to be respected. The payload reduction is so high that to bring the same payload to the final destination more than 2 flights are needed. Considering that the fuel saved is around 1.6 tons, globally the hybrid solution will consume more fuel. This is in line with the existing literature, in which the aircraft hybridization is proposed only for short range missions. Moreover, from Table 7.18 note that the battery mass is defined by the amount of energy that has to store and not to the power pick that has to provide. The obtained value of battery mass is higher than the one obtained in the analogous short mission.

Mass [kg]		
Variable	**Ref**	**DP1**
m_{OEW}	41413	41413
m_{Batt}	-	19402 (SE)
m_{PAY}	20276	4436
m_{FUEL}	6223	4582
Total $m_{ElecMot}$	-	3365
m_{PElec}	-	1125
$m_{ElecGen}$	-	3922
m_{tot}	67912	78244
Difference m_{tot} from Ref	-	+10332

Table 7.18: Medium range mission, 2 engines configuration, CASE 1: Comparison between the reference component masses and the component masses of the best result between DPref, DP1 and DP2.

CASE 1bis

	DPref	**DP1**	**DP2**	**Unit**
SFC_{init} **reduction**	-38	-38	38	%
SFC_{target}	3.69e^{-8}	3.69e^{-8}	3.69e^{-8}	$\frac{kg}{s \cdot W}$
m_{PAY}	10086	10496	9646	kg
m_{PAY} **reduction**	-10190	-9780	-10630	kg
	-50.3	-48.2	-52.4	%
Battery P_{max}	12.5	11.9	12.8	MW
GT P_{max}	37.3	37.3	37.2	MW
Battery energy used	2710	2632	2791	kWh
m_{FUEL}	4783	4761	4820	kg
Fuel saved wrt reference	+1440	+1462	+1404	kg

Table 7.19: Medium range mission analysis, 2 engines configuration: CASE 1bis results. From left to right the flight missions analyzed are the ones with number 30, 34 and 38 of Appendix A.

CASE 1bis shows results worst with respect the reference case, but better with respect CASE 1. In fact, even if the fuel saved is less than before, the value of m_{PAY} is higher. In

particular, referring to the engine HYB-CF1-2eng-DP1, the fuel saved is about 1.4 tons against 1.6 tons of CASE 1, but now m_{PAY} is 10 tons and not 4.4 tons. This result shows that with an higher range mission the level of hybridization should be lower. In fact, in this case the value of the battery mass is about 6 tons lower with respect CASE 1.

Mass [kg]

Variable	Ref	DP1
m_{OEW}	41413	41413
m_{Batt}	-	13161 (SE)
m_{PAY}	20276	10496
m_{FUEL}	6223	4761
Total $m_{ElecMot}$	-	3365
m_{PElec}	-	1125
$m_{ElecGen}$	-	3922
m_{tot}	67912	78243
Difference m_{tot} from Ref	-	+10331

Table 7.20: Medium range mission, 2 engines configuration, CASE 1bis: Comparison between the reference component masses and the component masses of the best result between DPref, DP1 and DP2.

CASE 2

	DPref	DP1	DP2	Unit
SFC_{init} **reduction**	-19	-18	-20	%
SFC_{target}	4.82e^{-8}	4.87e^{-8}	4.76e^{-8}	$\frac{kg}{s \cdot W}$
m_{PAY}	20276	20276	20276	kg
m_{PAY} **reduction**	0	0	0	kg
	0	0	0	%
GT P_{max}	35	34.9	35	MW
m_{FUEL}	6189	6218	6180	kg
Fuel saved wrt reference	+34	+5	+43	kg

Table 7.21: Medium range mission analysis, 2 engines configuration: CASE 2 results. From left to right the flight missions analyzed are the ones with number 31, 35 and 39 of Appendix A.

Looking the results in Table 7.21 it can be noted that, with respect the short mission case, now the value of SFC_{target} is lower. This means that globally the combo of GT plus electric CR fans consumes more fuel with respect the short mission case and, obvioulsy, also more fuel with respect the reference case. This result is confirmed also by looking Table 7.22. In fact, since the total increment of the aircraft mass is similar to the one obtained in the short mission case, the increment in the fuel consumption is not due to the mass increase, but it is due to a more inefficient system during the cruise phase.

Mass [kg]

Variable	Ref	DP1
m_{OEW}	41413	41413
m_{PAY}	20276	20276
m_{FUEL}	6223	6218
Total $m_{ElecMot}$	-	3353
m_{PElec}	-	552
$m_{ElecGen}$	-	3675
m_{tot}	67912	75489
Difference m_{tot} from Ref	-	+7577

Table 7.22: Medium range mission, 2 engines configuration, CASE 2: Comparison between the reference component masses and the component masses of the best result between DPref, DP1 and DP2.

CASE 2bis

	DPref	DP1	DP2	Unit
SFC_{init} **reduction**	-14	-13	-15	%
SFC_{target}	$5.53e^{-8}$	$5.65e^{-8}$	$5.41e^{-8}$	$\frac{kg}{s \cdot W}$
m_{PAY}	20276	20276	20276	kg
m_{PAY} **reduction**	0	0	0	kg
	0	0	0	%
GT P_{max}	33.8	33.3	34.2	MW
m_{FUEL}	6174	6208	6208	kg
Fuel saved wrt reference	+49	+15	+15	kg

Table 7.23: Medium range mission analysis, 2 engines configuration: CASE 2bis results. From left to right the flight missions analyzed are the ones with number 32, 36 and 40 of Appendix A.

The results obtained in CASE 2bis (Figure 7.23) confirms what was written in CASE 2.

7.2.3. Sensitivity analysis: Boeing 737-800 propelled by HYB-CF1 with 10 engines configuration

The different flight missions analyzed in this sub-section are the ones from 41 to 52 of Appendix A. These are the ones performed by Boeing 737-800 in which are alternatively mounted the engines HYB-CF1-10eng-DPref, HYB-CF1-10eng-DP1 and HYB-CF1-10eng-DP2. Again, the hybrid systems tested are CASE 1 and CASE 1bis with the layout hy-el se, and CASE 2 and CASE 2bis with the layout tu-el pc.

This sub-section is structured as the other ones. In Figure 7.32 is represented its structure.

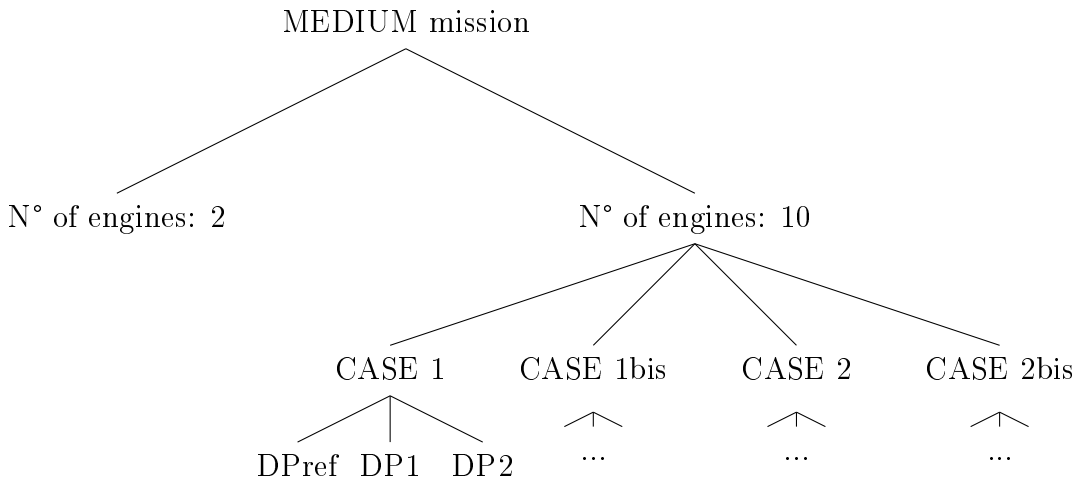

Figure 7.32: Tree diagram that describes the sensitivity analysis procedure in the case of short/medium mission range in 10 engines configuration.

The results obtained in CASE 1, CASE 1bis, CASE 2 and CASE 2bis are slightly worst with respect the ones obtained with the 2 engines configuration. The same thing happened with the short range case. Since similar considerations to the ones of the short range case can be done, in this sub-section will be only reported the results obtained in the different CASEs. The results will be reported for completeness, but they will not be commented in order to avoid useless ripetitions.

CASE 1

	DPref	DP1	DP2	Unit
SFC_{init} **reduction**	-38	-38	-38	%
SFC_{target}	3.69e^{-8}	3.69e^{-8}	3.69e^{-8}	$\frac{kg}{s \cdot W}$
m_{PAY}	3536	3956	2746	kg
m_{PAY} **reduction**	-16740	-16320	-17530	kg
	-82.6	-80.5	-86.5	%
Battery P_{max}	16.4	16.6	17.9	MW
GT P_{max}	37.3	37.2	37.3	MW
Battery energy used	4058	3976	4210	kWh
m_{FUEL}	4594	4580	4623	kg
Fuel saved wrt reference	+1629	+1643	+1600	kg

Table 7.24: Medium range mission analysis, 10 engines configuration: CASE 1 results. From left to right the flight missions analyzed are the ones with number 41, 45 and 49 of Appendix A.

Mass [kg]

Variable	Ref	DP1
m_{OEW}	41413	41413
m_{Batt}	-	16610 (SE)
m_{PAY}	20276	3956
m_{FUEL}	6223	4580
Total $m_{ElecMot}$	-	3362
m_{PElec}	-	1124
$m_{ElecGen}$	-	3918
m_{tot}	67912	78235
Difference m_{tot} from Ref	-	+10323

Table 7.25: Medium range mission, 10 engines configuration, CASE 1: Comparison between the reference component masses and the component masses of the best result between DPref, DP1 and DP2.

CASE 1bis

	DPref	DP1	DP2	Unit
SFC_{init} **reduction**	-38	-38	-38	%
SFC_{target}	$3.69e^{-8}$	$3.69e^{-8}$	$3.69e^{-8}$	$\frac{kg}{s \cdot W}$
m_{PAY}	10016	10416	9556	kg
m_{PAY} **reduction**	-10260	-9860	-10720	kg
	-50.6	-48.6	-52.9	%
Battery P_{max}	12.3	12	12.8	MW
GT P_{max}	37.3	37.2	37.3	MW
Battery energy used	2722	2646	2807	kWh
m_{FUEL}	4786	4772	4825	kg
Fuel saved wrt reference	+1437	+1451	+1398	kg

Table 7.26: Medium range mission analysis, 10 engines configuration: CASE 1bis results. From left to right the flight missions analyzed are the ones with number 42, 46 and 50 of Appendix A.

Mass [kg]

Variable	Ref	DP1
m_{OEW}	41413	41413
m_{Batt}	-	13229 (SE)
m_{PAY}	20276	10416
m_{FUEL}	6223	4772
Total $m_{ElecMot}$	-	3362
m_{PElec}	-	1124
$m_{ElecGen}$	-	3918
m_{tot}	67912	78234
Difference m_{tot} from Ref	-	+10332

Table 7.27: Medium range mission, 10 engines configuration, CASE 1bis: Comparison between the reference component masses and the component masses of the best result between DPref, DP1 and DP2.

CASE 2

	DPref	DP1	DP2	Unit
SFC_{init} **reduction**	-19	-19	-20	%
SFC_{target}	$5.23e^{-8}$	$5.35e^{-8}$	$5.11e^{-8}$	$\frac{kg}{s \cdot W}$
m_{PAY}	20276	20276	20276	kg
m_{PAY} **reduction**	0	0	0	kg
	0	0	0	%
GT P_{max}	35	35	35	MW
m_{FUEL}	6191	6158	6192	kg
Fuel saved wrt reference	+32	+65	+31	kg

Table 7.28: Medium range mission analysis, 10 engines configuration: CASE 2 results. From left to right the flight missions analyzed are the ones with number 43, 47 and 51 of Appendix A.

Mass [kg]

Variable	Ref	DP1
m_{OEW}	41413	41413
m_{PAY}	20276	20276
m_{FUEL}	6223	6158
Total $m_{ElecMot}$	-	3359
m_{PElec}	-	553
$m_{ElecGen}$	-	3681
m_{tot}	67912	75440
Difference m_{tot} from Ref	-	+7528

Table 7.29: Medium range mission, 10 engines configuration, CASE 2: Comparison between the reference component masses and the component masses of the best result between DPref, DP1 and DP2.

CASE 2bis

	DPref	DP1	DP2	Unit
SFC_{init} **reduction**	-14	-13	-15	%
SFC_{target}	5.11e^{-8}	5.17e^{-8}	5.05e^{-8}	$\frac{kg}{s \cdot W}$
m_{PAY}	20276	20276	20276	kg
m_{PAY} **reduction**	0	0	0	kg
	0	0	0	%
GT P_{max}	33.7	33.3	34.2	MW
m_{FUEL}	6185	6222	6222	kg
Fuel saved wrt reference	+38	+1	+1	kg

Table 7.30: Medium range mission analysis, 10 engines configuration: CASE 2bis results. From left to right the flight missions analyzed are the ones with number 44, 48 and 52 of Appendix A.

7.3. Long range mission analysis

In this last section the long range mission case will be analyzed. The structure of this section is the same as before, but note that CASE 1 and CASE 1bis will be not analyzed. From the medium range missions, it was seen that due to the high demand of power and energy the resulting battery weight is too high. Since in the long range missions the power request is in the order of 100 [MW], the resulting battery weight would be so high that the aircraft could not fly. Therefore, in this section only the configurations depicted in Figures 7.3 and 7.4 will be tested through CASE 2 and CASE 2bis.

7.3.1. Reference: Boeing 787-800 propelled by GEnx-1B64

The reference case for the long range mission is the one performed by the Boieng 787-800 propelled by GEnx-1B64. In Figures 7.33, 7.35, 7.34, 7.36, 7.37 are reported the component performance maps. Analogous considerations done for both the previous reference cases can be done. However, remember that now the engine is different. Hence, even if the shape of these maps are the same as before, the scaling factors are different.

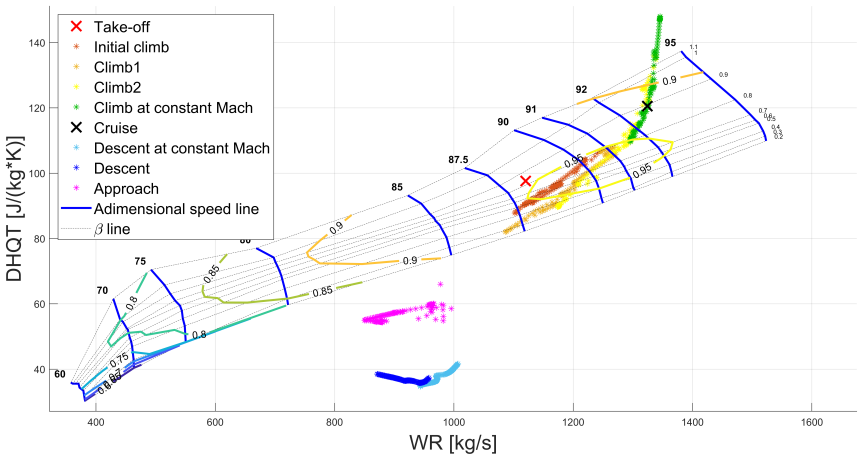

Figure 7.33: Reference long mission: GEnx-1B64 fan performance points during flight.

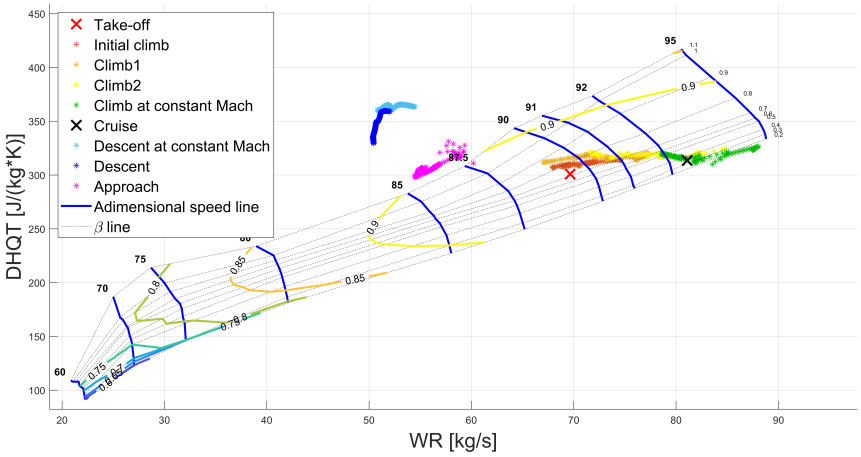

Figure 7.34: Reference long mission: GEnx-1B64 LP compressor performance points during flight.

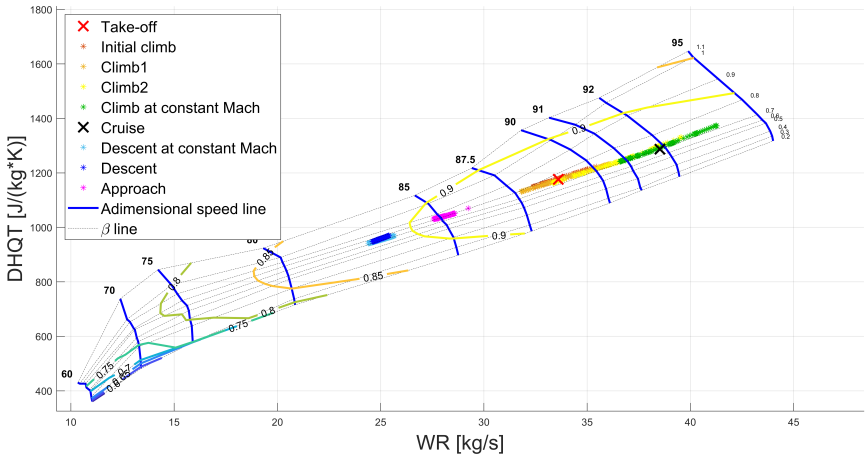

Figure 7.35: Reference long mission: GEnx-1B64 HP compressor performance points during flight.

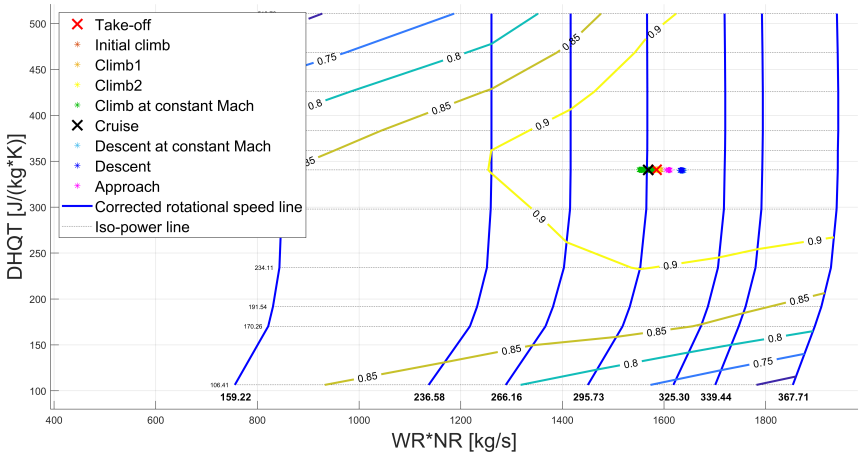

Figure 7.36: Reference long mission: GEnx-1B64 HP turbine performance points during flight.

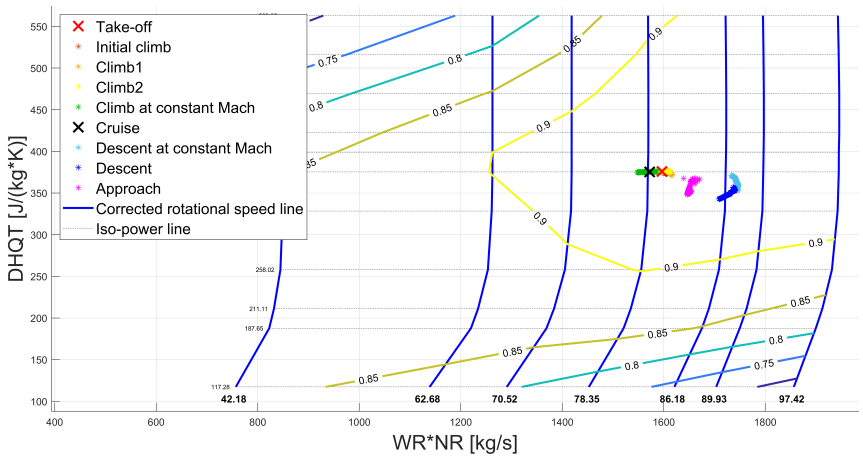

Figure 7.37: Reference long mission: GEnx-1B64 LP turbine performance points during flight.

In Table 7.31 are reported the results of the reference flight mission. Note that now the value of the fuel consumed is one order of magnitude bigger than before, therefore only a little improvement achieved can save a lot of fuel. Also these results are in line with what can be found in literature.

	Value	**Unit**
Total fuel consumed	46082	kg
Time of flight	444	min
Flight distance	6469	km

Table 7.31: Reference long range mission analysis final results.

In Figures 7.38, 7.39, 7.40, 7.40, 7.41 and 7.42 are reported the plots of the main important variables. The most important flight phase is the cruise, in which are achieved the highest values of altitude and mach with respect the other reference cases. Moreover, it can be noted that in a long range mission the aircraft mass can't be considered constant.

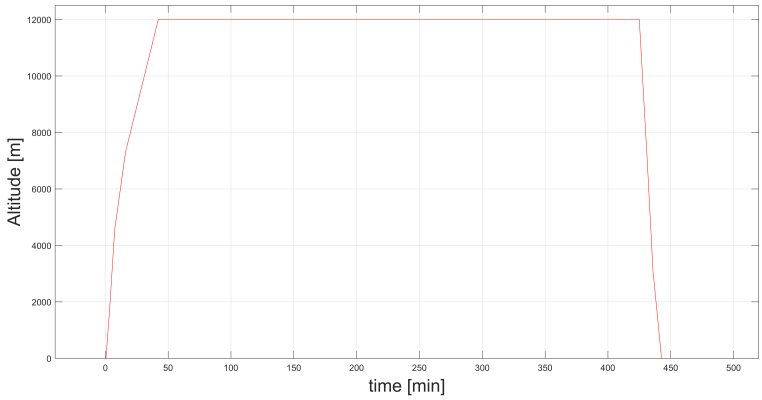

Figure 7.38: Reference long mission: Altitude vs time of flight.

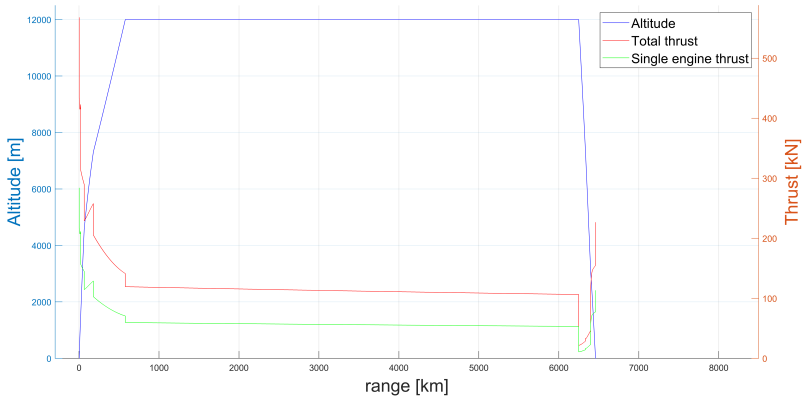

Figure 7.39: Reference long mission: Altitude and Thrust vs range.

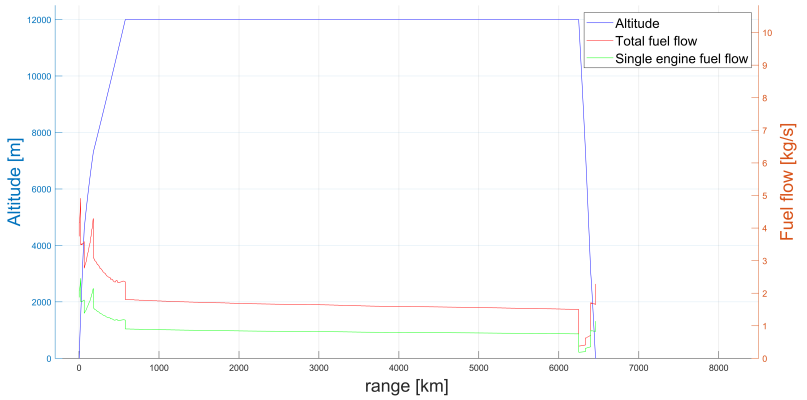

Figure 7.40: Reference long mission: Altitude and Fuel flow vs range.

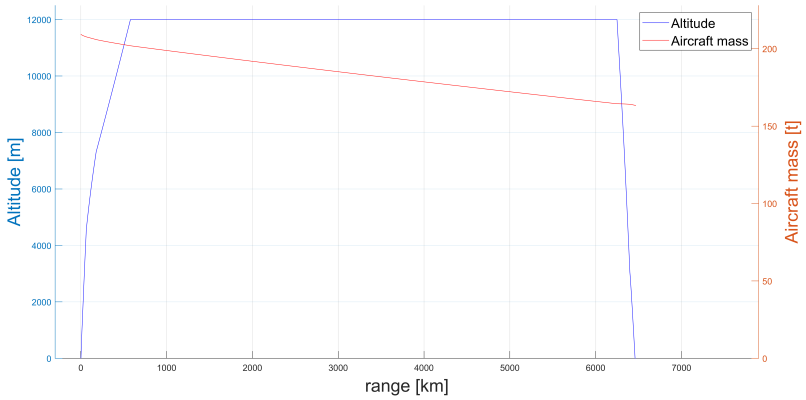

Figure 7.41: Reference long mission: Altitude and Aircraft mass vs range.

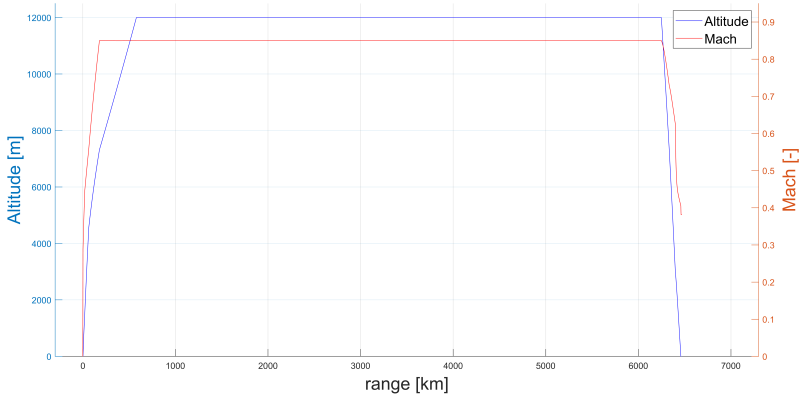

Figure 7.42: Reference long mission: Altitude and Mach vs range.

In the following Sub-sections 7.3.2 and 7.3.3 the flight missions with 2 or 10 engines configuration will be analyzed. The electric CR fans tested are respectively the ones of the group HYB-CF2-2eng and the ones of the group HYB-CF2-10eng. The difference from before, as explained in Chapter 5, is that now the CR fan engines HYB-CF2-2eng and the CR fan engines HYB-CF2-10eng have also a different value of β_c and not only a different $\dot{m}_{in}$. Hence, more different results are expeced between the 2 and the 10 engines configuration. In particular, since in the CR fan engines HYB-CF2-10eng the design value of β_c is lower, better results are expected for the distributed propulsion.

7.3.2. Sensitivity analysis: Boeing 787-800 propelled by HYB-CF2 with 2 engines configuration

The different flight missions analyzed in this sub-section are the ones from 54 to 59 of Appendix A. These are the ones performed by Boeing 787-800 in which are alternatively mounted the engines HYB-CF2-2eng-DPref, HYB-CF2-2eng-DP1 and HYB-CF2-2eng-DP2. The hybrid systems tested are only CASE 2 and CASE 2bis with the layout tu-el pc.

In Figure 7.43 is depicted the sub-section structure.

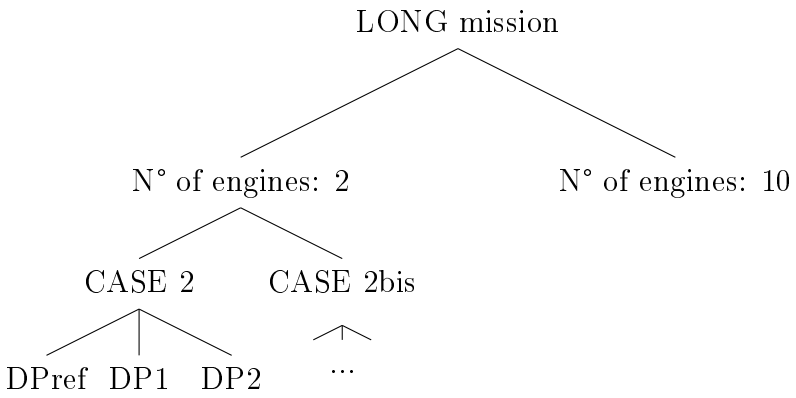

Figure 7.43: Tree diagram that describes the sensitivity analysis procedure in the case of long mission range in 2 engines configuration.

CASE 2

	DPref	DP1	DP2	Unit
SFC_{init} **reduction**	-38	-38	-38	%
SFC_{target}	$3.27e^{-8}$	$3.27e^{-8}$	$3.27e^{-8}$	$\frac{kg}{s \cdot W}$
m_{PAY}	42298	42508	41908	kg
m_{PAY} **reduction**	-1020	-810	-1410	kg
	-2.4	-1.9	-3.3	%
GT P_{max}	118.7	117.7	120	MW
m_{FUEL}	40324	40312	40375	kg
Fuel saved wrt reference	+5758	+5770	+5708	kg

Table 7.32: Long range mission analysis, 2 engines configuration: CASE 2 results. From left to right the flight missions analyzed are the ones with number 54, 56 and 58 of Appendix A.

From Table 7.32 can be seen that also in this case the engine designed with $N_{ratio} = 0.9$ has the best performances. Again, this was expected and it confirms what was seen in Chapter 5. The results show that the fuel saved is almost 6 tons and that the penalty in terms of m_{PAY} is very low. Unfortunately, the value of SFC_{target} found by the code is very low. From Table 7.33 it can be noted that the code reduced SFC_{init} in order to satisfy the condition of $m_{TOT} < m_{MTOW}$. In fact, due to the high electric power demand, the weight of the electric components increased the aircraft weight of about 9 %.

Mass [kg]

Variable	Ref	DP1
m_{OEW}	119950	11950
m_{PAY}	43318	42508
m_{FUEL}	46082	40312
Total $m_{ElecMot}$	-	11171
m_{PElec}	-	1839
$m_{ElecGen}$	-	12630
m_{tot}	209350	227871
Difference m_{tot} from Ref	-	+18521

Table 7.33: Long range mission, 2 engines configuration, CASE 2: Comparison between the reference component masses and the component masses of the best result between DPref, DP1 and DP2.

From Table 7.33 of CASE 2bis, it is interesting to note that the value of SFC_{target} is 25 % lower with respect SFC_{init}. It means that the combo GT plus electric CR fan engines consumes less fuel with respect the reference value only if SFC_{target} is at least 3.27e^{-8} $[\frac{kg}{s \cdot W}]$. The reduction of 25 % is higher compared to what was found for the short and medium range cases. This means that the CR fan engines work very well in short range missions in which for most of the time the aircraft is in a climb or descent phase. Instead, during the cruise phase the turbofan is still more efficient.

CASE 2bis

	DPref	DP1	DP2	Unit
SFC_{init} **reduction**	-25	-25	-25	%
SFC_{target}	3.96e^{-8}	3.96e^{-8}	3.96e^{-8}	$\frac{kg}{s \cdot W}$
m_{PAY}	43318	43318	43318	kg
m_{PAY} **reduction**	0	0	0	kg
	0	0	0	%
GT P_{max}	111.7	110.6	113.6	MW
m_{FUEL}	45592	45544	45854	kg
Fuel saved wrt reference	+491	+538	+228	kg

Table 7.34: Long range mission analysis, 2 engines configuration: CASE 2bis results. From left to right the flight missions analyzed are the ones with number 55, 57 and 59 of Appendix A.

7.3.3. Sensitivity analysis: Boeing 787-800 propelled by HYB-CF2 with 10 engines configuration

The different flight missions analyzed in this sub-section are the ones from 60 to 65 of Appendix A. These are the ones performed by Boeing 787-800 in which are alternatively mounted the engines HYB-CF2-10eng-DPref, HYB-CF2-10eng-DP1 and HYB-CF2-10eng-DP2. The hybrid systems tested are only CASE 2 and CASE 2bis with the layout tu-el pc.

In Figure 7.44 is represented how this sub-section is structured.

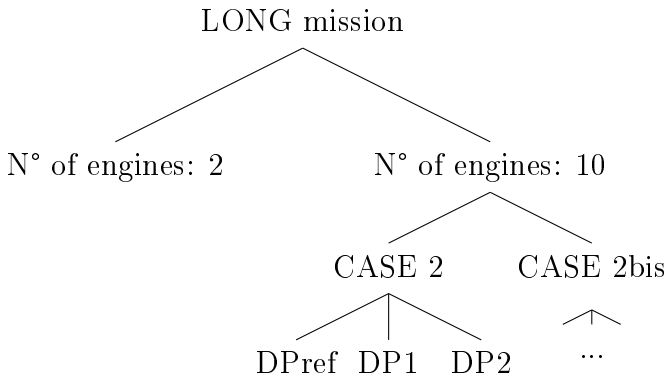

Figure 7.44: Tree diagram that describes the sensitivity analysis procedure in the case of long mission range in 10 engines configuration.

CASE 2

	DPref	DP1	DP2	Unit
SFC_{init} **reduction**	-36	-36	-36	%
SFC_{target}	$3.38e^{-8}$	$3.38e^{-8}$	$3.38e^{-8}$	$\frac{kg}{s \cdot W}$
m_{PAY}	43318	43318	43318	kg
m_{PAY} **reduction**	0	0	0	kg
	0	0	0	%
GT P_{max}	111.6	110.6	112.2	MW
m_{FUEL}	40539	40353	40578	kg
Fuel saved wrt reference	+5544	+5730	+5504	kg

Table 7.35: Long range mission analysis, 10 engines configuration: CASE 2 results. From left to right the flight missions analyzed are the ones with number 60, 62 and 64 of Appendix A.

The results of CASE 2 are reported in Table 7.35. As expected, the 10 engines configuration performs better with respect the 2 engines configuration. In fact, these electric CR fan engines have a lower value of β_c, hence an higher value of $\dot{m}_{in}$. Therefore, the propulsive efficiency is higher.

Mass [kg]

Variable	Ref	DP1
m_{OEW}	119950	119950
m_{PAY}	43318	43318
m_{FUEL}	46082	40353
Total $m_{ElecMot}$	-	10292
m_{PElec}	-	1694
$m_{ElecGen}$	-	11637
m_{tot}	209350	227244
Difference m_{tot} from Ref	-	+17894

Table 7.36: Long range mission, 10 engines configuration, CASE 2: Comparison between the reference component masses and the component masses of the best result between DPref, DP1 and DP2.

CASE 2bis

	DPref	DP1	DP2	Unit
SFC_{init} **reduction**	-23	-23	-23	%
SFC_{target}	$4.06e^{-8}$	$4.06e^{-8}$	$4.06e^{-8}$	$\frac{kg}{s \cdot W}$
m_{PAY}	43318	43318	43318	kg
m_{PAY} **reduction**	0	0	0	kg
	0	0	0	%
GT P_{max}	105.5	104.2	106.8	MW
m_{FUEL}	45740	45566	45947	kg
Fuel saved wrt reference	+342	+516	+135	kg

Table 7.37: Long range mission analysis, 10 engines configuration: CASE 2bis results. From left to right the flight missions analyzed are the ones with number 61, 63 and 65 of Appendix A.

The results in Table 7.37 of CASE 2 bis confirm the ones of CASE 2.

8 | Conclusions and future perspective

This thesis presents a global overview about electric CR fans, which were analyzed from different point of views. The component CR fan was created in EL, in such a way it was possible to use it with the other components in the turbojet library. Then, the electric CR fan engine schematic was builted. After that, different engines were modeled and their engine maps [1] created. A similar approach was used to obtain the engine maps of the two reference turbofans, the CFM56-7B24 and the GEnx-1B64. In the last part of the thesis different flight missions were performed. Each flight mission is defined by the range (short/medium/long), the hybrid system used (CASE 1 / CASE 1bis / CASE 2 / CASE 2bis) and the electric CR fan used (HYB-CF1 gruop / HYB-CF2 group). In Chapter 7 the flight missions results were presented.

First of all, the off-design analysis showed that the CR fans have a bigger rangeability with respect the turbofans. In fact, since a CR fan can works at different values of N_{ratio}, its total engine map is the sum of the three engine maps obtained at $N_{ratio} = 1$, $N_{ratio} = 0.9$ and $N_{ratio} = 1.1$. Moreover, also the single engine map at fixed N_{ratio} presents an higher rangeability. These results are in line with what can be found in the literature presented in Chapter 2. Among all the electric CR fan engines, the ones designed with $N_{ratio} = 0.9$ (i.e. DP1) showed the best performances in off-design. This result is confirmed also in the analysis of the flight missions, in which these engines are the ones that consume less energy. Note that these results are valid for the non-scaled engine maps used in this thesis, hence changing the engine maps the results can change.
The results obtained with the 10 engines configuration, compared to the ones obtained with the 2 engines configuration, are slightly worst in the short and medium range mis-

[1] Remember that the engine map is simple the result of the off-design analysis. This is a 3D plot in which the axis are z, M and $\dot{m}_f$ (or P). Each point of this plot is the result of a single off-design calculation performed at a specific value of z, M and $\dot{m}_f$ (or P). In that point are saved also all the other engine parameters obtained in that simulation. So, for example, this map tells to the user that the engine at a certain z, M and $\dot{m}_f$ (or P) generates a certain amount of T_h. This is why the name engine map.

sions, but they are better in the long ones. As explained in Chapter 7, the electric CR fan engines used in the short and medium range missions were modeled with very similar boundary conditions for both the configurations. The conclusion is that, increasing the number of engines, the global system is less efficient. Instead, for the long range missions the electric CR fan engines used in 10 engines configuration are more efficient because, with respect the ones used in the 2 engines configuration, they were modeled imposing a lower value of β_c and an higher value of $\dot{m}_{in}$. A suggestion for future studies is to analyze more in detail the distributed configuration, because it is easier to achieve an higher propulsive efficiency of the overall system while limiting the engine size.
Another result obtained is that the use of the battery makes sense only in short range missions, where relatively low level of power and energy are required. Moreover, the battery dimensioning parameter for the short range missions is the battery SP. Instead, starting from medium range missions, the battery dimensioning parameter is the SE. For medium and long range missions the hybrid layout tu-el pc is preferable, in which a GT provides electric power to the electric engines for the all duration of the flight. However, especially for the long range case, the problem is the weight of the electric components. In general, these results are very sensitive to the electric components technological level, hence a more detailed analysis is required in future studies. In particular, when high power is needed, these components should have very high SP. Therefore, should be interesting to analyze a tu-el pc layout with superconductive electric components and liquid hydrogen. The latter used to both maintain the superconductivity and as a fuel for the GT.
The last results provided are the ones obtained in CASEs 2bis. Here are highlighted the differencies between the fuel consumed by the turbofans and the one consumed by the system CR fans plus GT. These results showed that in the short range missions could be a certain advantage and this is the consequence of the high rangeability of the CR fans. Instead a more detailed analysis is required for the long range mission, in which the results depend mainly on the CR fan efficiency in cruise condition.
For all the flight missions analyzed the SFC_{target} value for the GT was computed. As explained in the thesis, this is the SFC that the GT should have in order to make first of all the flight possible (i.e. $m_{TOT} < m_{MTOW}$) and then also more sustainable (i.e. less fuel consumed with respect the reference case).

The future researches about that topic should use these results as guidelines and the models created in EcosimPro as a basis for more complete and detailed modelling. About EcosimPro, it should be preferable continue the studies in PROOSIS, which is a software compatible with EcosimPro, but designed specifically for the analysis of aeroengines.

Bibliography

[1] Elementi di meccanica del volo (parte 1). Università La Sapienza di Roma.

[2] *EcosimPro 5.2 modelling and simulation software - User Manual*.

[3] *A Review of Recent Research on Contra-Rotating Axial Flow Compressor Stage*, volume Volume 1: Turbomachinery of *Turbo Expo: Power for Land, Sea, and Air*, 06 1996. doi: 10.1115/96-GT-254. URL https://doi.org/10.1115/96-GT-254. V001T01A073.

[4] Aircraft drag polar estimation based on a stochastic hierarchical model. In *Eighth SESAR Innovation Days, 3rd – 7th December 2018, Salzburg, Austria*, 2018.

[5] A. Alexiou, I. Roumeliotis, N. Aretakis, A. Tsalavoutas, and K. Mathioudakis. Modeling Contra-Rotating Turbomachinery Components for Engine Performance Simulations: The Geared Turbofan With Contra-Rotating Core Case. *Journal of Engineering for Gas Turbines and Power*, 134(11), 09 2012. ISSN 0742-4795. doi: 10.1115/1.4007197. URL https://doi.org/10.1115/1.4007197. 111701.

[6] G. Colella. Design and preliminary optimization of a supersonic turbine for rotating detonation engine. master's degree thesis, Politecnico di Milano, Oct 2020.

[7] M. Daly. *Jane's Aero-Engines: 2019-2020*. Jane's by IHS Markit, 2019. ISBN 9780710633101.

[8] Eurocontrol. Boeing 737-800, . URL https://contentzone.eurocontrol.int/aircraftperformance/details.aspx?ICAO=B738&NameFilter=737. [12/03/2022].

[9] Eurocontrol. Boeing 787-800, . URL https://contentzone.eurocontrol.int/aircraftperformance/details.aspx?ICAO=B788&NameFilter=787. [12/03/2022].

[10] Flightradar24. URL https://www.flightradar24.com. [12/03/2022].

[11] F. G. Francesco Nasuti, Diego Lentini. Dispense del corso di propulsione aerospaziale, a.a. 2011/2012. Sapienza Università di Roma; Corso di Laurea di 1° livello in Ingegneria Aerospaziale.

[12] P. Gaetani. Notes from the turbomachinery course, a.a. 2020/2021. Politecnico di Milano; master's degree in aeronautical engineering.

[13] General Electric. Power gas turbine catalogue. https://www.ge.com/gas-power/products/gas-turbines, 2022. [Online; accessed 21-June-2022].

[14] H. Gesell, F. Wolters, and M. Plohr. System analysis of turbo-electric and hybrid-electric propulsion systems on a regional aircraft. *The Aeronautical Journal*, 123 (1268):1602–1617, 2019. doi: 10.1017/aer.2019.61.

[15] H. Gesell, F. Wolters, and M. Plohr. System analysis of turbo-electric and hybrid-electric propulsion systems on a regional aircraft. *The Aeronautical Journal*, 123 (1268):1602–1617, 2019. doi: 10.1017/aer.2019.61.

[16] Ispir, Ali Can, Gonçalves, Pedro Miguel, and Saracoglu, Bayindir H. Analysis of a combined cycle propulsion system for stratofly hypersonic vehicle over an extended trajectory. *MATEC Web Conf.*, 304:03001, 2019. doi: 10.1051/matecconf/201930403001. URL https://doi.org/10.1051/matecconf/201930403001.

[17] I. Kolias, A. Alexiou, N. Aretakis, and K. Mathioudakis. Axial compressor mean-line analysis: Choking modelling and fully-coupled integration in engine performance simulations. *International Journal of Turbomachinery, Propulsion and Power*, 6(1), 2021. ISSN 2504-186X. doi: 10.3390/ijtpp6010004. URL https://www.mdpi.com/2504-186X/6/1/4.

[18] E. P. Lesley. Experiments with a Counter-propeller. Mar. 1933. URL https://ntrs.nasa.gov/citations/19930081275.

[19] E. P. Lesley. Tandem Air Propellers. Feb. 1939. URL https://ntrs.nasa.gov/citations/19930081524.

[20] E. P. Lesley. Tandem Air Propellers - II. Aug. 1941. URL https://ntrs.nasa.gov/citations/19930081533.

[21] C. Mistry and A. Pradeep. Effect of variation in axial spacing and rotor speed combinations on the performance of a high aspect ratio contra-rotating axial fan stage. *Proceedings of the Institution of Mechanical Engineers, Part A: Journal of Power and Energy*, 227(2):138–146, 2013. doi: 10.1177/0957650912467453. URL https://doi.org/10.1177/0957650912467453.

[22] A. G. Newton. Aero gas turbine engines for commercial application. 1985.

[23] S. Platini. Master's thesis.

[24] B. Roy, K. Ravibabu, S. Rao, S. Basu, A. Raju, and M. P. N. Flow studies in ducted twin-rotor contra-rotating axial flow fans. 1992.

[25] N. T. Saunders and A. J. Glassman. Future directions in aero- propulsion technology, 7th international symposium on air breathing engines, beijing, china. 1985.

[26] P. Schimming. Counter rotating fans - an aircraft propulsion for the future? *Journal of Thermal Science*, 12:97–103, 05 2003. doi: 10.1007/s11630-003-0049-1.

[27] V. Sethi, G. Doulgeris, P. Pilidis, A. Nind, M. Doussinault, P. Cobas, and A. Rueda. The Map Fitting Tool Methodology: Gas Turbine Compressor Off-Design Performance Modeling. *Journal of Turbomachinery*, 135(6), 09 2013. ISSN 0889-504X. doi: 10.1115/1.4023903. URL `https://doi.org/10.1115/1.4023903`. 061010.

[28] P. B. Sharma and A. Adekoya. A review of recent research on contra-rotating axial flow compressor stage. 1996.

[29] P. B. Sharma, Y. P. Jain, N. K. Jha, and B. B. Khanna. Stalling behaviour of a contra-rotating stage, 7th international symposium on air breathing engines, beijing, china. 1985.

[30] H. S. Toru Shigemitsu, Junichiro Fukutomi. Influence of blade row distance on performance and flow condition of contra-rotating small-sized axial fan. *International Journal of Fluid Machinery and Systems*, 5, 2012.

[31] L. Trainelli, C. E. Riboldi, F. Salucci, and A. Rolando. A general preliminary sizing procedure for pure-electric and hybrid-electric airplanes. 03 2020.

[32] J. Wang. *Experimental study of two counter rotating axial flow fans*. Theses, Ecole nationale supérieure d'arts et métiers - ENSAM, Sept. 2014. URL `https://pastel.archives-ouvertes.fr/tel-01078162`.

[33] Wikipedia contributors. Boeing 737 — Wikipedia, the free encyclopedia. `https://en.wikipedia.org/w/index.php?title=Boeing_737&oldid=1094161033`, 2022. [Online; accessed 21-June-2022].

[34] Wikipedia contributors. Boeing 787 dreamliner — Wikipedia, the free encyclopedia. `https://en.wikipedia.org/w/index.php?title=Boeing_787_Dreamliner&oldid=1093996597`, 2022. [Online; accessed 21-June-2022].

[35] Wikipedia contributors. Cfm international cfm56 — Wikipedia, the free encyclopedia. `https://en.wikipedia.org/w/index.php?title=CFM_International_CFM56&oldid=1089999750`, 2022. [Online; accessed 17-June-2022].

[36] Wikipedia contributors. General electric genx — Wikipedia, the free encyclopedia. https://en.wikipedia.org/w/index.php?title=General_Electric_GEnx&oldid=1070017821, 2022. [Online; accessed 19-June-2022].

[37] Wikipedia contributors. Brayton cycle — Wikipedia, the free encyclopedia, 2022. URL https://en.wikipedia.org/w/index.php?title=Brayton_cycle&oldid=1090856050. [Online; accessed 7-June-2022].

[38] W. W. Wilcox. An analysis of the potentialities of a two-stage counter rotating supersonic compressor.

[39] R. H. Young. Contra-rotating axial-flow fans. *J. Inst. Heat. Ventilat*, 18(187):448–477, 1951.

[40] Zambonini and Gherardo. *Unsteady dynamics of corner separation in a linear compressor cascade*. PhD thesis, 12 2016.

[41] G. Zubi, R. Dufo-López, M. Carvalho, and G. Pasaoglu. The lithium-ion battery: State of the art and future perspectives. *Renewable and Sustainable Energy Reviews*, 89:292–308, 2018. ISSN 1364-0321. doi: https://doi.org/10.1016/j.rser.2018.03.002. URL https://www.sciencedirect.com/science/article/pii/S1364032118300728.

A | Flight mission list

All the flight missions analyzed in Chapter 7 are reported below. The symbology used is "(mission range) / (aircraft) / (engine mounted) / (hybrid system setting)". The flight missions are:

1. **short / Boeing 737-800 / CFM56-7B24 / -** $\longrightarrow$ **reference case**;
2. short / Boeing 737-800 / HYB-CF1-2eng-DPref / CASE 1;
3. short / Boeing 737-800 / HYB-CF1-2eng-DPref / CASE 1bis;
4. short / Boeing 737-800 / HYB-CF1-2eng-DPref / CASE 2;
5. short / Boeing 737-800 / HYB-CF1-2eng-DPref / CASE 2bis;
6. short / Boeing 737-800 / HYB-CF1-2eng-DP1 / CASE 1;
7. short / Boeing 737-800 / HYB-CF1-2eng-DP1 / CASE 1bis;
8. short / Boeing 737-800 / HYB-CF1-2eng-DP1 / CASE 2;
9. short / Boeing 737-800 / HYB-CF1-2eng-DP1 / CASE 2bis;
10. short / Boeing 737-800 / HYB-CF1-2eng-DP2 / CASE 1;
11. short / Boeing 737-800 / HYB-CF1-2eng-DP2 / CASE 1bis;
12. short / Boeing 737-800 / HYB-CF1-2eng-DP2 / CASE 2;
13. short / Boeing 737-800 / HYB-CF1-2eng-DP2 / CASE 2bis;
14. short / Boeing 737-800 / HYB-CF1-2eng-DP3 / CASE 1;
15. short / Boeing 737-800 / HYB-CF1-2eng-DP4 / CASE 1;
16. short / Boeing 737-800 / HYB-CF1-10eng-DPref / CASE 1;
17. short / Boeing 737-800 / HYB-CF1-10eng-DPref / CASE 1bis;
18. short / Boeing 737-800 / HYB-CF1-10eng-DPref / CASE 2;
19. short / Boeing 737-800 / HYB-CF1-10eng-DPref / CASE 2bis;

20. short / Boeing 737-800 / HYB-CF1-10eng-DP1 / CASE 1;
21. short / Boeing 737-800 / HYB-CF1-10eng-DP1 / CASE 1bis;
22. short / Boeing 737-800 / HYB-CF1-10eng-DP1 / CASE 2;
23. short / Boeing 737-800 / HYB-CF1-10eng-DP1 / CASE 2bis;
24. short / Boeing 737-800 / HYB-CF1-10eng-DP2 / CASE 1;
25. short / Boeing 737-800 / HYB-CF1-10eng-DP2 / CASE 1bis;
26. short / Boeing 737-800 / HYB-CF1-10eng-DP2 / CASE 2;
27. short / Boeing 737-800 / HYB-CF1-10eng-DP2 / CASE 2bis;
28. **medium / Boeing 737-800 / CFM56-7B24 / -** $\longrightarrow$ **reference case**;
29. medium / Boeing 737-800 / HYB-CF1-2eng-DPref / CASE 1;
30. medium / Boeing 737-800 / HYB-CF1-2eng-DPref / CASE 1bis;
31. medium / Boeing 737-800 / HYB-CF1-2eng-DPref / CASE 2;
32. medium / Boeing 737-800 / HYB-CF1-2eng-DPref / CASE 2bis;
33. medium / Boeing 737-800 / HYB-CF1-2eng-DP1 / CASE 1;
34. medium / Boeing 737-800 / HYB-CF1-2eng-DP1 / CASE 1bis;
35. medium / Boeing 737-800 / HYB-CF1-2eng-DP1 / CASE 2;
36. medium / Boeing 737-800 / HYB-CF1-2eng-DP1 / CASE 2bis;
37. medium / Boeing 737-800 / HYB-CF1-2eng-DP2 / CASE 1;
38. medium / Boeing 737-800 / HYB-CF1-2eng-DP2 / CASE 1bis;
39. medium / Boeing 737-800 / HYB-CF1-2eng-DP2 / CASE 2;
40. medium / Boeing 737-800 / HYB-CF1-2eng-DP2 / CASE 2bis;
41. medium / Boeing 737-800 / HYB-CF1-10eng-DPref / CASE 1;
42. medium / Boeing 737-800 / HYB-CF1-10eng-DPref / CASE 1bis;
43. medium / Boeing 737-800 / HYB-CF1-10eng-DPref / CASE 2;
44. medium / Boeing 737-800 / HYB-CF1-10eng-DPref / CASE 2bis;
45. medium / Boeing 737-800 / HYB-CF1-10eng-DP1 / CASE 1;

46. medium / Boeing 737-800 / HYB-CF1-10eng-DP1 / CASE 1bis;
47. medium / Boeing 737-800 / HYB-CF1-10eng-DP1 / CASE 2;
48. medium / Boeing 737-800 / HYB-CF1-10eng-DP1 / CASE 2bis;
49. medium / Boeing 737-800 / HYB-CF1-10eng-DP2 / CASE 1;
50. medium / Boeing 737-800 / HYB-CF1-10eng-DP2 / CASE 1bis;
51. medium / Boeing 737-800 / HYB-CF1-10eng-DP2 / CASE 2;
52. medium / Boeing 737-800 / HYB-CF1-10eng-DP2 / CASE 2bis;
53. **long / Boeing 787-800 / GEnx-1B64 / -** $\longrightarrow$ **reference case**;
54. long / Boeing 787-800 / HYB-CF2-2eng-DPref / CASE 2;
55. long / Boeing 787-800 / HYB-CF2-2eng-DPref / CASE 2bis;
56. long / Boeing 787-800 / HYB-CF2-2eng-DP1 / CASE 2;
57. long / Boeing 787-800 / HYB-CF2-2eng-DP1 / CASE 2bis;
58. long / Boeing 787-800 / HYB-CF2-2eng-DP2 / CASE 2;
59. long / Boeing 787-800 / HYB-CF2-2eng-DP2 / CASE 2bis;
60. long / Boeing 787-800 / HYB-CF2-10eng-DPref / CASE 2;
61. long / Boeing 787-800 / HYB-CF2-10eng-DPref / CASE 2bis;
62. long / Boeing 787-800 / HYB-CF2-10eng-DP1 / CASE 2;
63. long / Boeing 787-800 / HYB-CF2-10eng-DP1 / CASE 2bis;
64. long / Boeing 787-800 / HYB-CF2-10eng-DP2 / CASE 2;
65. long / Boeing 787-800 / HYB-CF2-10eng-DP2 / CASE 2bis.

B | Counter-rotating fan EL code

In this appendix is reported the CR fan component code in EcosimPro language (EL).

```
 1. ------------------------------------------------------------------------------
 2. -- AUTHOR: Matteo Baldassarri
 3. -- CREATION DATE: 25/04/2022
 4. ------------------------------------------------------------------------------
 5.
 6. -- Libraries
 7. USE PORTS_LIB
 8. USE CONTROL
 9. USE MATH
10. USE TURBOJET
11.
12. ------------------------------------------------------------------------------
13. -- Component that represents a Counter-rotating fan
14. ------------------------------------------------------------------------------
15. COMPONENT Electric_CrFan IS_A GasChannel
16.    "Counter rotating fan"
17.
18.  PORTS
19.       IN    Shaft sh1_in      "Front rotor input mechanical port"
20.       IN      Shaft sh2_in      "Rear rotor input mechanical port"
21.       OUT    Shaft sh1_out     "Front rotor output mechanical port"
22.       OUT    Shaft sh2_out     "Rear rotor output mechanical port"
23.
24.    DATA
25.       REAL ND1 = 10000.   UNITS   u_r_min      "Front rotor design rotational speed"
26.       REAL CG1 = 1.      UNITS no_units    "Correction coefficient for corrected mass flow"
27.       REAL CG2 = 1.      UNITS no_units    "Correction coefficient for efficiency"
28.       REAL CG4 = 1.      UNITS no_units    "Correction coefficient for compression work"
29.       REAL CG5 = 1.     UNITS   no_units      "Correction coefficient for torque ratio (trqR)"
30.       REAL NR  = 1.      UNITS no_units      "Speed ratio (NR = N1/N2)"
31.
32.       -- Compressor map
33.       TABLE_3D F1         UNITS u_J_kgK     "DHQT (J/kg*K) vs PCNR1 (-) and beta (-) and NR (-
    )"
34.       TABLE_3D F2         UNITS no_units    "EPD (-) vs PCNR1 (-) and beta (-) and NR (-)"
35.       TABLE_3D F3         UNITS u_kg_s      "EPD (kg/s) vs PCNR1 (-) and beta (-) and NR (-)"
36.       TABLE_3D F4         UNITS no_units      "trqR (-) vs PCNR1 (-) and beta (-) and NR (-)"
37.
38.    DECLS
39.       REAL WR            UNITS  u_kg_s      "Corrected Flow Rate"
40.       REAL PowerR       UNITS no_units      "Power ratio (PowerR = P1/P2)"
41.       REAL Power         UNITS  u_W         "Total Mechanical power"
42.       REAL Power1         UNITS  u_W         "Front rotor mechanical power"
43.       REAL Power2         UNITS  u_W         "Rear rotor mechanical power"
44.       REAL trq1         UNITS  u_Nm         "Front rotor torque"
45.       REAL trq2         UNITS  u_Nm         "Rear rotor torque"
46.       REAL N1            UNITS  u_r_min      "Front rotor - Rotational speed"
47.       REAL N2            UNITS  u_r_min      "Rear rotor - Rotational speed"
48.       REAL beta = 0.7   UNITS no_units      "Beta parameter"
49.       REAL PCNR1         UNITS u_pct        "Front rotor adimensional rotational speed"
50.       REAL DHQTJ         UNITS u_J_kgK      "Non scaled compression work"
51.       REAL EPDJ         UNITS no_units      "Non scaled efficiency"
52.       REAL WRJ           UNITS u_kg_s       "Non scaled corrected mass flow"
53.       REAL trqRJ         UNITS no_units      "Non scaled Torque ratio (trqR = trq1/trq2)"
54.       REAL DHQT         UNITS u_J_kgK      "Compression work"
55.       REAL EPD           UNITS no_units      "Efficiency"
56.       REAL trqR         UNITS no_units      "Torque ratio (trqR = trq1/trq2)"
57.
58.    CONTINUOUS
59.
60.       -- Conservation of air mass
61. <M>   g_in.W = g_out.W
```

```
62.
63.         -- Conservation of fuel mass
64.         g_in.FAR = g_out.FAR
65.
66.         -- Adimensional rotational speed
67.         PCNR1 = 100. * (sh1_in.N / ND1) / ssqrt(theta)
68.         DHQTJ = linearInterp3D(F1, PCNR1, beta, NR)
69.         EPDJ = linearInterp3D(F2, PCNR1, beta, NR)
70.         WRJ = linearInterp3D(F3, PCNR1, beta, NR)
71.         trqRJ = linearInterp3D(F4, PCNR1, beta, NR)
72.         trqR = CG5 * trqRJ
73.         DHQT = CG4 * DHQTJ
74.         EPD = CG2 * EPDJ
75.         IMPL(beta) g_in.W * ssqrt(theta) / delta = CG1 * WRJ
76.         g_out.H = g_in.H + DHQT * g_in.T
77.
78.         (Phi_T_FAR(g_out.T, g_in.FAR) - Phi_T_FAR(g_in.T, g_in.FAR)) * EPD = \
79.            R_FAR(g_in.FAR) * log(PQ)
80.
81.         -- Computation of (trqR1, N1) and (trqR2, N2)
82.
83.         WR = g_in.W * sqrt(theta) / delta
84.  <E>    Power = g_in.W * (g_in.H - g_out.H)
85.         PowerR = Power1/Power2
86.         N2 = N1 / NR
87.         0 = Power2 + sh2_in.Power - sh2_out.Power
88.         sh2_in.N = N2
89.         sh2_out.N = N2
90.         0 = Power1 + sh1_in.Power - sh1_out.Power
91.         sh1_in.N = N1
92.         sh1_out.N = N1
93.         trq1 = (30. * Power * trqR * NR) / (PI * N1 * (1 + trqR * NR))
94.         trqR = trq1 / trq2
95.         Power1 = trq1*N1*PI/30
96.         Power2 = trq2*N2*PI/30
97.
98.  END COMPONENT
```

List of Figures

List of Tables

List of main Symbols

Variable	Description	SI unit
$\boldsymbol{\beta_c}$	compression ratio	-
$\boldsymbol{\eta}$	efficiency	-
$\boldsymbol{\eta_{is}}$	isentropic efficiency	-
$\boldsymbol{\rho}$	density	$\frac{\mathrm{kg}}{\mathrm{m}^3}$
$\boldsymbol{\vec{\sigma}_n}$	surface force	$\frac{\mathrm{N}}{\mathrm{m}^2}$
$\boldsymbol{\omega}$	rotational frequency	$\frac{1}{\mathrm{s}}$
$\overline{(\cdot)}$	average in time	-
$\overline{\overline{(\cdot)}}$	average in time and space	-
$(\cdot)_{\boldsymbol{FR}}$	front rotor quantity	-
$(\cdot)_{\boldsymbol{RR}}$	rear rotor quantity	-
$(\cdot)_{\boldsymbol{target}}$	target value	-
$\boldsymbol{BPR}$	bypass ratio	-
$\boldsymbol{C_p}$	specific heat at costant p	$\frac{\mathrm{J}}{\mathrm{kg \cdot K}}$
$\boldsymbol{\vec{f}}$	volume forces	$\frac{\mathrm{N}}{\mathrm{m}^3}$
$\boldsymbol{h}$	static enthalpy	$\frac{\mathrm{J}}{\mathrm{kg}}$
$\boldsymbol{h_T}$	total enthalpy	$\frac{\mathrm{J}}{\mathrm{kg}}$
$\boldsymbol{m}$	mass	kg
$\boldsymbol{M}$	Mach	-
$\boldsymbol{m_{Batt}}$	battery mass	kg
$\boldsymbol{m_{ElecGen}}$	electric generator mass	kg
$\boldsymbol{m_{ElecMot}}$	electric motor mass	kg
$\boldsymbol{\dot{m}}$	mass flow	$\frac{\mathrm{kg}}{\mathrm{s}}$
$\boldsymbol{\dot{m}_f}$	fuel flow	$\frac{\mathrm{kg}}{\mathrm{s}}$
$\boldsymbol{m_{FUEL}}$	fuel mass	kg
$\boldsymbol{m_{MTOW}}$	max take-off weight	kg

$\boldsymbol{m_{OEW}}$	overall empty weight	kg
$\boldsymbol{m_{PAY}}$	payload mass	kg
$\boldsymbol{m_{PElec}}$	power electronics mass	kg
$\boldsymbol{m_{TOT}}$	total aircraft mass	kg
$\boldsymbol{N_{eng}}$	number of engines mounted on the aircraft	-
$\boldsymbol{N_{ratio}}$	speed ratio	-
$\boldsymbol{p}$	static pressure	Pa
$\boldsymbol{P}$	power	W
$\boldsymbol{P_{ratio}}$	power ratio	-
$\boldsymbol{p_T}$	total pressure	Pa
$\boldsymbol{SE}$	specific energy	$\frac{\mathrm{J}}{\mathrm{kg}}$
$\boldsymbol{SFC}$	specific fuel consumption	$\frac{\mathrm{kg}}{\mathrm{s \cdot N}}$ or $\frac{\mathrm{kg}}{\mathrm{s \cdot W}}$
$\boldsymbol{SP}$	specific power	$\frac{\mathrm{W}}{\mathrm{kg}}$
$\boldsymbol{T}$	static temperature	K
$\boldsymbol{T_h}$	thrust	N
$\boldsymbol{T_{r_{ratio}}}$	torque ratio	-
$\boldsymbol{T_T}$	total temperature	K
$\boldsymbol{t_{TO}}$	take-off duration	s
$\boldsymbol{V}$	absolute velocity	$\frac{\mathrm{m}}{\mathrm{s}}$
$\boldsymbol{V_n}$	normal velocity	$\frac{\mathrm{m}}{\mathrm{s}}$
$\boldsymbol{V_t}$	tangential velocity	$\frac{\mathrm{m}}{\mathrm{s}}$
$\boldsymbol{z}$	altitude	[m]

Abbreviations and Acronyms

$\boldsymbol{CR}$	countr-rotating
$\boldsymbol{EL}$	EcosimPro language
$\boldsymbol{FR}$	front-rotor
$\boldsymbol{GT}$	turbogas generator
$\boldsymbol{HP}$	high pressure
$\boldsymbol{HYB}$	hybrid
$\boldsymbol{hy-el\ se}$	hybrid electric serial
$\boldsymbol{LP}$	low pressure
$\boldsymbol{p-e}$	pure electric
$\boldsymbol{Ref}$	reference
$\boldsymbol{RR}$	rear-rotor
$\boldsymbol{tu-el\ dir}$	turbo electric direct
$\boldsymbol{tu-el\ pc}$	turbo electric power controlled

Acknowledgements

Firstly, I want to thank my thesis supervisor Prof. Paolo Gaetani for giving me the possibility to develop my master's thesis at the von Karman Institute. This experience abroad was very instructive for me from both a technical and a personal point of view.
My deep gratitude goes to my co-advisors from VKI Prof. Fabrizio Fontaneto and Dr. Manas Madasseri Payyappalli, who both closely supported me during these months and answered my questions.
From VKI I want also to thank all the people that I met during this experiences. They always helped me during the difficulties and with some of them I shared beautiful days in visiting Belgium. I am also thankful to all my close friends from both Milano and Pesaro, who accompanied me during these years. I want just to say a few words about Carlo, who was my roommate in Milano. Thank you for the support during this years in Milano.
A very special thank goes to my girlfriend Martina who gave me the strenth to always go on and never stop against difficulties. I want to thank her also for her continuos presence and love also during the days in which we were far.
Last but not least, I want to thank my family for their continuosly support both from an emotional and economical point view. Study is very expensive, I will never forget all the sacrifices that they have done for me.